Enhanced Barrier Properties of Renewable Multiphase Polymer Coatings and Films

by

Binh-Minh Trinh

A Thesis

Presented to the University of Waterloo

In the fulfillment of the

Thesis requirement for the degree of

Master of Applied Science

in

Chemical Engineering

Waterloo, Ontario, Canada, 2021

AUTHOR'S DECLARATION

This thesis consists of materials all of which I authored or co-authored: see Statement of Contributions included in the thesis. This is a true copy of the thesis, including any required final revisions, as accepted by my examiners.

I understand that my thesis may be made electronically available to the public.

STATEMENT OF CONTRIBUTIONS

Chapter 2 of this thesis comprises background information and literature reviews on moisture and gas barrier properties of renewable polymer films and coatings. The information used in this chapter was adapted from part of a draft review manuscript. The manuscript is being prepared by myself, a post-doctoral fellow (Dr. Boon Cheng), a Ph.D. student (Debela Tadele) under the guidance of Dr. Mekonnen.

Chapter 3 is adapted from a published manuscript "**Facile fabrication of thermoplastic starch/poly (lactic acid) multilayer films with superior gas and moisture barrier properties, Polymer, 223** (2021) **123679**" in which I am the first author. Another student in Dr. Mekonnen's group, Christina Chang supported me in carrying out the experiments, analyzing the results, and preparing the draft manuscript. Dr. Mekonnen initiated the project, provided guidance and supervision, and reviewed the manuscript.

Chapter 4 is also adapted from a recently accepted manuscript "**A nanomaterial-stabilized starch-beeswax Pickering emulsion coating to extend produce shelf-life**. **Chemical Engineering Journal 431** (2022) **133905**". I am the first author of this work. I designed all the experiments and analyzed the results under the guidance of Prof. Mekonnen. I also prepared the draft manuscript. Michael Smith, a co-op student in Dr. Mekonnen's group, carried out some experiments under my guidance and reviewed the manuscript. Dr. Mekonnen initiated the project, provided guidance and supervision, and reviewed the manuscript.

ABSTRACT

The use of traditional synthetic polymer in the food industries imposes great sustainability issues in conjuncture with plastic waste accumulation and consumers' health concerns. This drives innovation in bioplastics with acceptable physical properties. However, most single-phase biodegradable and bio-based bioplastics typically have poor moisture or oxygen barrier properties or both than traditional fossil fuel-based plastics, making it a challenging task to replace these plastics. This thesis presents multiple robust approaches to fabricate sustainable food packaging films and coating materials, considering various stratagems to combine different renewable components to enhance barrier properties. The use of multiphase systems, including blends, multilayer assembly, and nanocomposites as well as the employment of novel compatibilization techniques, such as surface modifications and emulsion stabilizations, are evaluated to fabricate the new generation of sustainable multiphase packaging materials.

The first part of the thesis is on multilayer film systems made from two poly(lactic acid) (PLA) layers and one center thermoplastic starch (TPS) layer embedded with nano-clay. Maleic anhydride (MA) modification enhanced the interaction between each layer. This multilayer film assembly provided 92.4% improvement in moisture barrier compared to TPS films and 3300% improvement in oxygen barrier properties compared to PLA. The second part of the thesis has focused on fabricating Pickering emulsion-based coatings made from cornstarch and beeswax (BW) stabilized with modified cellulose nanocrystals (CNCs). Different fruits were dip-coated with a formulated edible coating, which displayed magnificent color and freshness preservation by reducing oxygen activities and preventing moisture losses. These preliminary findings show a promising outlook in food packaging and coating applications.

ACKNOWLEDGEMENTS

First and most importantly, I would like to express my utmost respect and gratitude to my supervisor and mentor, Dr. Tizazu Mekonnen, for supporting my development and giving me such incredible guidance to finish multiple projects for this Master thesis. Dr. Mekonnen is the one who gave me an amazing opportunity to work in his lab as a co-op and inspired me to pursue my Master, and possibly Ph.D. in the future. Thus, I am forever grateful for his guidance and expertise in the field of academia. I considered Prof. Mekonnen the ultimate role model in my life, and his approval meant a lot to me. I would also want to show my appreciation to my committee members, Prof. Costas Tzoganakis and Prof. Evelyn Yim, for their time and constructive feedback on my thesis.

Next, I would like to thank my colleagues with who I have been working in the past and present. A special mention to Rohan Shorey, and Dylan Jubinville, with who I am the closest and offer me many supports and assistance during my graduate studies. I would also like to thank the rest of my colleagues: Dr. Boon Cheng, Dr. Arvind Gupta, Dr. Emmanuel Ogunsona, Dr. Hormoz Eslami, Azin Adibi, Curtis Seto, Debela Tadele, Ewomazino Ojogbo, Karelle Guiao, and Rachel Blanchard for making the lab an enjoyable workplace. I hope we can all meet together again someday and maybe even collaborate in the future.

Special gratitudes to my dear friends, Aimee Wu, Andy Yang, Aubrey Gambito, Danielle Skeba, Maddy Jang, Gavin Lee, Kevin Lee, Mahir Rashid, Michael Girgis, Nishita Saha, Thomas Sun, and many others. I cannot thank them all enough for their support and encouragement, as well as all the best experiences and unforgettable memories in universities that I can ever ask for.

DEDICATION

I want to dedicate this work to all of my family members, especially my beloved parents, who always support and provide me with unconditional love and support. They are the reasons why I can get to where I am today. A special thank you to my sister, Thao, and my nephew, Duc Anh, for always being there for me and giving me all the strength that I needed to finish my undergraduate and graduate studies. I also want to show my appreciation to my cousin, Kien, whom I considered my brother, for giving me all the supports and advice that I needed to complete my Master's at the University of Waterloo.

Last but not least, I would also like to dedicate all of this work to my late grandparents, who unfortunately cannot see my achievements today. I love you all, and I hope you will be proud of me.

TABLE OF CONTENTS

LIST OF FIGURES

LIST OF TABLES

LIST OF ABBREVIATIONS

AFM	Atomic force spectroscopy
BNC	Bacterial nanocrystal
BW	Beeswax
CNC	Cellulose nanocrystal
CNF	Cellulose nanofibril
DDSA	Dodecenyl succinic anhydride
DMA	Dynamic mechanical analysis
FTIR	Fourier transform infrared
HCl	Hydrochloric acid
KBr	Potassium bromide
MA	Maleic anhydride
MAP	Modified atmosphere packaging
MMT	Montmorillonite
MTPS	Maleated thermoplastic starch
NaOH	Sodium hydroxide
NMR	Nuclear magnetic resonance
OMMT	Organo-Montmorillonite
OTR	Oxygen transmission rate
OP	Oxygen permeability
PBAT	Poly (butylene adipate terephthalate)

PBS	Poly (butylene succinate)
PCL	Polycaprolactone
PE	Poly (ethylene)
PET	Poly (ethylene terephthalate)
PGA	Poly (glycolic acid)
PH	Poly (hydroxy ether of bisphenol A)
PHA	Poly (hydroxyalkanoic acid)
PHB	Poly (3-hydroxybutyrate)
PHBV	Poly(3-hydroxybutyrate-co-3- hydroxyvalerate)
PLA	Poly (lactic acid)
PP	Polypropylene
PVA/PVOH	Poly (vinyl alcohol)
PVC	Poly (vinyl chloride)
RH	Relative humidity
S	Starch
SEM	Scanning electron microscopy
T_g	Glass transition temperature
TGA	Thermogravimetric analysis
TPS	Thermoplastic starch
WVTR	Water vapor transmission rate
WVP	Water vapor permeability
ZnO	Zinc Oxide

CHAPTER 1: INTRODUCTION

Figure 1.1. Different categories and functionalities of food packaging materials

1.1.Overview and Motivation

Polymer coatings and films have been widely utilized in various engineering applications and have continued to grow over the past decades[1,2]. Polymer coatings and films are primarily applied as decorative or protective layers to shield wanted goods from undesirable environmental factors. They are generally applied in diverse material engineering applications, such as automotive, furniture, papers, food, and electronic sectors. These coatings can also be spread over substrates

using different techniques, such as brushing, spray-coating, dip-coating, roll-coating, and spin-coating. Most commercial polymer coatings and films are derived from synthetic fossil-fuel materials. The use of polymer films and coatings in food packaging applications can be divided into three main categories, as shown in **Figure 1.1.** These are enhanced barrier, active, and intelligent/smart packaging materials, each with their own unique functionalities. In this thesis, the role of coatings and films acting as enhanced barrier material for food packaging applications will be summarized.

It is important to highlight that the food packaging industry is highly dependent on polymer coating due to transportation and distribution necessities of food products, which would enable quality preservation and external protection against physical, chemical, thermal, and microbial contamination[3,4]. The most common polymers utilized as flexible packaging and coating materials includes poly(ethylene) (PE), poly(propylene) (PP), poly(amide) (PA), poly(vinyl chloride) (PVC), poly(vinyl alcohol) (PVA), poly(ethylene glycol) (PEG), and ethylene vinyl acetate (EVA). These materials have the mutual traits of being comparatively inexpensive and easy for processing. Moreover, the production of synthetic polymers can be extremely efficient as the process utilize a continuous extrusion process with minimal waste generation and the capability to recycle scraps and some waste.

Despite the fact that most synthetic polymer coatings possess many convenient and beneficial attributes, they also impose major sustainability issues, can be a concern for the environment, and in some cases health and safety concerns. Food packaging films and coatings contribute to one of the largest plastic landfill waste fraction with about 275 million tons of waste generation in 2018 [5]. The exceptional barrier properties of synthetic polymers together with their resistance to chemical, biological, or microbial agents can be a double-edged sword as those resistance properties can make synthetic polymers extremely difficult to remove from the environment in

their end life [6].The presence of food residue in conjuncture with the complexity of their, which often contains multi-layers composed of other types of polymers, paper, and metals (e.g., aluminum) further complicates recycling options of food packaging and coating materials. Thus, most synthetic polymer based films and coatings are disposed of as wastes in landfills, that often get incinerated with air pollution concerns [7,8]. Plastic waste from food packaging films and coatings can be observed everywhere, ranging from streets, to drainage systems, rivers and lakes, and oceans. In terms of health risks to consumers, these non-biodegradable plastics can release harmful chemicals (e.g., Bisphenol A from epoxy coatings) and partially break down into microplastics. The absorption of toxic chemicals and microplastics over time would have an accumulating negative health effect to consumers. Overall, there is growing concern over the environmental pollution, resource depletion, and health and safety impacts associated with the use and disposal of petroleum-derived polymers [9–11].

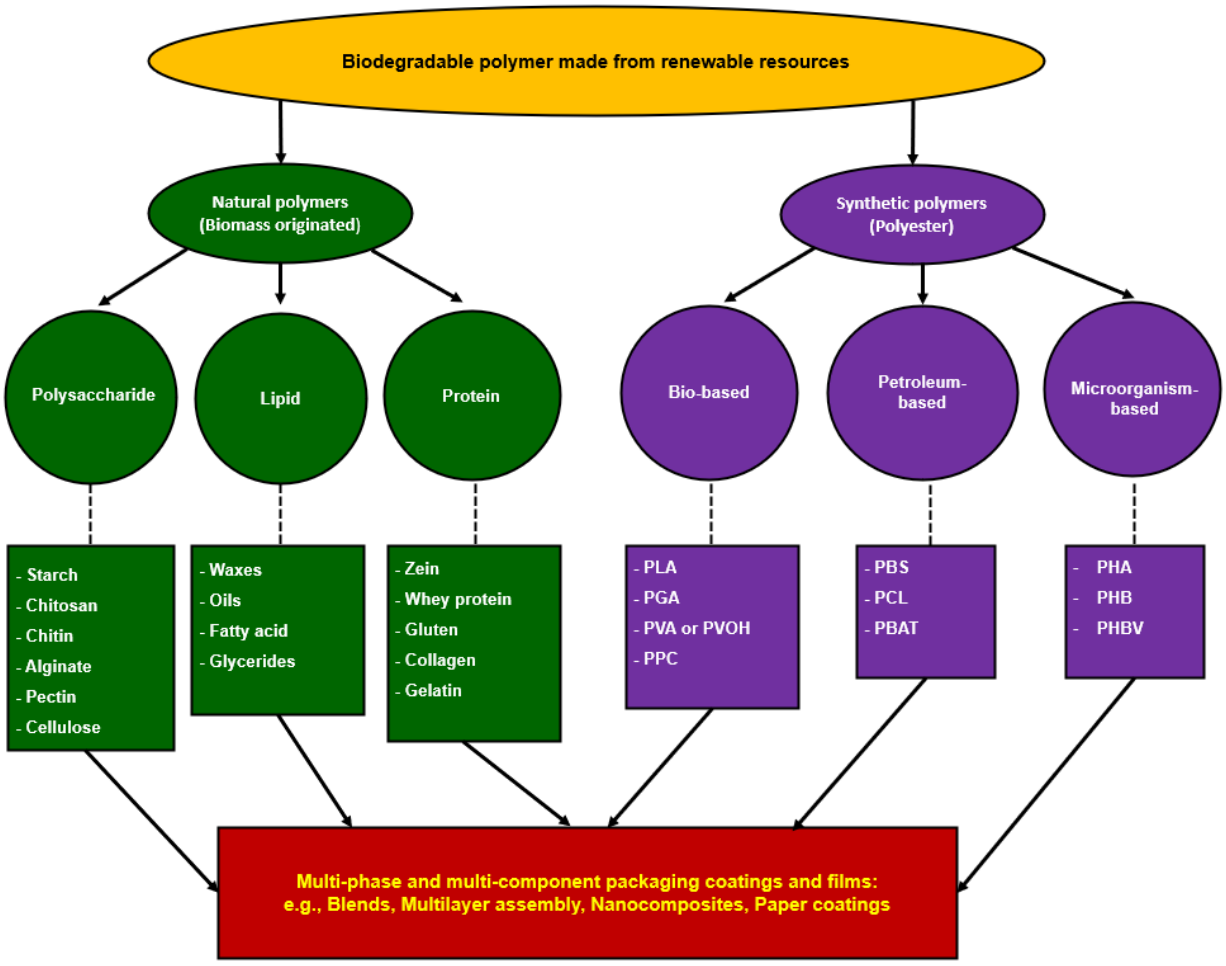

Figure 1.2. Classification of renewable polymers

Many solutions have been proposed to minimize the use of synthetic polymer coatings and help solving the problem. The most common solutions are to replace these synthetic coatings with bio-based plastic materials with compostability or biodegradability attributes. Bio-based materials, are derived from natural biomass and renewable feedstock and in some cases they can imitate the advanced functional barrier properties of synthetic materials for appropriate applications [12]. In comparison to synthetic polymers, biodegradable polymers are much better candidates as they can be quickly degraded via microorganisms. Especially, the use of biopolymers can be desirable in the pharmaceutical and food manufacturing industries since these natural materials often satisfy

both health & safety regulations and customer demand, unlike synthetic polymers which can sometimes have health and safety concerns for consumers[13,14]. Moreover, some biopolymer based materials can be edible, for instance edible fruit coatings that provide an extra layer that reduce transpiration rate and weight loss [15]. So far, there are several food coatings that originated from biomass or eco-friendly natural resources and extensively utilized in the food industry. Examples of natural materials or biopolymers that are gaining interest in the food packaging film and coating applications include biopolyesters (poly(lactic acid) (PLA), poly(hydroxyalkanoates) (PHA), Poly(butylene succinate) (PBS), and poly(caprolactone) (PCL)) [16–18], polysaccharide-based biopolymers (starch, cellulose, and chitosan)[19–21], lipid-based compounds (waxes, oils, and fatty acids)[22–24], protein-based biopolymers (zein, whey protein, gluten, and gelatin) [25–27], or multi-phase blend, multilayer, or composite coatings and films [28–30], as seen in **Figure 1.2**. Despite the fact that biopolymer coatings showed appealing potentials to be used in a variety of application markets compared to synthetic polymers, they still have a few obstacles that needs to be overcame. For instance, most biopolymers have unsatisfactory mechanical and barrier properties compared to traditional petroleum-based polymers[28].

The strong drive for bioplastics that provide good barrier properties against moisture and oxygen while simultaneously displaying good mechanical properties without compromising their biodegradability is ever-increasing, mainly for food packaging and coating applications [31]. Coatings and films need to have excellent barrier properties to promote appropriate isolation of food from the environment and minimize contact with oxygen (oxidation reaction, aerobic microorganisms' growth) or moisture (microbial growth, water activities, flavor change), as well as to avoid dehydration of food, such as fruits and vegetables. There are many strategies that can be employed to improve the barrier properties of polymeric coatings. Most commonly used strategies are the implementations of multiphase and multilayer coating materials by combining

two or more different polymers or materials in the film coating systems in the form of blend, layer-by-layer, or composite system.

1.2. Research objectives

The aim of this thesis is to investigate ways of enhancing the moisture and oxygen barrier properties of renewable (bio-based, biodegradable, compostable) polymer films and coatings. , Two separate scientific directions were carried out and presented. In both studies, detailed investigations on the development of multiphase renewable films and coatings are thoroughly conducted, and the material functionalities in food packaging films and coatings are closely examined.

The first part of the research focuses on the production of a multilayer films comprised of TPS and PLA fabricated via a reactive extrusion, compression molding, and dip coating processes. The goal of this work was to improve the interfacial adhesion between TPS and PLA layers of the multilayer film via maleation of TPS. Moreover, the incorporation of low concentration nanoclays to reduce the polymer free volume and subsequently enhance the barrier properties of the films is investigated.

The second part of the research has focused on stabilizing thermoplastic starch – beeswax (BW) coating formulations for fresh produce coating applications. Native and aliphatic succinic anhydride-modified cellulose nanocrystals (CNCs) were employed as a Pickering emulsifiers to stabilize lipid BW particles in the starch solution. The effect of emulsion stabilizers loading on the enhancement of physical properties, reduction of water vapor loss, and decrease in oxygen permeability were evaluated. Furthermore, the application of the coatings in fruit preservation was explored, which involved the dip-coating of various fruits type (bananas, strawberries, and apples) and a comprehensive time-lapse study.

1.3. Thesis outline

The subsequent sections of the thesis are structured as follows: Chapter 2 provides a literature review that focuses on the topics related to the barrier properties of multiphase biodegradable materials in the food packaging industries such as: barrier requirement, barrier mathematical models, and factors that affect barrier properties of coatings and films. Chapter 3 presents the completed research work on biodegradable food packaging materials, which presents a detailed fabrication process and characterization of a facile TPS/PLA multilayer film with superior gas barrier properties. Chapter 4 covers the complete experimentation, characterization, and functionalization of a Starch/Beeswax Pickering-emulsion film study that can be used as edible coatings in fresh fruits and other produces. Finally, Chapter 5 provides the overall conclusions and recommendations of the thesis.

CHAPTER 2: BACKGROUND INFORMATION

2.1. Barrier requirements of polymer coatings in various applications

The permeation and dissolution of moisture and gases through thin polymer films (or layers) is directly correlated to the barrier capabilities of polymer coatings and films utilized in many industries, such as pharmaceutical, biomedical, and food packaging. While the barrier properties of traditional polymers utilized in food packaging films and coatings is well established, such properties for the newer bioplastics are usually inferior and requires further investigation. Comparison between packaging requirement and single-component biodegradable and bio-resourced materials are summarized in **Figure 2.1.** In most cases, stand-alone single component polymer films and coatings could not satisfy the barrier requirement of packaging materials for several food products such as instant coffee, cheese, or fresh meat. These individual materials lack either moisture barrier or oxygen barrier properties, and in some cases completely lack both requirements. The only exception of biodegradable polymer with both superior moisture and oxygen barrier properties in packaging application is poly(glycolic acid) (PGA) [32]. Compared to the common polymers used in food packaging films and coatings (PET, PE, and PP) , PGA exhibits superior moisture and gas barrier properties. However, the production of PGA is much more complicated, energy consuming, and costly. As a result, PGA is not yet widely used in food packaging applications.

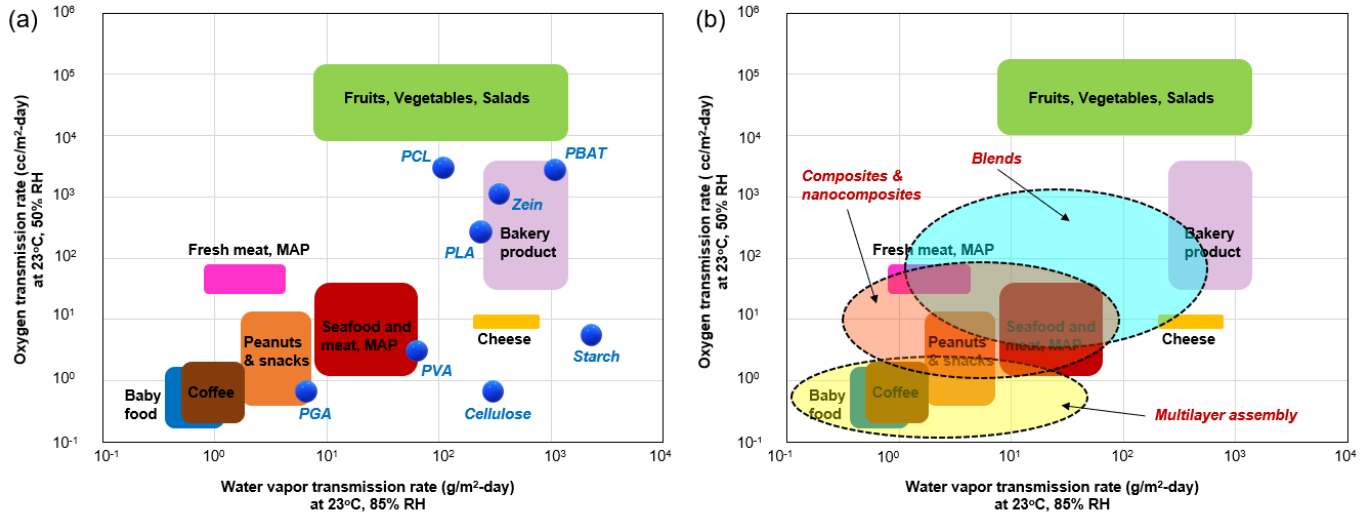

Figure 2.1. Comparison of various food packaging water vapor/oxygen transmission rate requirement with (a) Individual polymers and (b) Multi-phase polymer systems.

To obtain enhanced barrier performance, combining bioplastics with other traditional polymers, which possess excellent moisture and oxygen barrier properties, such as PET, PE, and PP are common practices among many premier "green" packaging providers like Novamont (Italy), Biotec (Germany), and Dupont (USA)[33,34]. However, the incorporation of non-biodegradable parts within the multi-phase packaging coatings and films still constitutes a major challenge as the disintegration of such multiphase polymer systems with stark degradation difference leads to the generation of microplastics. Therefore, it is now widely accepted that such packaging films and coatings should be constructed from 100% biodegradable or compostable components to satisfy the sustainability requirement in addition to their physicochemical performance.

Promising developments are in progress on multicomponent and multiphase biodegradable system that satisfy the barrier requirement of packaging materials, which significantly reduce the overall moisture and oxygen transmission rate to the food products, as shown in **Figure 2.1**. For instance, recent works on TPS/PLA multilayer, TPS/PBAT multilayer, PLA/ PPC blend [35], PBAT-hemp

biocomposites [36], and starch ester/CNC nanocomposites [37] demonstrated promising barrier performance. Barrier properties are highly dependent on the polymers morphology, polarity, structure attributes, including the crystallinity, chain orientation, branching, free volume, and molecular interaction within polymer matrices [38]. To enhance the barrier properties of multiphase films and coatings, compatibilization techniques that involve chemical/physical modification, as well as novel structure designs, incorporation of nanomaterials with specific morphologies are under intense investigation. This chapter reviewed key factors that influence the barrier properties of polymer packaging films and coatings used in food packaging applications.

2.2. Models for permeations and barrier properties of polymer films and coatings

2.2.1. Simple transport mechanism

For polymeric materials, the permeation of moisture and oxygen gases involves the absorption capabilities of materials, diffusion, as well as desorption of these particles from the films or coating surfaces as shown in **Figure 2.2**. The absorption of moisture or gas depends on the "solubility" of the permeants in the polymers. In another term, the ability to allow fluidic gas to pass through depends on the absorptive capabilities of the materials, which is dependent on factors such as degree of crystallinity (morphology), polarity, and molecular weight. In general, nature derived biodegradable and renewable polymers have much worse barrier properties than those presented in petroleum-based polymers due to their inherent structures and chemical compositions. This is not surprising as these macromolecules are not purposefully designed for packaging applications as opposed to the synthetic counterparts used in packaging.

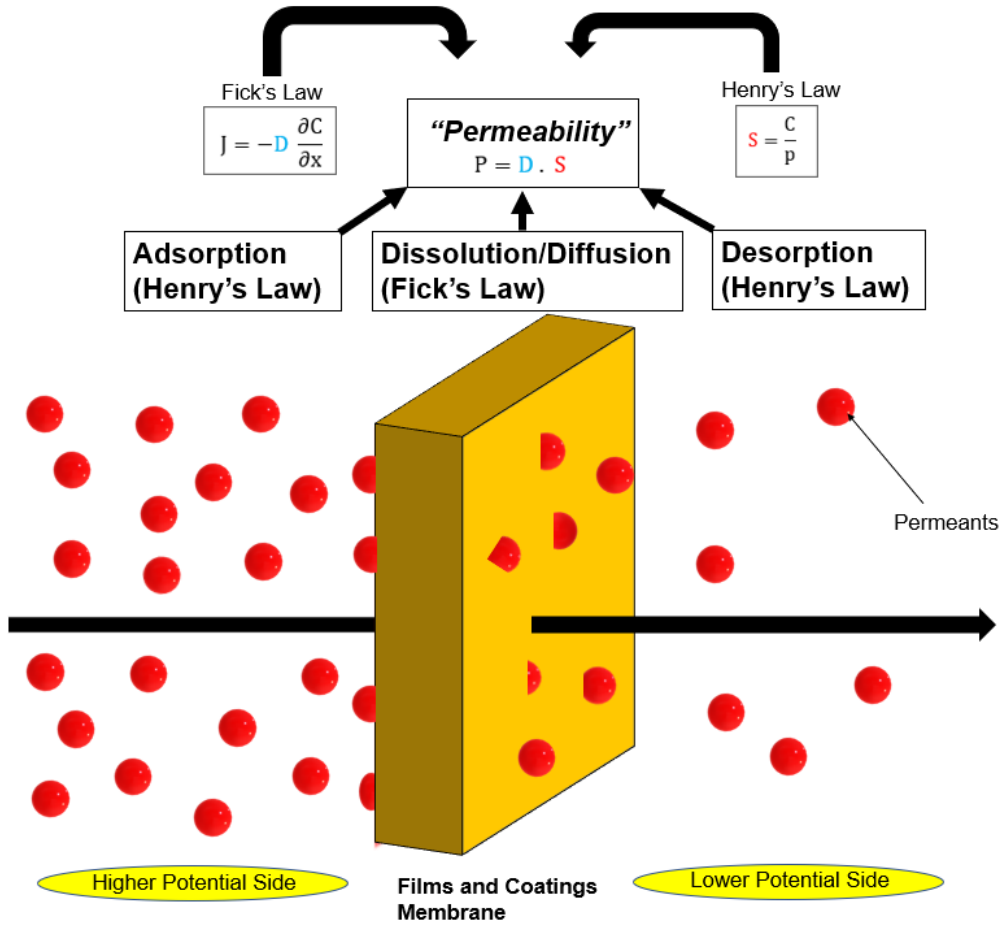

Figure 2.2. Simple permeability model across a polymer film or membrane

The simplest and most widely used mechanism of gas and moisture permeability is often illustrated and described as the idealized "Dissolution-Diffusion" (or "Solubilization-Diffusion") model, which can be summarized into three main consecutive steps. The first step is adsorption, in which the moisture and gas molecules move on to one side of the membrane due to gradient potential difference of pressure, concentration or temperature. The second step is diffusion or dissolution. In this step, the molecules get solubilized inside the films or coatings and travel through the void space (or free volume) of the polymeric materials. The third and final stage is desorption, which entails the escape of the diffused molecules on the other side of the film or coatings[39,40]. **Figure 2.2** shows a simplified mechanism of this permeation model. The movement of water vapor

through a polymer layer or membrane can also be viewed as water molecules dissolving into the solid mass, traveling through the material, and finally evaporating on the other side of the layer or membrane. The diffusion/dissolution step primarily determine the absorbent properties of the material. Based on this mechanism, the permeability (P), can be related to the solubility (S) and diffusivity (D) coefficients as presented in Eq.1:

$$P = D.S \tag{1}$$

The diffusivity coefficient term (D) can simply be described by either Fick's first (Eq.2) and second law (Eq.3), which describe the kinetic movement of low molecular penetrants (typically gas) across a polymer film or coating in terms of mass transfer proportional to the concentration gradient:

$$J = -D.\frac{\partial C}{\partial x} \tag{2}$$

$$\frac{\partial C}{\partial t} = -\frac{\partial J}{\partial x} = D.\ \frac{\partial^2 C}{\partial x^2} \tag{3}$$

Where J is the flux of penetrant (amount of permeant passing thought unit area per unit time), C is the concentration of the penetrant, and x is the one-dimensional direction of the concentration gradient. Fick's second law is used when the diffusion coefficient is considered to be independent of concentration, distance, or time. The diffusivity constant is dictated by both the polymer membrane and the diffusing permeant in terms of molecular size, temperature, pressure, and concentration gradients

In order to integrate the Fick's first law equation, steady state assumption must be implemented in the system. Additionally, the gas and vapor permeant concentration at equilibrium must also kept constant on both sides of the film or membrane for simplicity. Thus, Eq. 2 can be written as:

$$\frac{\mathrm{Q}}{\mathrm{A.t}} = \mathrm{J} = \mathrm{D} \,.\, \frac{\mathrm{C}_H - \mathrm{C}_L}{\mathrm{L}} \tag{4}$$

In this case, the flux J is expanded as the amount (Q) passing through unit area (A) per unit time (t). C_H and C_L represent the permeant concentration at higher and lower potentials, respectively. The denominator, L, denotes the thickness of the polymeric films or coatings.

The solubility coefficient term (S) can be determined from the ratio of concentration of gas or vapor relative to the pressure in the gaseous state in the form of Henry's law:

$$\mathrm{S} = \frac{\mathrm{C}}{\mathrm{p}} \tag{5}$$

Where C is the surface concentration of dissolved gas or vapor, and p is the partial pressure of the permeant gas. However, this method of determining solubility model does not take the effect of plasticization of polymer film or membrane into account, which is not representative for polymeric materials in general. In order to consider the plasticization effect, an extended dual sorption model to determine solubility adsorption of polymeric membrane matrix can be employed by the addition of extra terms for concentration of dissolved gas or vapor (C), which is the combination of Henry's law and Langmuir's adsorption[41]:

$$\mathrm{C} = \mathrm{C_H} + \left(\frac{\mathrm{C_L b}}{\mathrm{K_D}}\right) \frac{\mathrm{C_D}}{1 + \mathrm{b C_D / K_D}} \tag{6}$$

where C_H and C_L are the concentration of dissolved gas or vapor defined by Henry and Langmuir solubility, b is the affinity of gas molecules being absorbed in the polymer, and K_D is the Henry's law dissolution constant. The second term of this equation originate from the non-equilibrium nature of glassy polymers. The modified surface concentration will then be used to determine solubility coefficient term through Henry's law (Eq.4).

Combining Eq.4 and Eq.5 and substituting them into Eq. 1, the permeability constant can simply be determined as [42]:

$$P = \frac{\mathrm{Q.\,L}}{\mathrm{A.\,t.\,\Delta p}} \tag{7}$$

Δp represents pressure difference on the two sides of the polymeric films or coatings. This pressure difference is influenced mainly by factors, such as gas type, humidity, and temperature. The dependence of permeability and transmission rate on temperature can be modified using Arrhenius equation [43]. As seen in Eq.7, the units of permeability for gases are generally expressed as volume-length/area-time-pressure. In the case of moisture permeability, the units are expressed as weight-length/area-time-pressure instead. Overall, this units of permeability and transmission rate can vary, depending on the measuring methods; e.g "barrer" or "mol/m.s.Pa" for gas permeability and "perm" or "kg/m.s.Pa" for water permeability.

2.2.2. Developed models for multi-component polymer films and coatings

In reality, the dissolution and diffusion of permeants in polymers are much more complicated process to predict accurately. Especially in multi-component systems, Fick's model is insufficient in predicting the solubility of multiple components as the theory neglect the interaction between permeants and polymer chains as well as one polymer chain from the other. Moreover, Fick's diffusion assumes a linear gradient concentration across the moving boundary of the films or coatings, which would only happen in an ideal situation [44]. The random orientations of the free volume of polymer matrix and swelling of polymer chains suggest that the concentration gradients behave more similarly to a non-linear model, which is attributed to abruption of permeants when they get in contact with different segments of polymeric multi-phase components [45]. Therefore, it is important to predict and develop the dissolution and diffusion behaviors of different renewable polymer systems by the means of experimental modelling and characterization.

2.2.2.1. Multi-phase blends and multilayer assembly

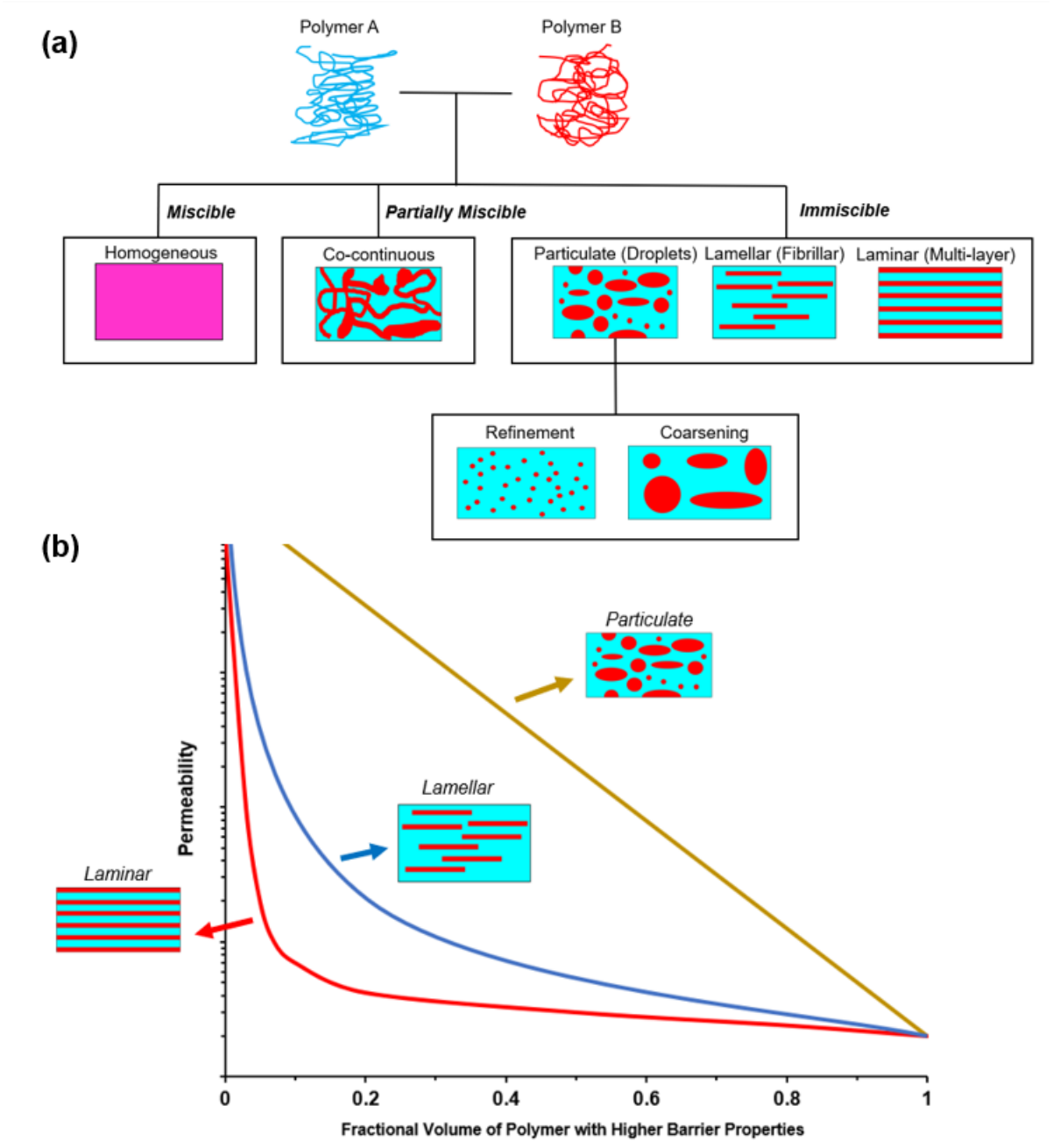

Figure 2.3: (a) Different morphological categories of multi-phase polymer blends. (b) Comparison of overall Permeability values between particulate, lamellar, and laminar system [46] (Copyright ©2020. Adapted with permission from Wiley Online Library)

Table 2.1. Mathematical models of moisture/ gas permeability through multi-phase blends and multilayer coatings and films.

Blend system	**Model**	**Equation**	**Eq. #**
Particulate	Voight[47,48]	$\ln P = \emptyset_d \ln P_d + \emptyset_c \ln P_c$ or $\ln P = \sum_{i=1}^{n} \emptyset_i \ln P_i$	(8)
Particulate	Maxwell [49]	$P = P_c \left[\frac{P_d + 2P_c - 2\emptyset_d(P_c - P_d)}{P_d + 2P_c + \emptyset_d(P_c - P_d)}\right]$	(9)
Particulate and co-continuous	Bruggeman [50]	$\left(\frac{P}{P_c} - \frac{P_d}{P_c}\right)\left(\frac{P}{P_c}\right)^{-1/3} = (1 - \emptyset_d)\left(1 - \frac{P_d}{P_c}\right)$	(10)
Particulate	Higuchi [51,52]	$P = P_c\left[1 + \frac{3\emptyset_d\left(\frac{P_d - P_c}{P_d + 2P_c}\right)}{1 - \emptyset_d\left(\frac{P_d - P_c}{P_d + 2P_c}\right) - K(1 - \emptyset_d)\left(\frac{P_d - P_c}{P_d + 2P_c}\right)^2}\right]$; K=0.78	(11)
Particulate and Lamellar	Lewis-Nielsen [53]	$P = P_c\left[\frac{1 + 2\emptyset_d\left(\frac{P_d - P_c}{P_d + 2P_c}\right)}{1 - \Psi\emptyset_d\left(\frac{P_d - P_c}{P_d + 2P_c}\right)}\right]; \Psi = 1 + \left[\frac{1 - \emptyset_m}{{\emptyset_m}^2}\right]\emptyset_d$ $\emptyset_m$ = 0.785 for square fibrillar packing, $\emptyset_m$ = 0.82 for random packing	(12)
Lamellar	Maxwell-Wagner-Sillar [54]	$P = P_c\left[\frac{nP_d + (1-n)P_c + (1-n)(P_d - P_c)\emptyset_d}{nP_d + (1-n)P_c - n(P_d - P_c)\,\emptyset_d}\right]$ $0 \le n \le 1/3$ for prolate ellipsoid, n=1/3 for spherical, $1/3 \le n \le 1$ for oblate ellipsoid	(13)
Co-continuous	Geometric Mean[55]	$P = {P_c}^{\emptyset_c} + {P_d}^{\emptyset_d}$ or $P = \sum_{i=1}^{n} {P_i}^{\emptyset_i}$	(14)
Laminar	Reuss[55]	$\frac{1}{P} = \frac{\emptyset_c}{P_c} + \frac{\emptyset_d}{P_d}$ or $\frac{1}{P} = \sum_{i=1}^{n} \frac{\emptyset_i}{P_i}$	(15)

Note: Pc and Pd are the permeability of the permeant in the continuous and dispersed polymer phases, respectively. $\emptyset_c$ and $\emptyset_d$ are the fractional volumes of the continuous and dispersed polymer phases, respectively

Blending is a common technique to produce barrier films and coatings that utilize limited amounts of the expensive high barrier polymer in an inferior and low-cost polymer matrix to fabricate a material with balanced performance and cost. The blends are often produced in a simple and solvent-free process, such as extrusion and injection process making it a very desirable technique to be used in the food packaging industries. Since blending is the combination of two or more materials, the properties of polymer blend will often fall between those components. However, on rare occasions, the compatibilities and synergies between the blends can be so good that it might establish a system with improved properties that surpass its parent materials [56,57]. The barrier properties of any polymer blends depend strongly on the miscibility of the components. The morphologies of blending can be divided into 3 main categories: miscible, partially miscible, and immiscible (**Figure 2.3a**). Miscible blend refers to mixtures of polymers with similar chemical structure and viscosity that can combine together into one homogeneous phase. It must be noted that achieving a miscible blend of two or more materials is a remarkably challenging task because of the unfavorable kinetic and entropy of mixing [47]. Thus far, there has been no report of permeation model development for biodegradable and renewable polymer blends with complete miscibility.

On the other hand, analytical models that predict the permeability of moisture and gases for binary immiscible blends have been extensively studied and well-presented over the last few decades, especially on the particulate (dispersed droplets) and lamellar (fibrillar) distribution of a polymer in another polymer matrix. A number of reviews such as Aroon et al. [58], Gonzo et al.[59], and Wu et al. [60]have investigated and compiled various possible mathematical models that would be fitting to describe polymer blend systems. Among the developed models presented in these reviews, a few important and common mathematical equations are selected and summarized in **Table 2.1**.

Various approaches are developed to take the permeability for the particulate distribution of dispersed phases in polymer films or coatings into account. The maximum permeability of immiscible blend coating can simply be described by an equation that is analogous to Voight model from the Rule of Mixture (**Eq.1**)[48]. This predictive model is used when the dispersed phases are parallel to the direction of permeation flux, which gives the Voight model another name, known as Parallel model. Since the Voight model acts as the upper boundary for permeability, all of the developed models should predict lower values of permeability. Among the equations, the most widely accepted model to depict the permeability in polymer blends is the equation proposed by Maxwell. Maxwell's model was initially used to estimate the dielectric conductivity properties of polymer blends, but the formula was later developed into an equation to predict permeability as shown in **Eq. 9** [49]**.** The limitation of this model is that it is adequate only in the prediction of spherical refinement morphology of the blended polymer matrices and only with dispersed volume fraction ($\emptyset$) < 0.2. Many other analytical models were adapted from Maxwell equation and were extensively investigated with the most prevalent examples being Bruggeman, Higuchi, Lewis-Nielsen, and Maxwell-Wagner-Sillar. Bruggerman expressed the permeability of a particulate system blend by the use of effective medium theory approach in (**Eq. 10**), which can be applied for both particulate and co-continuous systems [50]. This equation is appropriate when there is a small difference in the permeability of two polymer phases, as well as for compositions near 50%. The formula expressed by Higuchi (**Eq. 11**) was derived from experimental data and is applicable to predict particulate blend systems regardless of distributions or sizes, including refinement and coarsening morphology [51]. From the collection of dielectric constants, Higuchi determine the empirical constant (K) for spherical systems to be 0.78. Lewis and Nielsen experimentally developed their own model (**Eq. 12)** by exploring the relative elastic modulus and volume fraction of the spherical particulate model [53]. This model considers the maximum packing fraction ($\emptyset_m$)

and can predict the permeability of a square lamellar distribution systems by setting $\emptyset_m$ to 0.785 [61]. For the specific case of dilute dispersion of ellipsoid fillers in lamellar orientation, the modified Maxwell-Wagner-Sillar equation (**Eq. 13**) can be applied with a shape factor (n) ≤ 1/3 [54]. The expression will be reduced down to Maxwell equation when n = 1/3. Based on these models proposed for the lamellar system, the P values of such morphologies would typically fall between the values of the particulate and laminar system, as observed in **Figure 2.3b**.

Laminar blends refer to a system of complete immiscible morphology between polymer blends that are separated into different layers in the direction that is perpendicular to the route of molecular diffusion. In fact, this laminar system is normally regarded as multilayer assembly.

A partially miscible blend system typically refers to the morphology of co-continuous distribution. Since a network system of co-continuous system is randomized, it is especially challenging to come up with a specific system that can accurately predict the moisture and gas permeability values based on the orientation of the dispersed matrices. Predicting the permeability of co-continuous (or lamellar) blend can be estimated by utilization a simple Geometric Mean model, which is presented in **Eq. 14** [55]. This Geometric Mean model assumes random distribution of phases, and takes the weighed geometric mean as a mean to calculate polymer permeability.

The permeability of multilayer films or coating (laminar) systems can simply be calculated through the lower bound of permeability model described by Reuss model from Rule of Mixtures (**Eq. 15**) [55]. Comparison of the permeability of ideal multilayer system to those of the blend system is illustrated in **Figure 2.3b**. It is evident that multilayer assembly would achieve effective enhanced barrier properties with less amount of high barrier polymers, indicating it is a superior approach to improve the barrier properties of renewable and sustainable materials.

2.2.2.2. Fillers and nanocomposites

With the current interest in nanotechnology, nanocomposite materials have attracted a substantial research interest for packaging films and coatings. Different modeling approaches have proved that significant improvement of barrier properties can be achieved with high aspect ratio nanoparticles [62] in polymer matrices, with the leading example being the Nielsen model as shown in **Table 2.2**. Over the years, models of permeability of nanoparticles have been proposed for three main categories of nanofillers, depending on their shape. Iso-dimensional particles, which have unity dimension in all lattice directions (e.g., silica, spherical CNC, TiO_2); elongated particles, which consist of fibrils with diameter < 100 nm but with much higher length up to hundreds or thousands nanometers (e.g., platelets CNT, CNF, collagen); and nanoplatelets

(layered) particles, which consist of flat-shaped particles with thickness ranging from 1-10nm (e.g., graphite, nanoclay, CNC) [63]. Categories of nanoparticles can be shown in **Figure 2.4a**.

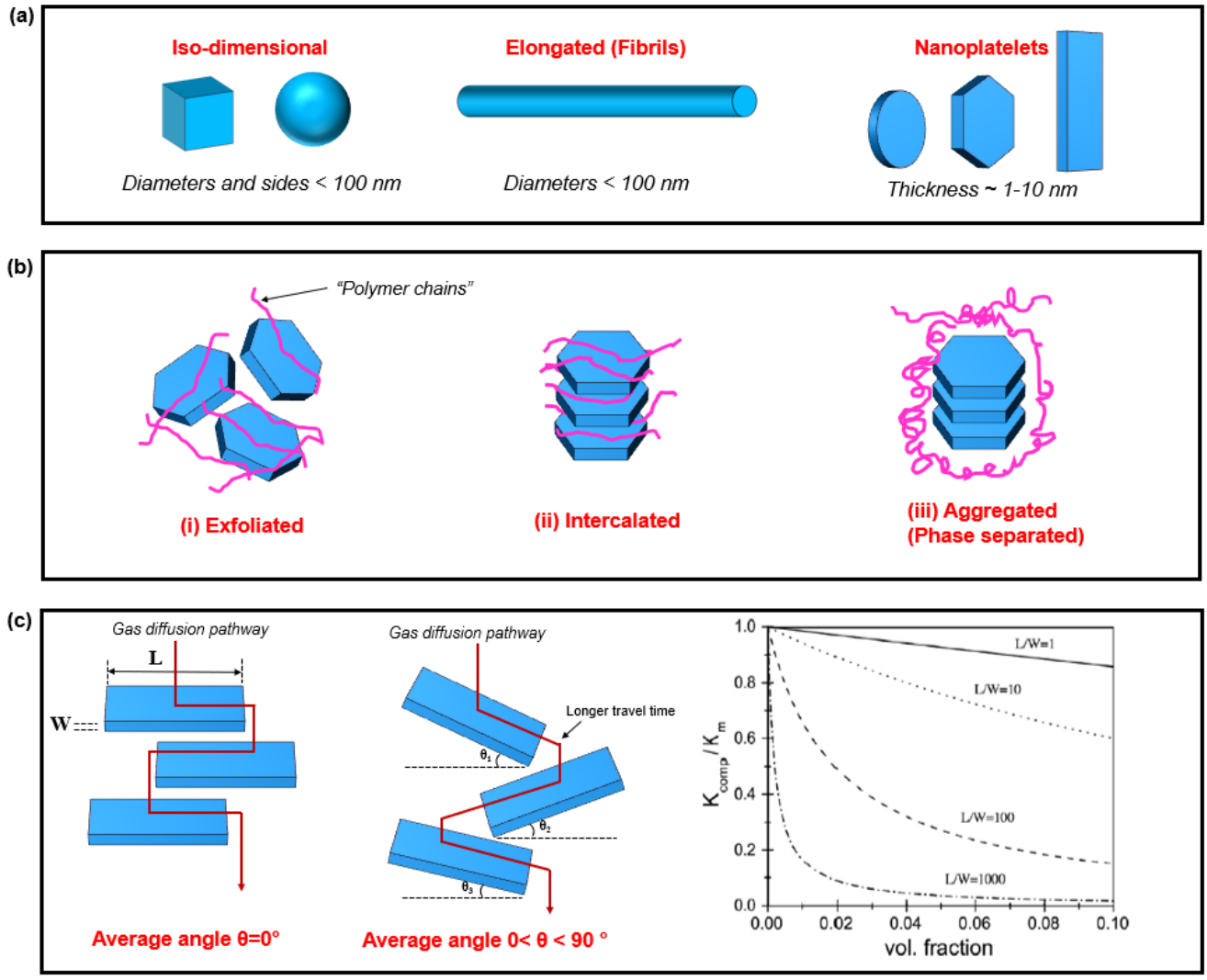

Figure 2.4. (a) Different shapes of bio-based nanoparticles. (b) Formation of exfoliation, intercalation, and aggregation of nanoplatelets in polymer matrices. (c) Schematic on the orientation influence of tortuosity on the network of layered nanoplatelets. Influence of aspect ratio on the relative permeability of nanocomposites (as shown by Nielsen's model); K_{comp}/K_m stands for relative permeability [64] (Copyright ©2009. Reproduced with permission from Elsevier)

The models presented in **Table 2.1** for blends can also be applied for the permeability's of isometric nanoparticle filled composites, namely **Eq. (9-12)** for spherical shape and Eq. (10 & 12) for cuboid shape nanoparticles. In the case of nanoparticle network dispersed uniformly in polymer

matrices, the fillers would be considered impermeable due to the high crystalline structures and high aspect ratio of nanoparticles. Thus, these aforementioned models would use the assumption that the permeability of the disperse phase (P_c) = 0.

In the case of nanotubes in polymer matrices, the second generalized Maxwell equation can be used:

$$P = P_c\left[1 + \frac{(1+G) - \emptyset_d}{\left(\frac{P_d/P_c + G}{P_d/P_c - 1}\right) - \emptyset_d}\right] \quad (16)$$

where G is the geometric factor accounting for the shape of the dispersants, which can be determined experimentally. This model was adapted by Ge et al. [65] and used for the gas permeability through the CNT-polymer matrix membrane structure.

Among all the three types of nanoparticles, nanoplatelets have shown to improve the barrier properties inside a polymer matrix considerably. Thus, there are significantly more models developed to predict the permeability of this type of nanoparticles compared to those of isodimensional and elongated particles. A review by Choudalaski and Gotsis provided an in-depth description of the models for the permeation of nanoplatelet systems in polymer, in which the formula can be generalized to other nanoplatelet systems [64]. For platelet-shaped nanoparticles, there are three main types of morphologies: exfoliated, intercalated, and aggregated (phase separated), which can be observed in **Figure 2.4b**. The equations used to describe the moisture and gas permeation through these three nanoplatelet morphologies are outlined in **Table 2.2**. These models typically assume the nanoparticles to have either parallel orientations that are

perpendicular or random orientation at average angles (θ) to the direction of diffusion, as illustrated in **Figure 2.4c**.

Table 2.2. Mathematical models of moisture/ gas permeability through nanoplatelets-type nanocomposites. (Adapted from Choudalakis and Gotsis [64], Elsevier copyright ©2009).

Array/Orientation (cross-section)	**Model**	**Equation**	**Eq #**
All	Percolation threshold [59]	$P = P_c(\emptyset_d - \emptyset_t)^t$	(17)
Intercalated	Nielsen [66]	$P = P_c\left(\frac{1-\emptyset_d}{\tau}\right);\ \tau = 1 + \frac{\propto}{2}\emptyset_d;\ \propto = \frac{L}{W}$	(18)
Intercalated	Cussler [67,68]	$P = P_c\left(1 + \frac{\propto^2 {\emptyset_d}^2}{1-\emptyset_d}\right)^{-1}$	(19)
Intercalated	Moggridge [69]	$P = P_c\left(1 + \frac{2}{27}\frac{\propto^2 {\emptyset_d}^2}{1-\emptyset_d}\right)^{-1}$	(20)
Exfoliated	Bharadwaj [70]	$P = P_c\left[\frac{1-\emptyset_d}{\tau}\right];\ \tau = 1 + \frac{\propto}{3}\left(\mu + \frac{1}{2}\right)\emptyset_d;\ \mu = \frac{1}{2}(3cos^2\theta - 1)$ μ =-1/2 for parallel orientation, μ =0 for random direction, μ =1 for perpendicular orientation	(21)
Aggregated (Phase separated)	Nazarenko [71]	$P = P_c\left(\frac{1-\emptyset_d}{1 + \frac{\propto}{2N}\emptyset_d}\right)$	(22)
Exfoliated and Aggregated (Phase separated)	Combined Bharadwaj-Nazarenko [64]	$P = P_c\left[\frac{1-\emptyset_d}{1 + \frac{\propto}{3N}\left(\mu + \frac{1}{2}\right)\emptyset_d}\right]$	(23)

Note: Pc and Pd are the permeability of the permeant in the continuous and dispersed polymer phases, respectively. $\emptyset_c$ and $\emptyset_d$ are the fractional volumes of the continuous and dispersed polymer phases, respectively. $\emptyset_t$ is the fractional volume at percolation threshold and t is the critical exponent. τ is the tortuosity and α is the aspect ratio of nanoplatelets. μ *is the orientation factor; and N is the number of layers in a layer stack.*

The first permeability model for nanocomposites was developed based on percolation theory. Thus, a simple power law can describe the relationship between the nanocomposite permeability

within the critical percolation threshold, as shown in **Eq. 17** [59]. Another simple permeability model for the parallel arrangement of rectangular platelets with thickness, W and length, L are presented in **Eq. 18** [66]. This expression is the Nielsen model, and it is one of the most basic equation to predict the permeability of polymer matrix with nanoplatelets acting as impermeable barriers to the diffusing permeant molecules. This formula accounts for both aspect ratio of nanoparticles, and the tortuosity provided by the arrangement of platelets. It should be noted that the tortuosity is correlated to the aspect ratio of nanoparticles; thus, a change in aspect ratio would directly affect the permeability through the nanocomposites. The significant effects of aspect ratio and tortuosity on the diffusion of permeants are illustrated in **Figure 2.4c**. The overall diffusion of gases through random arrays of single laminae was intensively studied by Cussler's group [69,72,73]. They extended Nielsen's model and proposed a different formula (**Eq. 19**) that connects the diffusion through the film or coating with the pore/slit distance between particles [67]. Compared to Nielsen's model, Cussler's model showed a substantial reduction in permeability at smaller nanofiller volumetric fraction due to the more restrictions it accounted [67]. In order to consider the permeability of hexagonal flake nanoparticles arranged in parallel arrays (i.e. nanostarch, silica, or ZnO), Moggridge et al. gave an extension of the Cussler model and added a specific hexagonal platelet-shape coefficient (2/27), as indicated in (**Eq. 20**) [69]. This coefficient suggested that hexagonal shape nanoparticles objectively have barrier properties reducing effect in the nanocomposite systems compared to regular rectangular shape ones.

The assumption of parallel array orientations of nanoplatelets can lead to underestimating actual moisture and gas permeability values. To account for different geometry and orientation of the dispersed nanofiller phase inside matrix coatings, Bharadwaj proposed a two-dimensional model that was another modified version of Nielsen's model [70]. This model provided more considerations for the physical orientations of the nanoplatelets fillers (μ), which can be beneficial

in predicting the permeability performance of exfoliated polymer structures. It is highly suggested that the orientation at angles will force permeants to take longer tortuous pathways to travel across the film/coating (**Figure 2.4c**); thus, reducing the overall moisture/oxygen barrier properties. Based on the developed formula, Bharadwaj concluded that the dispersion of nanoplatelet fillers at a perpendicular orientation to the direction of permeation would give the highest barrier performances, indicating that intercalated structures are more preferable than exfoliated structures in terms of obtaining enhanced barrier properties.

In many cases, the permeability of renewable and biodegradable nanocomposites can be affected by the aggregation of nanoplatelet particles due to poor compatibility between the fillers and polymer matrices. The aggregation can especially happen at high concentrations of nanoparticles and can act as a low resistance pathway for moistures and gases transport within the composites. A model proposed by Nazarenko et al. (**Eq. 22**), derived from Nielsen's permeability equation, considers the aggregated morphologies that are present in the matrix by providing the term N to represent the number of layers in the layer stack [71]. The larger the value of N is, the larger the degree of aggregation, resulting in deficient barrier performances. One limitation in Nazarenko's formula is that it assumes the stacked nanoplatelets all have a perpendicular orientation to the flux direction. To account for the random orientation of the aggregated layers, an expression (**Eq. 23**) was developed from a combination of (**Eq. 21 and Eq. 22)** [64]**.** This expression is versatile, as it can calculate permeability as a function of volume fraction, geometry, orientation, and degree of orientation.

2.3. Factors affecting water vapor and gas permeability of multi-component renewable polymer film and coating systems

Most renewable and sustainable materials are susceptible to the permeation of moisture and/or gases, however, to a very different extent, which is primarily dictated by the intrinsic nature of either the polymers or the permeants. Thus, to fabricate high barrier packaging coatings and films, many researches focus on figuring out how the attributes of the polymer materials can affect the barrier properties. It has been widely reported that the barrier performance of renewable food packaging coatings and films can be influenced by multiple factors, such as chemical structures, polymer architecture and morphologies, polymer crystallinity and orientation, as well as the combination of different systems like polymer blend/multilayer assembly or the incorporation of nanofillers and other additives. Understanding the fundamental basis and the prominent impacts of these factors on the permeability performance of biodegradable packaging materials is crucial for future development and practical purposes to high barrier sustainable packaging materials.

2.3.1. Chemical structure and polarity

One of the most significant factors that tremendously contribute to the barrier properties of sustainable polymers is the inherent chemical structures or architecture of the polymer chains and the resulting morphologies. Parameters such as polarity, free volume, intermolecular cohesion, and cross linking are important factors that determine the barrier properties of the particular polymer systems. These factors are highly dependent on each other, and one should consider all of them when selecting appropriate materials for high barrier packaging coatings and films.

As mentioned in the mathematical model, a significant aspect that contributes to the permeability through polymer coatings or films is the ability of the particular material to absorb penetrating gases or vapor. The “solubility” of is the permeant in is highly dependent on the chemical structure and polarity of the polymer and the constituting monomers. In polymer science, the study of

surface functionality/polarity and chemical interaction is extensively to understand the overall functional performances of both non-biodegradable and biodegradable polymer systems, including but not limited to the mechanical, physical, thermal, as well as moisture and gas barrier properties. The chemical interaction between the permeant fluids and polymeric chains can affect the permeability and barrier performance of packaging materials, which is especially more prevalent for moisture vapor permeability. It is widely accepted that the water barrier activities of hydrophilic polymers are significantly higher than hydrophobic polymers. Specifically, natural and bio-based polymeric materials tend to contain much more polar functional groups than traditional petroleum-based polymers that subsequently make these polymers much more susceptible to moisture attack via polar-polar interaction and hydrogen bonding. Thus, surface tailoring and modification are typically implemented as a stratagem to either (i) improve and optimize the properties of existing polymers, or (ii) introduce desirable functional attributes to the polymer. Representative examples are polysaccharide-based materials, such as TPS or cellulose are the prime subjects of surface modification to improve the barrier properties. This is attributed to the abundant hydrophilic -OH group present on the polymer backbone, allowing easy moisture association via hydrogen bonding. On the other hand, these hydrophilic polysaccharide-based materials provide an excellent barrier against nonpolar O_2. A multitude of researches have been conducted to partially substitute the –OH functional groups of cellulose with more hydrophobic functional groups to improve the moisture barrier properties, with various degrees of success[74–76].

Most chemical modification of packaging coatings and films involves tailoring and controlling the polymer structure on the surface, which does not change the fundamental backbone and can keep most of their physicochemical and biochemical properties. Mashkour et al. synthesized biodegradable acetylated nanofibrillated cellulose (ANFC) using acetic anhydride that can be used

as coatings for paper packaging applications [77]. The authors observed that the air resistance of the ANFC coatings has drastically increased by about 1090% (6.4 times) compared to the unmodified paper coatings, indicating a significant improvement in terms of gas barrier properties. Another study carried out by Trinh et al. observed that surface grafting of maleic anhydride slightly reduced the water vapor permeability (WVP) values of TPS by about 12% [74]. However, the surface modification did not intend to reduce the WVP of TPS directly but rather to improve the barrier properties by promoting the TPS's interaction with hydrophobic PLA in a multilayer assembly. Due to the limitation in the reaction sites of surface grafting, it should be expected that barrier properties can only be marginally enhanced, though not as much of an improvement as other methods such as blending, multilayer construction, or composites. On another note, it must also be acknowledged that changing the chemical structures of biodegradable polymer backbones or monomers could potentially eliminate the desirable biodegradability traits of renewable coatings and films [78]. As suggested by Witt et al., the biodegradability of materials depend on the chemical structure rather than the feedstock [79].

2.3.2. Polymer structure/architecture and morphological factors

The permeability of polymer coatings and films can also be affected by the "diffusivity" element. Another physical and morphology factor that affects the diffusivity properties of renewable coatings and films is the polymer free volumes and intermolecular cohesion. Free volume in any polymeric material is defined as the internal space available inside the polymer that would allow polymer chains mobility. This available space within polymer matrices can act as open "pathways", which ultimately allows diffusive activities of penetrants across polymeric films and coatings[80]. Free volume in polymer stems mainly from the addition of plasticizers. Plasticizers are commonly incorporated in bioplastics (e.g., glycerol and other polyols in thermoplastic starch and protein) to increase the free volume among polymer chains and ease processability, which

subsequently improves the elasticity and flexibility of the final packaging coatings and films. However, plasticizers reduce the glass transition temperature (T_g) and worsen permeability as a tradeoff.

It is also noted that the intermolecular cohesion of polymer chains directly affects the barrier performance of polymer matrices. Typically, high intermolecular cohesion energy between polymer chains improves the barrier transport against moisture and gases penetrants. This is because higher intermolecular cohesion energy decreases the free volume within polymer by restricting polymer chain mobility and consequently reduces the voids and diffusive mobility of permeant gases or vapor [81]. A recent study by Corres et al. elucidated the role of free volume in the barrier properties of films using PCL with Poly(hydroxy ether of Bisphenol A) (PH) models. The study provided good insight on the topic, which can be extended to other renewable polymer systems[82]. In the study, both the water vapor transmission rate (WVTR) and oxygen permeability (OP) values of PCL significantly reduced; in other words, enhanced the barrier properties with the increase in the PH concentration. This was attributed to the reduction in the free volume sizes contributed by PH (**Figure 2.5**). Though the free volume size and barrier properties seem to be directly correlated, the authors also suggest that the chemical compatibility between PCL and PH also plays a strong part in reducing the overall permeability.

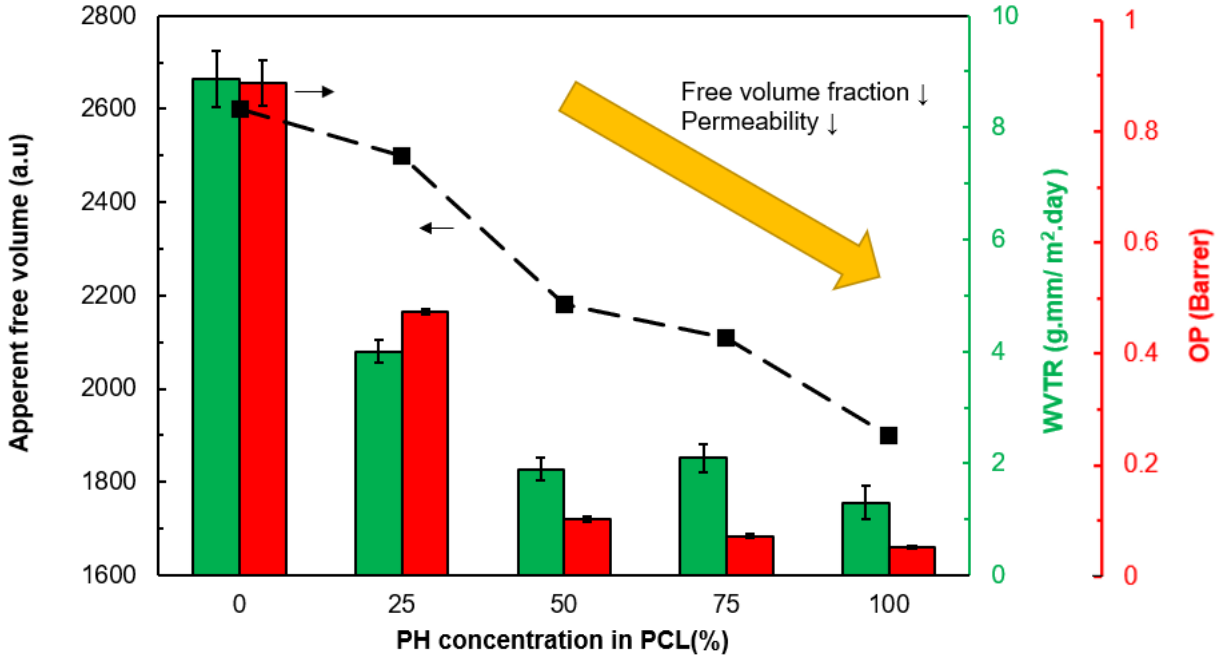

Figure 2.5. Reduction in WVTR and OP of PCL/PH blends as free volume decreased with the higher loading of PH in the matrices [82] (Copyright ©2020. Adapted with permission from Elsevier)

The barrier performance of polymers can also be improved via chemical crosslinking that involve the covalent linking of two or more molecular chains using a crosslinking agent. Crosslinking is an appealing technique that can limit the mobility of polymer chains and decrease the free volume within the polymer structures, which can lead to the reduction in oxygen uptake and water activities of biomass-derived polymers, such as polysaccharides or proteins [83]. However, crosslinking is especially favorable for protein-based plastics, such as gelatin because protein-based materials have abundant primary functional groups, such as amines, carboxyl, hydroxyl, and sulfhydryl that are amenable to form covalent. Most studies showed that higher crosslinking degree can result in improved moisture and oxygen resistant with structural flexibility tradeoff[84,85]. Muñoz et al. mentioned that the use of aldehyde crosslinking agents such as formaldehyde, glutaraldehyde, and glyoxal all reduce the WVP values by up to 30% after crosslinking treatments, although the WVP are still poor in comparison to synthetic plastics used in packaging applications [86]. A recent

study by Gao et al. showed that the crosslinking of zein protein films with glutaraldehyde can produce packaging materials that have superior oxygen barrier properties that can even compete with commercial PE and PP [87]. However, crosslinking does not always improve the barrier properties of biodegradable polymer coatings or films. Depending on the crosslinking agent, crosslinking can have detrimental effect on the moisture and gas barrier properties of the materials in some cases. Uranga and Leceta reported an increase in the WVP values of their fish gelatin crosslinking with citric acid, which was attributed to the unreacted hydrophilic citric acid –COOH remaining inside the structure of the films and absorbing more moisture [88]. The correlations between crosslinking and moisture and oxygen barrier properties are often unpredictable in practice; and thus, investigations through experimental designs are required to confirm such relationships.

2.3.3. Polymer crystallinity and molecular orientation

For the last few decades, polymer crystallinity and molecular orientation have been observed to play a major role in controlling the barrier properties of renewable polymers. Overall, the crystalline phase of polymers is considered impermeable due to the chain immobilization effect, and the barrier properties are primarily dictated by the amorphous phase. In addition, the lamellar crystals of semi-crystalline polymers reduce the amorphous phase chain mobility that further reduces the diffusion rate of permeants. Previous investigations on synthetic plastics have confirmed the validity of the relationship between the degree of crystallinity and barrier properties. Yuniarto et al. developed a solvent casted PLA film with PEG additives, in which the PEG was incorporated to accelerate the crystal formation in the PLA film matrix [89]. The authors reported a maximum increase (20%) in the oxygen barrier properties with an increase in the degree of crystallinity from 17.71% in the neat PLA to 34.64% in the PLA-PEG films. Some sustainable thermoplastic polyesters, such as PLA, PHA, PGA, and PBS generally possess higher degree of

crystallinity and as such lower free volume compared to natural macromolecule derived polymers, such as polysaccharide-based, lipid-based, and protein-based materials [90].

Several studies have also pointed out that the barrier properties of semi-crystalline polymers can be improved through a stress-induced crystallization and orientation in the remaining amorphous phase. The orientation of crystalline structure is dependent on the strain imposed during the processing of polymer. Spherulitic morphologies are formed under low level of strain, while "shish kebab" structure is generated under high level of strain (**Figure 2.6a**) [80]. Typically, the "shish kebab" morphologies would result in increase in permeability, in comparison to spherulitic structures, due to the increase in crystallites tortuous arrangement. Bai et al. [91] have proposed a mechanism (**Figure 2.6b**) to overcome the obstacle presented in the "shish kebab" morphologies of PLA. In this study, the authors designed an impermeable building block boundaries by interlocking the spherulites with each other by utilizing N,N′,N″-tricyclohexyl-1,3,5-benzene-tricarboxylamide (TMC-328) nucleating agents. The resulting interlocked "shish kebab" structure showed a remarkable oxygen permeability reduction by up to 500 times in comparison to the control PLA, as displayed in **Figure 2.6 (c)**. This is a simple yet robust strategy that has the potential to be applied to other semi-crystalline biopolymers such as PBS, PHA, and PCL.

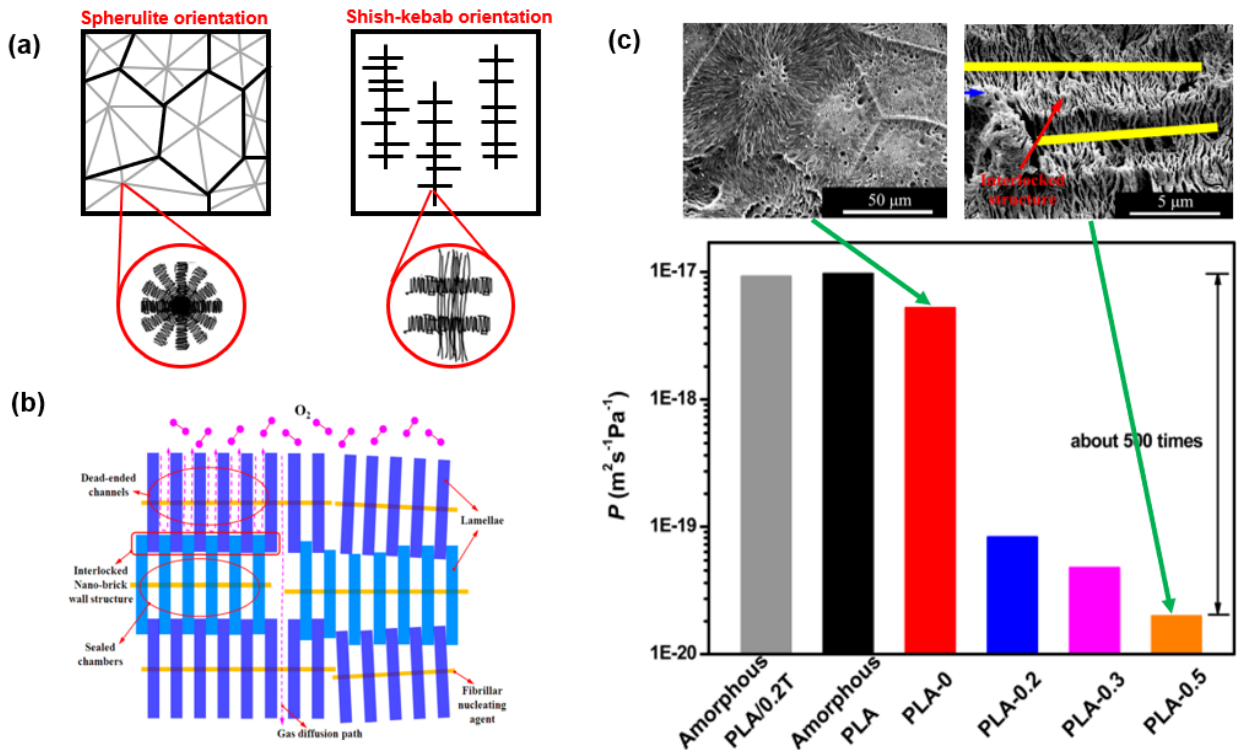

Figure 2.6. (a) Different crystalline structure in semicrystalline polymers. (b) Mechanism of the interlocked parallel "shish kebab" structure that inhibit oxygen permeation and (c) The improved oxygen barrier of PLA with the parallel "shish-kebab" structure [91](Copyright ©2014. Reproduced with permission from American Chemical Society).

Overall, obtaining oriented morphologies to achieve high crystallinity in biodegradable and sustainable polymers is still a major challenge , especially for polymers with rich-crystalline phases like PLA or PGA. Maintaining maximum crystalline structure in industrial-scale processes like extrusion, compression molding, or injection molding require either longer annealing time or specialized and optimized processing conditions. In order to maximize moisture and gas barrier properties of renewable packaging coatings and films, future studies should focus on structure-properties relationship and establish the optimum fabrication process to maintain the highest degree of crystalline structures within the material.

2.3.4. Renewable polymer blends

Polymer blending is one of the most utilized technique in the industry as it is a straightforward, cost-effective, and scalable strategy to improve the physical, mechanical, and barrier properties of many biodegradable and renewable polymers. Nevertheless, most polymer blends suffer from lack of interfacial compatibility and viscosity variation that result in separated morphologies and hence inferior barrier performances. As mentioned previously in **Section 2.2.2.1**, most renewable and biodegradable blends are immiscible or partially miscible blends that can form particulate (droplets), lamellar (fibrillar), or co-continuous phases (**Figure 2.3a**). One common problem with biodegradable polymer blends is that it is usually a challenge to generate blend coatings and films that are balanced in both barrier and mechanical properties, as such materials also suffer from lack of appropriate mechanical properties. Different strategies, with various degree of success, have been employed to improve the interaction between sustainable polymer blends in an effort to simultaneous enhance the mechanical and barrier properties. Compatibilization strategies, such as bridging using chain extension, graft co-polymer, block-copolymer, and maleic anhydride grafted polymer are shown to improve the barrier properties of blends [12].

Another type of renewable polymer blends that are commonly applied in the food packaging industries is the emulsion-based blend. Emulsion-based blend coatings and films can be found as protective layers that can prolong the shelf-life of both fresh and processed food products such as fruits and vegetables, cheeses, meat, and bakery products. These emulsion-based coating typically contain lipid-based materials, which can provide enhanced barrier performance compared to edible coatings made from one component, including polysaccharide-based [92] or protein-based [93] coatings. Lipid-based materials that originate from bio-resources such as waxes, fatty acids, and vegetable oils are utilized as blends for edible fruits coatings and films because they provide extra resistance to moisture due to the non-polar nature of such materials [3,94]. Since the lipid phase

needs to be stabilized in the aqueous phase of the edible coating and film formulations, emulsification process by employing emulsion stabilizing agents, is essential. Recent researches on emulsion coatings and films have investigated a wide variety of food-grade emulsifying agent that can stabilize the emulsion and increase the lipid particles distribution. The use of either classical emulsion stabilizers like lecithin, polysorbates, mono and di-glyceride ester [95] and Pickering emulsion stabilizer such as surface modified starch, chitosan, hydroxyapatite, and nanocellulose [96] displayed appealing results. However, there are still some concerns in terms of the longevity of stability and safety of these materials that needs to be addressed before commercial deployment. The concern is especially true for nanomaterial Pickering emulsifiers as their safety is not widely established.

2.3.5. Multilayer assembly

Another scalable technology that is commonly used in food packaging application is multilayer assembly. Compared to polymer blends, multi-layer assembly has the potential to achieve much higher moisture and/or oxygen barrier properties in food packaging [97]. The various layers of polymer stacking on each other in multi-layer coatings and films resembles the laminar structure in polymer blending, which would theoretically provide the most optimal moisture and oxygen gas barrier, as previously mentioned in **Section 2.2.2.2. (Figure 2.3b)**. Due to the superior structures they constitute and barrier properties they offer, multilayer assembly films are extensively utilized in various packaging applications, such as beverage, food, cosmetics, pharmaceutical, and electronics. Multilayer assembled films, sheets and films dominate the food packaging industry by constituting about 73.5 % of the total amount **(Figure 2.7)** of packaging used[98,99]. However, the performance of the multilayer coatings and films is also highly dependent on the adhesive strength and chemical interaction between each level of layers. Similar to polymer blends, the bio-originated and biodegradable polymer used in multilayer assembly must have a certain degree of

compatibility, which can either be achieved through selection of materials or by using compatibilization techniques.

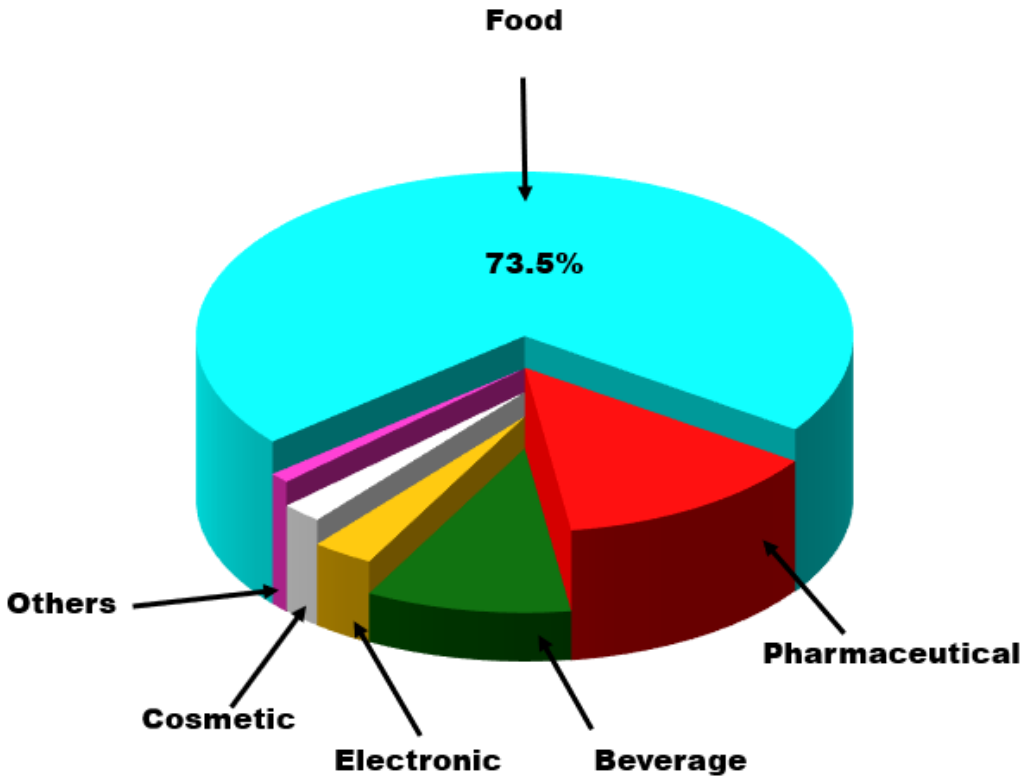

Figure 2.7. A graphical breakdown of multilayer technology coatings and films by industrial applications in 2019. [98,99]

Conventional multilayer films typically use two to five different polymers that can be fabricated into multilayer assembly of two to eleven layers arrangement, and can further be increased up to thousands of layers with microscale thickness by micro co-extrusion process [100,101]. Common methods to manufacture biodegradable multilayers coatings and films include either dry process such as co-extrusion/ lamination/compression molding or wet process such as solvent-coating/ aqueous dispersion/ vacuum coating [97].

Standard multilayer films typically comprise of many types of layer: outer, adhesion (tie), barrier and inner seal layer, as shown in **Figure 2.8**. For enhanced barrier packaging application, the most

two important layers are the adhesion and the barrier layers. The adhesion layers are incorporated to allow different barrier layers to adhere and interact with each other within the multi-phase polymer system, as well as to prevent delamination [102]. For renewable materials, the interactions between polymers are mostly poor due to the chemical incompatibility and immiscible coupling chain diffusion. Thus, the adhesion layers are made up of modified polymers with enhanced interfacial affinity with barrier layers. Examples of modifications on the adhesion layer includes: grafted co-polymers [103], maleic anhydride (MA) grafted polymers [74,104], and reactive surface blends [105]. On the other hand, barrier layer is the protective layer that provide the improved permeability properties in the packaging material. Some candidates for biodegradable polymer that can act as barrier components for multilayer assembly are PVOH, PGA, PHB and TPS for oxygen barrier properties [62] and PGA, PLA, and hydrophobic protein biopolymers (zein, gelatin, gluten) for moisture barrier properties [38]. One of the most appealing polymer used for multilayer coatings and films is PVOH, which can act as an additional supportive layers that provide excellent oxygen barrier properties in structures like tri-layer PHA/PVOH/PHA [104], tri-layer LDPE/PVOH-TPS blend/LDPE [106], bilayer silk fibroin/PVOH [9], and bilayer PVOH/CNC films [107]. To further enhance the moisture and oxygen barrier properties, the addition of micro and nanofillers into the barrier layers such as nanoclay, nanocellulose, graphene, and metal oxide can also be employed [107–109].

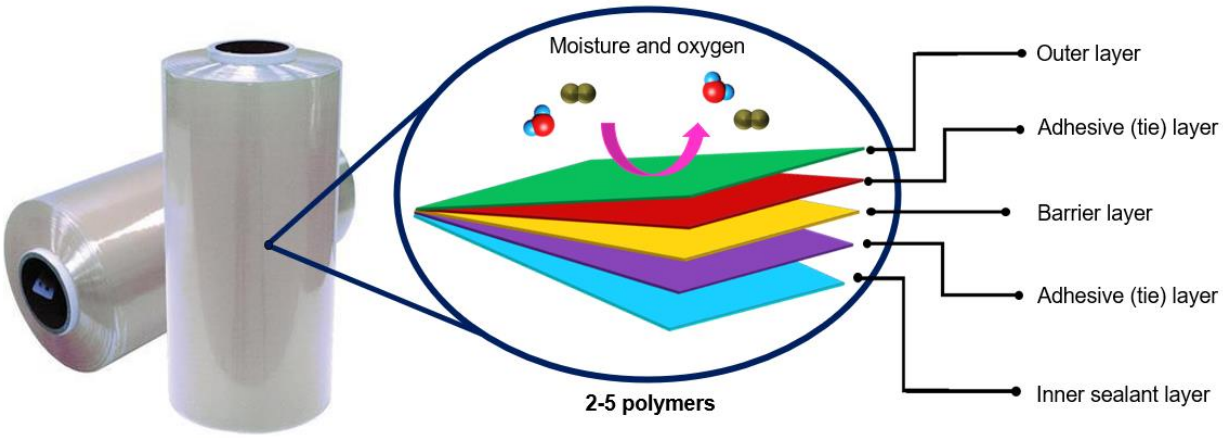

Figure 2.8. Layer-by-layer arrangement of a standard multilayer film system.

Overall, the technology of multilayer coatings and films can be applied to vastly upgrade the overall barrier properties of bio-based and biodegradable materials by providing extra barrier layers tailored to moisture/oxygen permeability. However, one crucial problem that these industrial multilayer coatings and films need to address is that all components and layers in the assembly, including the adhesive layer need to satisfy the sustainability requirement to ensure that the whole structure provides the desired environmental attribute. Thus, more researches on the bio-compatibility and variation of existing polymer multilayer combination should be carried out to help fabricating high barrier coatings and films while maintaining the biodegradability and recycling capacities of the plastics.

2.3.6. Nanocomposites and other additives

Incorporation of nanofillers and additives into packaging coatings and film can tremendously enhance the overall barrier performance, by filling the free volume and thus reducing the porosity as well as by providing tortuous pathway for the diffusion of permeants. In the last few decades, the use of nanoparticles and nanocomposites as novel materials has been extensively studied, and many researches have demonstrated successful attempts of improving the barrier properties of

polymer matrices with the incorporation of minimal amount (<10 wt.%) of these nano-sized fillers [71,110,111].

The selection of impermeable nanoparticles to moisture, oxygen, and other gases is crucial to inhibit the diffusion path of such permeants in the polymer matrices. Moreover, obtaining high barrier performance often requires the nanofillers to have a uniform and homogenous dispersion inside the composite systems. It is not rare to see nanoparticles to aggregate and agglomerate due to thermodynamic reasons and poor chemical incompatibility with the polymer matrices, which can ultimately cause detrimental effects to the polymer such as brittleness, weakened mechanical properties, reduced transparency, as well as diminished barrier performances [42]. However, these problems can be mitigated by employing appropriate chemical modifications of the fillers or the polymers, using surfactants and/or compatibilizers, or by exploiting advanced processing techniques, such as the use of ball milling, high shear mixing, and ultrasonic treatment [112,113]. Exemplary nanofillers and their effect on the barrier properties is summarized in Figure 2.9 and discussions are provided in the subsequent sections.

2.3.6.1. Nanoclay-based nanocomposites

Nanoclays are appealing nanomaterials because they are nature-derived, abundant, low cost, safe, etc [114,115]. One of the most widely used nanoclays for food packaging and coatings application is montomorillonite (MMT) layered silica platelets with particle thickness of 1-2 nm and a high surface area of more than 700 m^2/g [115]. Due to this high surface area and aspect ratio, host polymer matrices can achieve high barrier properties with a low loading percentage of the dispersed nanoclay particles. It is widely reported that MMT can easily be dispersed in either exfoliated or intercalated structure in hydrophilic polymers, such as polysaccharide-based or protein-based films using typical solvent or thermomechanical polymer processing techniques. On the other hand, MMT is not suitable as a barrier nanomaterials for hydrophobic polymers,

including several hydrophobic polyesters as it forms aggregates and agglomerates due to low compatibility. For MMT to be utilized in biodegradable polyesters, such as PLA, PHBV, PBS, PBAT, and PCL, the hydrophilic silicate surface must be modified into organophilic OMMT to reduce the surface energy and improve its interaction with these hydrophobic polymers [114]. It is worth mentioning that the barrier properties nano-clay offers can be highly dependent on the nature of the host polymer and can be overshadowed by the barrier properties of the polymer matrices. Research by Crétois et al. [116] shed light on this topic by studying the influence of OMMT in the PHBV/OMMT nanocomposite in terms of mechanical and barrier properties. The results showed that the moisture permeability of the PHBV/OMMT nanocomposites was not affected by the nanoclay content in the matrices, even at high concentration loading (>10 wt.%). The authors suggested that the high crystallinity contributed by PHBV already have higher barrier properties than the nanoclay, which makes it redundant to add nanoclay as a moisture barrier material.

2.3.5.2. Cellulose-based nanocomposites

Cellulose-based nanoparticles (CNC, CNF, BNC) are appealing bio-resourced nanofillers that can contribute to high barrier properties when incorporated into the proper polymer coatings and films. This is attributed to the little to no amorphous region in these nanocellulose structures that leave behind predominantly crystalline regions [117]. Moreover, the high aspect ratio of nanocellulose, the abundancy and safe-for-consumption quality makes them very attractive for barrier materials in food packaging application. In the last few decades, research on nanocellulose use in nanocomposite materials for packaging coatings and films has been extensively explored and steadily increasing [118]. Chemical modification and surface grafting by utilizing the –OH group is a widely employed strategy that aims to the polarity of nanocellulose and enhances its compatibility with hydrophobic polymer matrices. Moreover, surface-modified nanocelluloses can also act as stabilizing agents for emulsions, which makes modified nanocellulose suitable for

edible emulsion coating applications. Surface modification chemistries of nanocellulose reported for food coatings and film applications include, but not limited to succinylation [119,120], phosphorylation [121], oxidation [122], and enzymatic esterification [123].

2.3.5.3. Other nanocomposite fillers

Researches on other nanomaterials for renewable coatings and film composite applications that provide barrier property improvement includes lignin [124,125], silica [126], calcium carbonate ($CaCO_3$)[127], and metal zinc oxide (ZnO) [128,129]. However, barrier property enhancement is not as straightforward as mechanical and thermal strength, and there are usually some drawbacks to the nanocomposites associated with it. Batra et al. [126] reported the inclusion of silica nanoparticles in their gelatin/chitosan/and silica bio-nanocomposite films. The results of the study showed a WVP reduction by 80% with the incorporation of 10 wt.% silica nanoparticles [126]. However, the authors also reported the incorporation of silica nanoparticles increased the moisture absorption and entrapped water vapor inside the gelatin channels, likely because of the blockage caused by the nanoparticles. Sun et al. investigated the mechanical properties and moisture barrier permeability of corn starch/$CaCO_3$, and found that the nanocomposites' WVP of has significantly reduced by up to 70% with $CaCO_3$ loading of 0.06 wt.% [127]. Nevertheless, the surface morphology of the nanocomposite films displayed deep cracks with the increase in the $CaCO_3$ nanoparticles loading, which made the surface structures more fragile. In terms of oxygen permeability, Nafchi et al. successfully enhanced the gas barrier properties of both gelatin and sago starch active packaging films by incorporating nanorod ZnO at 2 wt.% concentration[130]. However, ZnO nanoparticles can pose environmental hazards to aquatic life as they cannot be easily assimilated in the ecosystem, raising some concern about biodegradability such renewable nanocomposite films.

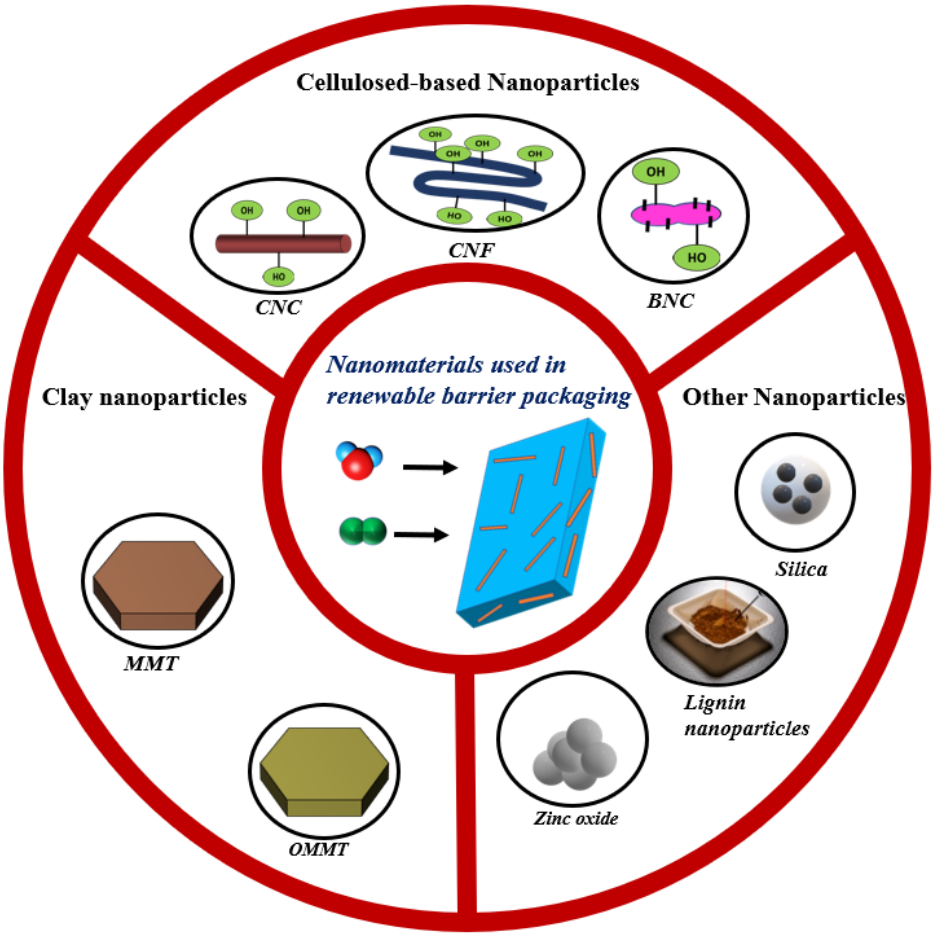

Figure 2.9: Different types of nanoparticles used in renewable packaging coatings and films

CHAPTER 3: FACILE FABRICATION OF THERMOPLASTIC STARCH/POLY (LACTIC ACID) MULTILAYER FILMS WITH SUPERIOR GAS AND MOISTURE BARRIER PROPERTIES

3.1. Introduction

Thermoplastics are commonly used in a wide variety of commercial applications such as automotive, cosmetic, packaging, construction, paper, pharmaceutical, and coating industries [2,131]. Among those applications, the main contributor for widespread usage of thermoplastic is the food packaging industry [97]. Petroleum-based plastics, such as polyethylene (PE), polypropylene (PP), and polyamide (PA), are the most commonly used plastics in the food packaging industry due to their flexibility, strength and good barrier properties [6,97,132]. Despite having superior mechanical and barrier properties for food packaging, these thermoplastic materials are non-biodegradable and poses a major environmental threat. Generation of greenhouse gases during the production process along with the pollution of land and water associated with their disposal are two of the many environmental concerns that comes with the usage of synthetic plastics [8,133]. Thus, the design of a new film packaging material with compostability or biodegradability options, suitable to replace synthetic polymers, is necessary to mitigate concerns associated with plastic pollution.

Starch is one of the most attractive and promising natural material that has potential for use in food packaging industries due to its biodegradability, renewability, abundancy, and low-cost [134]. Thermoplastic starch (TPS) can be produced from native starch by using plasticizers, mainly low molecular weight compounds such as glycerol and water [84], and thermomechanical process. TPS, similar to other polysaccharides, exhibits excellent oxygen barrier properties making it attractive for packaging materials [107]. However, it can be extremely water sensitive, possess poor moisture barrier capacity, and have relatively low tensile strength. An excellent strategy to overcome these drawbacks is to combine TPS with other polymers and conjoin them into a

multilayer film system. Previous studies have investigated the combinations of TPS with other thermoplastic materials such as low-density polyethylene (LDPE) [103], polycaprolactone (PCL) [18], polylactic acid (PLA) [135–137], and polyhydroxyalkanoate (PHA) [10], with varying degrees of success. Among these materials, PLA has proved itself to be one of, if not, the best candidate to complement the weaknesses of TPS due to its excellent water barrier properties, relatively good strength and modulus, biodegradability, and thermal stability [138].

Poly(lactic acid) (PLA) is a promising biodegradable thermoplastic polymer for food packaging applications due to its ease of processing, good mechanical properties and biodegradability, which makes it especially appealing [139,140]. Nevertheless, PLA has some major limitations such as poor oxygen barrier properties, brittleness, and high cost, which restricts its widespread use in the food packaging industry. The combination of TPS and PLA can potentially complement and overcome the weaknesses the two polymers possess, thereby, creating a multilayer film that has excellent oxygen and moisture barrier properties, high mechanical strength, and optimized cost structure. However, one particular problem with using PLA directly together with TPS stems from the fact that the two materials are inherently incompatible due to polarity difference among several other factors. While starch is highly polar, PLA is non-polar and displays better compatibility with other hydrophobic polymers [103]. Thus, compatibilization techniques need to be adapted to improve the molecular interaction. Maleic anhydride (MA) is a highly reactive compatibilizer that has been extensively studied for the modification of several polymers including starch [141–143]. The grafting of MA on starch can be conducted via a reactive extrusion process that avoids the use of toxic solvents and downstream process. The maleated starch is expected to demonstrate better interfacial adhesion with hydrophobic polymers. Moreover, MA is approved as a food-grade additive due to low its low toxicity, making it appealing for food packaging and containment applications [144,145].

In order to further improve the mechanical properties and barrier capacity, the use of a nanofiller in TPS was implemented for this study. Hydrophilic montmorillonite nanoclays was selected due to its compatibility with TPS, sustainability, and excellent strength enhancement properties [146]. The reinforcing effect of nanoclays, similar to other nanomaterials, is dependent on the level of dispersion in the starch. A scalable, and continuous process, such as extrusion can be employed to exfoliate and disperse the clay platelets in the TPS matrix[147]. The addition of nanoclays is expected to improve the structural integrity of TPS, as well as to reduce oxygen and water permeability through the films.

The main objective of this research was to investigate the development of a starch-based packaging material that displays enhanced mechanical and barrier properties, while maintaining its environmental attributes, as a drop-in replacement of the typical polyolefin-based food packaging materials. The fabrication of the film entails the modification of TPS, incorporation of PLA layers, in conjuncture with the incorporation of nanoclays. The modification of TPS and fabrication of the multilayer film utilized reactive extrusion process as it is cost effective, scalable, and a solvent free and green process. This research also aimed to optimize and down-gauge the nanoclays-filled TPS/PLA multilayer films while enhancing the film mechanical and barrier properties as compared to the neat TPS films.

3.2. Materials and Methods

3.2.1 Materials

Corn starch containing approximately 73% amylopectin and 27% amylose was supplied by Sigma Aldrich, USA. Glycerol (99%) obtained from Thermo Fisher Scientific was used as the plasticizer reagent. Polylactide (PLA) resins in pellet form (Ingeo™ biopolymer 4043D general grade) was obtained from NatureWorks LLC, Minnetonka, MN, USA. Hydrophilic bentonite

(montmorillonite) nanoclays ($H_2Al_2O_6Si$), maleic anhydride (MA), potassium bromide (KBr) in powder form, sodium hydroxide (NaOH) pellets, 12 M hydrochloric acid (HCl), dimethyl sulfoxide (99.0%), deuterated dimethyl sulfoxide (DMSO-d6), phenolphthalein, chloroform (99.8%), acetone (99.9%), and ethanol (99.0%) were all purchased from Sigma Aldrich, USA.

3.2.2. Methods

3.2.2.1. Preparation of TPS and MTPS material

Regular corn starch and MA were dried at 70 ^oC overnight to obtain a moisture level of below 1%. MA was dissolved in acetone (10 w/v %) mixed with dried corn starch at various levels. Formulations for the varying amounts of MA are presented in **Table 3.1**. The corn starch - MA was further dried in a vacuum oven to remove the acetone. Glycerol at 30% w/w concentration with respect to the corn starch mass was added, mixed evenly, and left inside a sealed container for 24 h before processing it with a reactive extrusion process.

Table 3.1. Formulations of TPS and MTPS and their nanocomposite films

Formulation with nanoclays			
Sample	Composition (phr)		
	Starch	Maleic Anhydride	Nanoclays
TPS	100	-	-
TPS-1C	100	-	1
TPS-3C	100	-	3
TPS-5C	100	-	5
MTPS	100	2.5	-
MTPS-1C	100	2.5	1
MTPS-3C	100	2.5	3
MTPS-5C	100	2.5	5

3.2.2.2. Maleation of TPS

The preparation of maleic anhydride grafted thermoplastic starch (MTPS) for characterization was carried out in an internal batch mixer (HAAKE PolyLab QC System, Thermo Fisher Scientific)

equipped with Banbury rotors at a temperature and rotor speed of 120°C and 100 rpm, respectively. The MA concentrations used for the characterization of the maleation process were 1, 2.5, and 5 phr. The mixed corn starch, glycerol, and MA materials were charged into the batch mixer and allowed for plasticization to occur for 10 min. The resulting MTPS produced was then collected and suspended in acetone at room temperature followed by centrifugation, and this cycle is repeated four times to solubilize and remove excess MA before characterization. The possible mechanism for the maleation of TPS is presented in **Figure 3.1**.

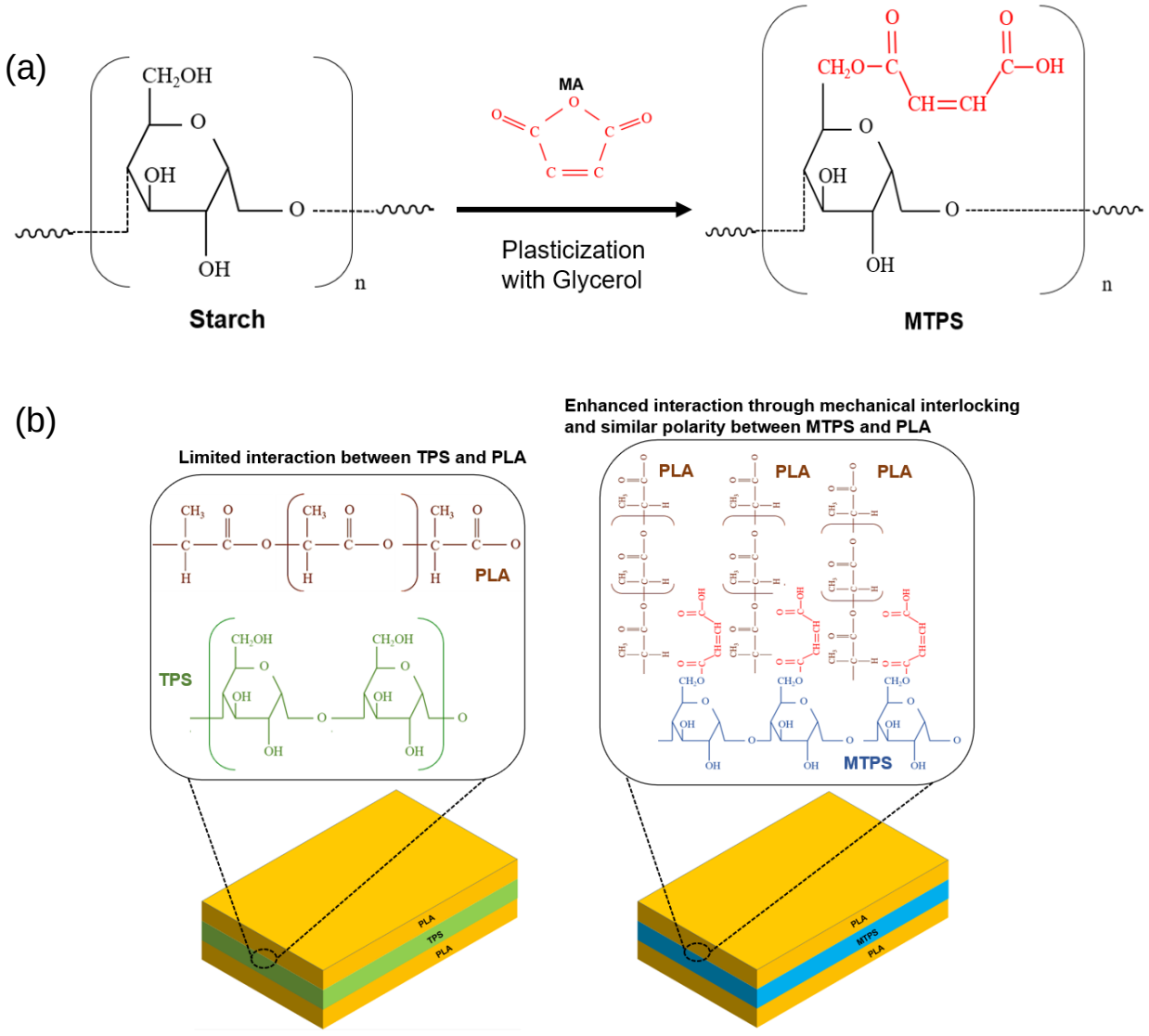

Figure 3.1. Chemical illustration for (a) the maleation of starch units to produce maleated thermoplastic starch (MTPS) and (b) enhanced interaction in the multilayer film

3.2.2.3. Characterization of the maleation reactions

Proton nuclear magnetic resonance (H-NMR)

Proton nuclear magnetic resonance (H-NMR) spectra of the baseline starch, TPS, MTPS were recorded to analyze the chemical changes as a result of the reactive extrusion based maleation process. For this, the samples were dissolved in deuterated dimethyl sulfoxide (DMSO-d6) and sealed in 5 mm NMR analysis tubes with a ratio of 10 mg solid sample to 0.7 mL of solvent. The H-NMR spectra were collected within the range of 1 to 7 ppm using Bruker 500 MHz high-resolution NMR (Bruker-SpectroSpin 500 MHz Ultra shield, Bruker Corporation, MA).

Fourier transform infrared spectroscopy (FTIR)

The IR spectra of starch, TPS and MTPS were recorded at ambient temperature using a Fourier transform infrared spectrometer (FTIR, model Nicolett 6700, Thermo Scientific). Pure starch samples for the IR were prepared by mixing the powder with KBr pellets (5 mg sample and 200 mg KBr) pressing it into pellets at 10,000 psi for 2 min. On the other hand, TPS and MTPS bioplastic samples were prepared by solubilizing the pellets in DMSO (at 90 ^{o}C) and casting on potassium bromide (KBr) salt pellets. The pellets were then dried in a vacuum oven to evaporate all of the DMSO solvent. FTIR scans, in transmittance mode, were recorded in the range of 4000 to 500 cm^{-1} under the same conditions as the background.

Titration test

The percentage of MA grafted onto the MTPS was determined using a titration method adopted from Alissandratos et al. [24]. For this, 1 g of blank TPS or MTPS (acetone washed and dried) was dissolved in a solution containing 10 mL of 75% ethanol in DI water and 10 mL of 0.5 M NaOH solution. The solution was heated to 90 ^{o}C and stirred for 45 min on a magnetic stir plate. The excess alkali was back-titrated to a phenolphthalein endpoint with a 0.5 M HCl. The percent

grafted MA on starch and the degree of substitution of –OH moieties on starch were then calculated according to equations (1) and (2):

$$\text{Grafted \%MA} = \frac{C_{HCl} \times 98.1 \times (V_0 - V_1)}{2 \times W_{sample} \times 1000} \quad (1)$$

$$DS_{Titration} = \frac{162 \times \text{Grafted \%MA}}{98.1 \times (100 - \text{Grafted \%MA})} \quad (2)$$

where C_{HCl} is the concentration in molarity of the HCl solution; V_0 and V_1 are the volume (mL) of the HCl solution required for the back titration of blank TPS and MTPS, respectively; W_{sample} is the weight (g) of dried TPS or MTPS sample.

3.2.2.4. Extrusion of TPS and MTPS

After selecting the optimal degree of maleation of TPS, hydrophilic montmorillonite nanoclays that demonstrate good dispersion in TPS was incorporated into the formulation. The formulations investigated in this study are listed in **Table 3.1**. For formulations that contain nanoclay, the nanoclay at the desired concentrations was first mixed with glycerol and mixed at a very high speed (25,000 rpm) using a rotor stator homogenizer (Homogenizer, PowerGen 700) to produce a stable dispersion. The calculated clay - glycerol was then blended with corn starch using a KitchenAid blender and equilibrated in an air sealed container for at least 24h. The blend was then manually fed into a twin-screw extruder (Process 11 Parallel Twin-Screw Extruder, Thermo Fisher Scientific) with a barrel diameter of 11 mm and L/D ratio of 40. The temperature profile used for extrusion was 110/115/115/120/120/120/125/125^{o}C from the feed throat to the exit die, and the screw speed was set at 150 rpm. The extruded samples were air chilled, pelletized and stored in an airtight container.

3.2.2.5. Fabrication of monolayer and multilayer films

To fabricate the monolayer films, the pellets were first dried in an oven (70 ^{o}C for 24 h) to remove residual moisture. A measured quantity of the dried compositions was then melt-pressed into thin bioplastic films via compression molding (Carver press, IN, USA) using a 0.2 mm mold spacer for 5 min at a temperature and pressure of 120 ^{o}C and 5,000 psi, respectively. The films were then cooled to room temperature and cut into appropriate specimen dimensions for further characterization.

To fabricate the multilayer films, the monolayer films were dip-coated in a PLA solution (5 % (w/v) PLA in chloroform) at room temperature for 10 s to obtain thin (thickness ~ 20 µm) skin coat on both sides of the core monolayers. The coated multilayer films were then dried at room temperature and prepared for further characterization.

3.2.2.6. Monolayer and multilayer physico-mechanical properties

UV-VIS characterization

The light transmittance measurements of the bioplastic samples were performed using Cary 100 Bio UV-Vis spectrophotometer to determine the transparency of the films. All films were cut into rectangular strips with a width of 10 mm and the data was recorded in the wavelength range of 400 to 800 nm.

Mechanical test

Tensile tests were carried out using a tensile testing unit (AGS-X series, Shimadzu, Japan) with a 500 N load cell according to ASTM D882-18. Films produced by compression molding were cut into 70 x 10 mm pieces, with a gauge length of 50 mm. The sample's thickness was collected by taking the average values of 3 measurement points across each sample. Testing was conducted at

room temperature and at a crosshead rate of 5 mm/min. For each formulation, at least 5 samples were tested, and the average was reported.

Shear test

To prepare samples for the shear test, a single layer of PLA was carefully peeled off from each multilayer sample in order to make bilayer films for testing. The films were put in contact between two metal wedges with an overlapping area of 20 x 10 mm^2. Epoxy glue was added on both side of the bilayer films and glued to the metal wedges to promote shearing between the bilayer films. The shear test was then conducted at a crosshead speed of 1.5 mm/min in accordance with ASTM D3163-14. Shear adhesive strength was then determined as the maximum point of the force-deformation curve. For each formulation, 5 samples were tested, and the average was reported.

Dynamic mechanical analysis (DMA)

The thermo-mechanical properties of the films were studied using a dynamic mechanical analyzer (TA Instrument, DMA Q800) in tension mode. Films were cut into strips with a width of 6.5 mm and an initial grip separation of 12 mm. The storage modulus and tan delta of the bioplastic films were scanned at a rate of 3 ^oC/min from -90 to 50^oC at a frequency, amplitude, and pre-load force of 1 Hz, 15 μm, and 0.01 N, respectively.

Morphology analysis with scanning electron microscopy (SEM) and energy dispersive X-ray (EDX)

The fractured surface morphologies of the multilayer films and the dispersion of nanoclays in the bioplastic were studied using a FEI SEM (Quanta FEG-SEM 250, Oxford Instrument) with EDX capability at an accelerating voltage of 20kV. For the multilayer films, the fractured surfaces were coated with gold sputtering and mounted onto stubs with double-sided carbon adhesive tape prior to scanning.

Water barrier property

The water permeability test of the various films was carried out in accordance with ASTM E96/E96M-16. Water vapor transmission rates (WVT) were measured using barrier cups with an exposed area of 8 cm^2. The barrier cups were filled with distilled water (RH=100%) with the film placed over the cup opening and tightly sealed. The cups were then placed inside a desiccator chamber at 23^oC and relative humidity (RH) of 30%. The weight loss resulting from water permeation through the film was recorded at different time interval up to seven days. WVT values ($g/m^2.h$) were determined according to the following equation:

$$WVT = \frac{\Delta G}{t} \times \frac{1}{A} \quad (3)$$

Where *ΔG/t (g/h)* is the linear slope of best fit of the weight loss vs. time graph; and *A* (m^2) was the exposed area of the water barrier cup. WVP values (kg. $m/m^2.s.Pa$), was calculated based on the following equation (4):

$$WVP = \frac{WVT\ x\ l}{S\ (RH_1 - RH_2)} \quad (4)$$

where *l (m)* was the thickness of the films; *S* was the saturation vapor pressure at 23^oC; RH_1 and RH_2 were the fractional relative humidity on the inside and outside of the test cup, respectively. Three specimens for each sample were used and the average values were reported.

Oxygen barrier property

The oxygen permeability (OP) tests were performed using a customized bubble flow rate system. Films (18.10 cm^2) were used to seal a two-chamber cartridge that was attached to an oxygen gas source on one end and a bubble flow meter on the other end. The pressure difference between the 2 chambers was set at 5 psi, allowing the oxygen to permeate through the membrane. The flux of

bubbles was determined by counting the time the bubbles take to travel 20 mL volumetric unit. The OP values ($cm^3.m/m^2.day.Pa$) was then calculated using equation (5):

$$OP = \left(\frac{V}{t.A}\right) \times \frac{l}{\Delta P} \quad (5)$$

where *V/(t.A) (cc/m^2.day)* is the flux of oxygen; *l* (m) was the thickness of the films; and *ΔP* (Pa) is the pressure difference between two side of the film. Triplicate measurements were conducted at room temperature and 50% RH.

3.2.2.7. Statistical analysis

Statistical differences in data were determined using multi-factor analysis of variance (ANOVA) and Tukey's HSD mean comparison test with a 95% confidence level ($P<0.05$).

3.3. Results and discussions

3.3.1. Characterization of Maleic Anhydride Grafted TPS

3.3.1.1. Degree of substitution (DS) analysis and H-NMR

The degree of substitution was determined in this study in order to optimize the MA content in the MTPS films. The substitution of –OH groups with MA on the anhydroglucose units of starch, associated with the grafting reaction, was estimated using a titration technique. **Figure 3.2d** presents the percentage of MA grafted on the anhydroglucose unit. The titration degree of substitution was calculated using equation (2). The results showed that the DS and % MA grafting have increased from 0.05 to 0.07, and 2.86 % to 3.80 %, respectively with increasing the concentration of MA in the reaction from 1 phr to 5 phr. This indicated that the reactive extrusion process was effective in grafting the MA, which was especially true at lower MA levels. Further increase in MA did not seem to increase the grafting levels by much indicating that the MA could have cause steric hinderance for additional reactions [148]. In comparison to other studies, Zuo et

al. reported a low grafting DS of 0.043 at 3 wt. % of MA in their corn starch TPS [142]. Bergel et al obtained a substantially higher DS (0.45) but at an elevated MA loading (20 wt.%) in their potato starch derived TPS samples.

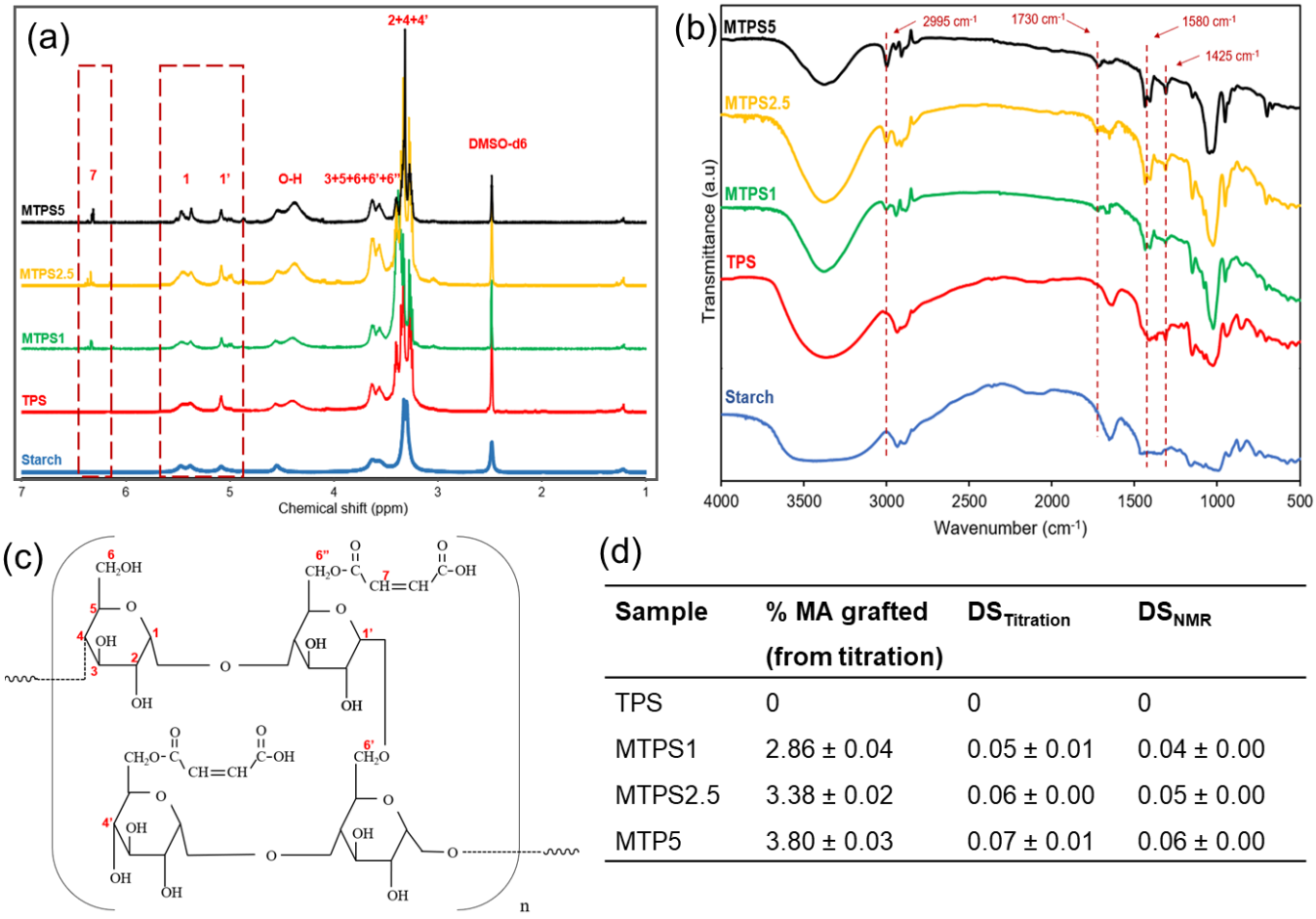

Sample	% MA grafted (from titration)	$DS_{Titration}$	DS_{NMR}
TPS	0	0	0
MTPS1	2.86 ± 0.04	0.05 ± 0.01	0.04 ± 0.00
MTPS2.5	3.38 ± 0.02	0.06 ± 0.00	0.05 ± 0.00
MTP5	3.80 ± 0.03	0.07 ± 0.01	0.06 ± 0.00

Figure 3.2. (a) H-NMR spectra of starch, TPS and MTPS samples at different maleation level (1,2.5, and 5 phr), (b) FTIR spectra comparison between native starch, pristine TPS and maleated MTPS samples at different modification level (1, 2.5, and 5 phr) (c) Chemical structure of maleated MTPS unit (d) % MA grafted, DS calculated from titration method ($DS_{Titration}$), and DS calculated from H-NMR (DS_{NMR})

The level of maleation resulting from the grafting of MA onto TPS was further analyzed using the H-NMR spectra (**Figure 3.2a)**. The peak at 2.5 ppm was associated with deuterated DMSO (DMSO-d6), which was the solvent used to dissolve the TPS and MTPS samples. All spectra exhibited characteristic peaks of anhydroglucose units from starch at 4.45 ppm (protons in O-H

group), 3.60 ppm (protons at positions 3/5/6/6'/6"), and 3.30 ppm (protons at positions 2/4/4') [149–151]. The NMR spectra of TPS and MTPS samples also demonstrated characteristic peaks of glycerol protons at 4.40 ppm (O-H group) and 3.50-3.30 ppm (methylene group) that was used for the plasticization of TPS [152]. However, the signals from glycerol overlapped with existing signals from starch, which was clearly observed in the TPS and MTPS samples. The peaks noted at 5.50-5.35 and 5.20-5.05 ppm corresponded to the proton atom of the linear α-1,4 linkages (position 1) and branching α-1,6 linkages (position 1') of starch, respectively [149,150,153].

The spectra of the MTPS samples revealed a distinctive peak at around 6.30 ppm that was not observed in neither the starch nor the TPS. This peak was assigned to the protons of the vinyl double bond (HC=CH) at position 7 of the open-ring maleic anhydride (**Figure 3.2c**). The appearance of this signal has also been reported in several other studies in the literature [141,143,154,155]. It was also noted that there is a gradual increase in the intensity of this peak (6.30 ppm) with an increase in the concentration of MA, indicating that more open-ring maleic anhydride group was grafted onto TPS as more MA was used.

The degree of substitution can also be determined by integrating the NMR spectra, specifically using the signals corresponding to the reference proton atoms of glycosidic linkages at position 1 + 1' (5.65-5.20 ppm) and the functionalized vinyl double bond of MA (6.30 ppm). The DS of modified TPS can then be calculated using Equation (6), which was adapted from the work of Sungho Lee [156]:

$$DS_{NMR} = \frac{\frac{I_{6.30}}{2}}{I_{5.65-5.20}} \quad (6)$$

where $I_{6.30}$ is the integrated area of the vinyl protons of MA presented at 6.30 ppm. The $I_{6.30}$ values is divided by two in the calculation to account for the 2 protons from each vinyl group. $I_{5.65\text{-}5.20}$ is

the contribution from both internal linear α-1,4 and branching α-1,6 linkages of the glucose unit, which is observed at around 5.65-5.20 ppm.

Comparison of the DS values calculated from the titration method to that of H-NMR (**Figure 3.2d**) indicated good agreement. However, the values obtained from H-NMR were overall lower than the titration values. Among all MTPS samples, MTPS2.5 shows the most promising potential as it exhibited an excellent DS while consuming lower MA in the formulation. Thus, MTPS2.5 was selected as a representative resin for further multilayer film fabrication.

3.3.1.2. Fourier transform infrared spectroscopy (FTIR) analysis

To further verify the grafting of MA onto TPS at various esterification levels, IR analysis was conducted and the spectra of native starch, pristine TPS, and maleated MTPS samples are presented in **Figure 3.2b**. Native starch showed characteristic IR peaks of the anhydroglucose units at 3600-3000 cm^{-1} (O-H stretching), 2920-2850 cm^{-1} (C-H stretching), 1200-980 cm^{-1} (C-O stretching, C-C stretching, and C-O-H bending), and 950 cm^{-1} (α-glycosidic linkages), similar to other studies [76,157,158]. The plasticization for neat TPS and all maleated MTPS was verified by the peak noted at 1425 cm^{-1}, representing the methylene H-C-H bending of glycerol [20]. The maleation of TPS was also demonstrated by the appearance of new IR peaks and the reduction of some existing signals. One of the most notable changes was the emergence of a new vibration peak at 1580 cm^{-1}, which was attributed to the C=C stretching as a result of the grafted MA groups[142,144]. Likewise, a new vibration peak was observed at 1730 cm^{-1} for all the maleated samples, which corresponded to the ester bond C=O stretching. This signal was the result of the carbonyl group in the open-ring MA grafted to TPS. Similar observation on the emergence of this peak was reported in the literature [142,159,160]. Because the MTPS were thoroughly washed with acetone before characterization, all of the unreacted MA had been washed away. Thus, all of

these changes in the IR spectra evidently confirms the presence of grafted MA on the TPS bioplastic.

Additional evidence for the grafting of MA on TPS was shown by the introduction of sp^2 C-H stretching from the alkene bond at 2995 cm^{-1} across all the MTPS samples [142,160]. Further comparison of the IR spectra for TPS and MTPS sample revealed a substantial reduction in the broad O-H peak at around 3600-3000 cm^{-1}. The reduction of this signal was more evident as more MA was added to the TPS formulation. The progressive reduction of this vibration provide supplementary evidence for the replacement of starch's O-H groups with open-ring MA groups [21,153]. Overall, the results obtained from FTIR validated the titration and H-NMR results that MA was successfully grafted onto the TPS via the esterification reaction.

3.3.1.3. Thermal analysis of TPS and MTPS

Thermal analysis was carried out to investigate changes in thermal stability or decomposition of starch as a result of plasticization and maleation. TG and DTG curves of starch, TPS, and MTPS were evaluated up to 500^{o}C and results are presented in **Figure 3.3 (a and b).** For the native starch sample, rapid thermal decomposition was observed peaking at around 310 ^{o}C. This decomposition of starch corresponding to the burning of anhydroglucose ring resulted in 20 wt. % of solid residue, which is in agreement with other studies [161,162]. TPS and MTPS thermograms were seen to begin deviating from starch at around 240^{o}C, which can be attributed to evaporative loss of glycerol. The weight loss for TPS and MTPS was more gradual as compared to native starch, indicating higher thermal stability of TPS and MTPS due to the plasticization [141].

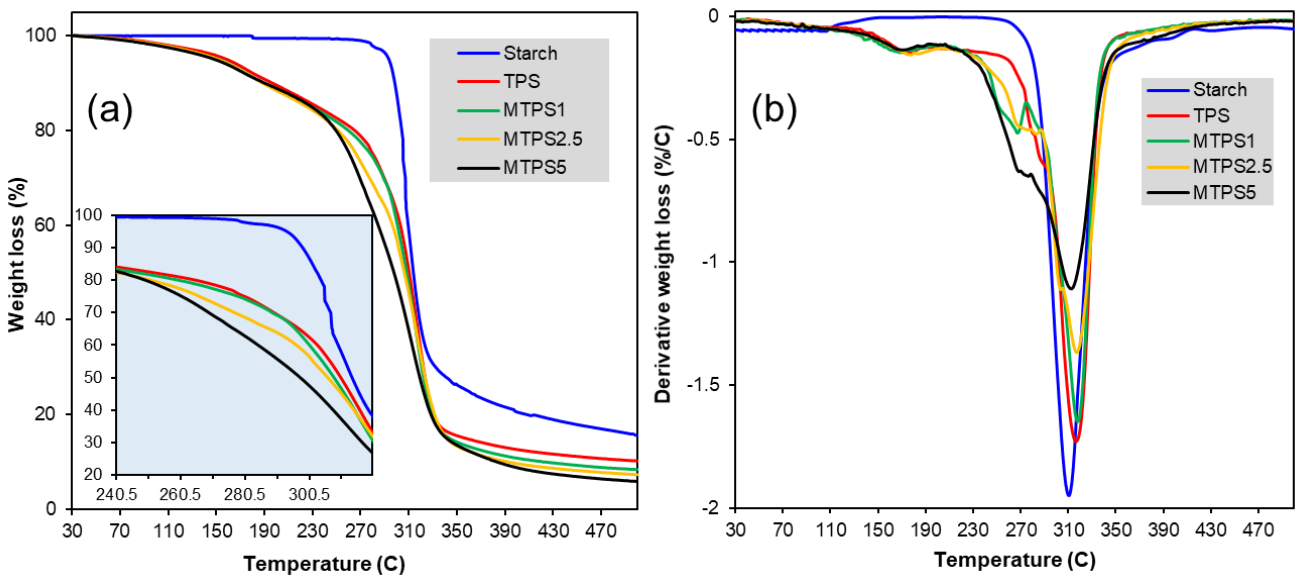

Figure 3.3. **(**a) TGA and (b) DTG of starch, TPS and MTPS materials

Thermal degradation behavior between TPS and MTPS samples were compared to see the effect of maleation. The results from the TG curves demonstrated that the decomposition initiation temperature of MTPS was lower than TPS. As anticipated, the slope of the TG decomposition curve was seen to diminish as the concentration of MA was increased. Zuo et al. also reported similar observations, and suggested the trend was due to the crystalline structure destruction as a result of the maleation reaction [142]. Furthermore, all MTPS samples demonstrated two degradation peaks in the DTG curves which again confirmed that the crystalline structure of the starch was significantly modified. The reduction in crystallinity showed great promise in extrusion processing as the material would theoretically be less rigid and have better viscosity for mixing [163].

3.3.2. TPS and MTPS – clay nanocomposites

3.3.2.1. Dispersion of nanoclays

Montmorillonite nanoclay is among the most extensively utilized nanomaterials in polymers, which can provide outstanding mechanical and barrier properties with affordable cost-structure

owing to its inherent platelet-nanolayer structure [164]. It is crucial to efficiently disperse nanoclays in TPS and MTPS bioplastic films in order to optimize the stress distribution for reinforcement or bring about a tortuous path for moisture and gas that result in good barrier properties. The dispersion and distribution of nanoclays in TPS and MTPS was investigated using SEM-EDX elemental mapping. Aluminum (Al) atoms of montmorillonite nanoclays was selected here to infer the dispersion of the clay nanoparticles in the fractured surface of the film. Al atoms was chosen over silicon (Si) in this study due to the fact that the number of Al atoms was twice as much as that of Si for this specific nanoclays, which would allow for better visualization of nanoclays in the bioplastic films.

Figure 3.4. shows the SEM and EDX mapping of both TPS and MTPS at different nanoclays loading. As expected, the frequency of yellow dots, which represent the Al element, was observed to be amplified as the nanoclays loadings increase. For the TPS sample, nanoclays appeared to be more finely dispersed at lower loadings, i.e.1 and 3 phr, which indicated a good exfoliated dispersion of nanoclay via the extrusion process [146]. This was not surprising considering that the nanoclay used for this study is hydrophilic, which can interact better with the hydrophilic TPS. However, some small agglomerates emerged as the loading increased to 5 phr as noted from the particle clusters detected in the TPS matrix. These agglomerations could have been the result of the high nanoclays loading, which increases the viscosity during extrusion process leading to less optimal dispersion[112,165].

On the contrary, inferior dispersion of nanoclays was observed in the MTPS films as compared to TPS. Comparatively higher aggregations of nanoclays were detected in MTPS at 5 phr loading as observed from the particle clumps. This phenomenon was associated with the fact that maleation causes MTPS to be more hydrophobic, which in turn lowers the interaction between the films and hydrophilic nanoclays [163]. I Nevertheless, the MTPS films at 1 and 3 phr nanoclays displayed a

homogenous distribution of the Al element, indicating a good dispersion of nanoclays despite the hydrophobicity of MTPS. Since the maleation generated relatively low substation of the –OH moieties on the anhydroglucose units of starch, the MTPS retained sufficient polar moieties to interact with the hydrophilic clay that resulted in the good dispersion of the nanoclays.

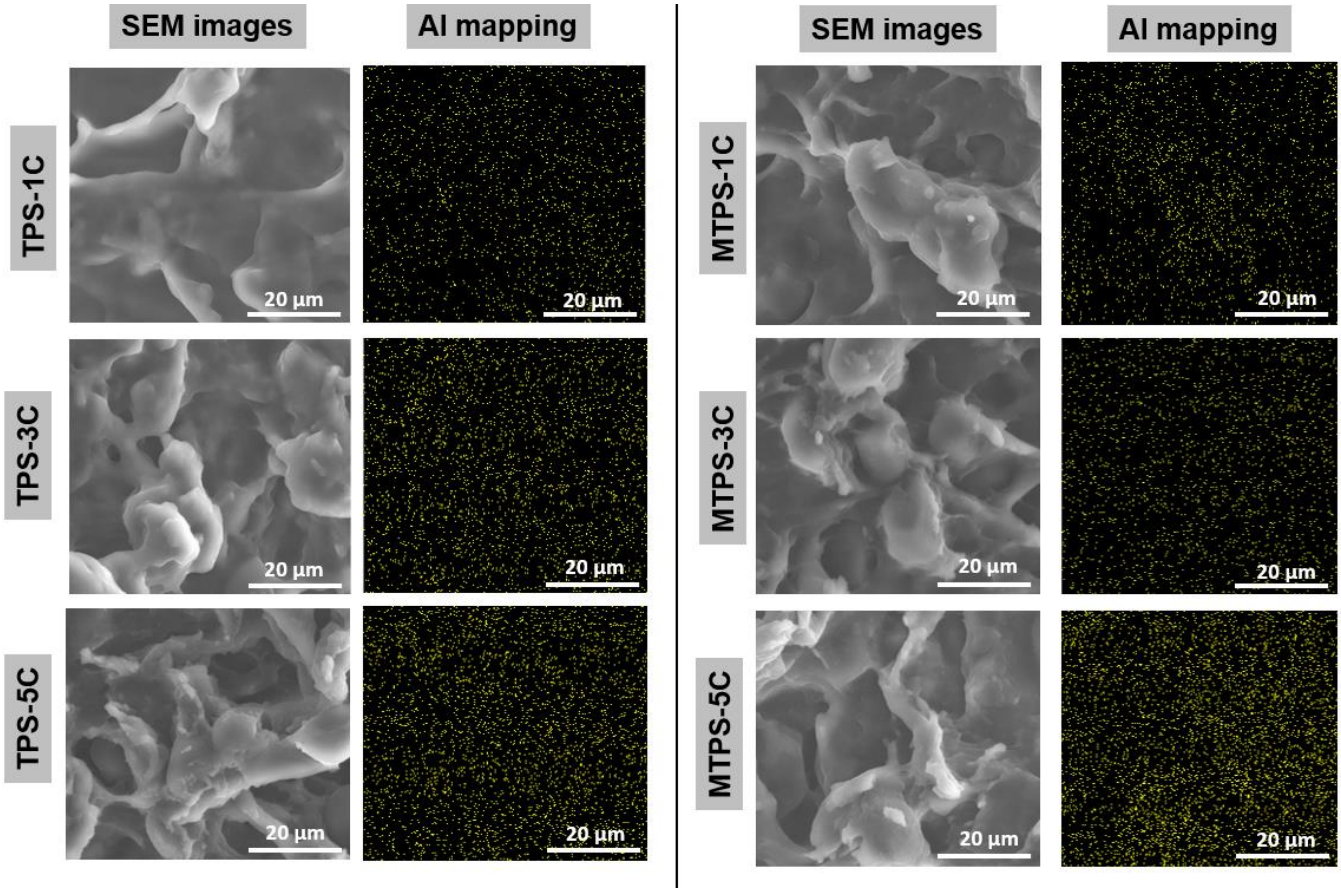

Figure 3.4. EDX mapping of aluminum (Al) element for the dispersion of montmorillonite nanoclays in the reinforced TPS/MTP nanocomposite films

3.3.3.2. Optical clarity

The transparency of films is a desirable property for materials used in packaging applications where the visibility of wrapped content is required [166]. Overall, both the TPS and MTPS films showed good transparency to the naked eye, even at high nanoclay loading levels (**Figure 3.5c**). To further evaluate the optical properties of TPS and MTPS films, UV-Vis spectrophotometer was used to measure the transmittance of light through the film in the visible light region (between

400-750 nm)**. Figure 4** showed that both the TPS and MTPS have a decreasing trend in optical clarity with an increase in nanoclay loading. This was because a higher nanoclay loading will increase light scattering and hence transmittance [167].

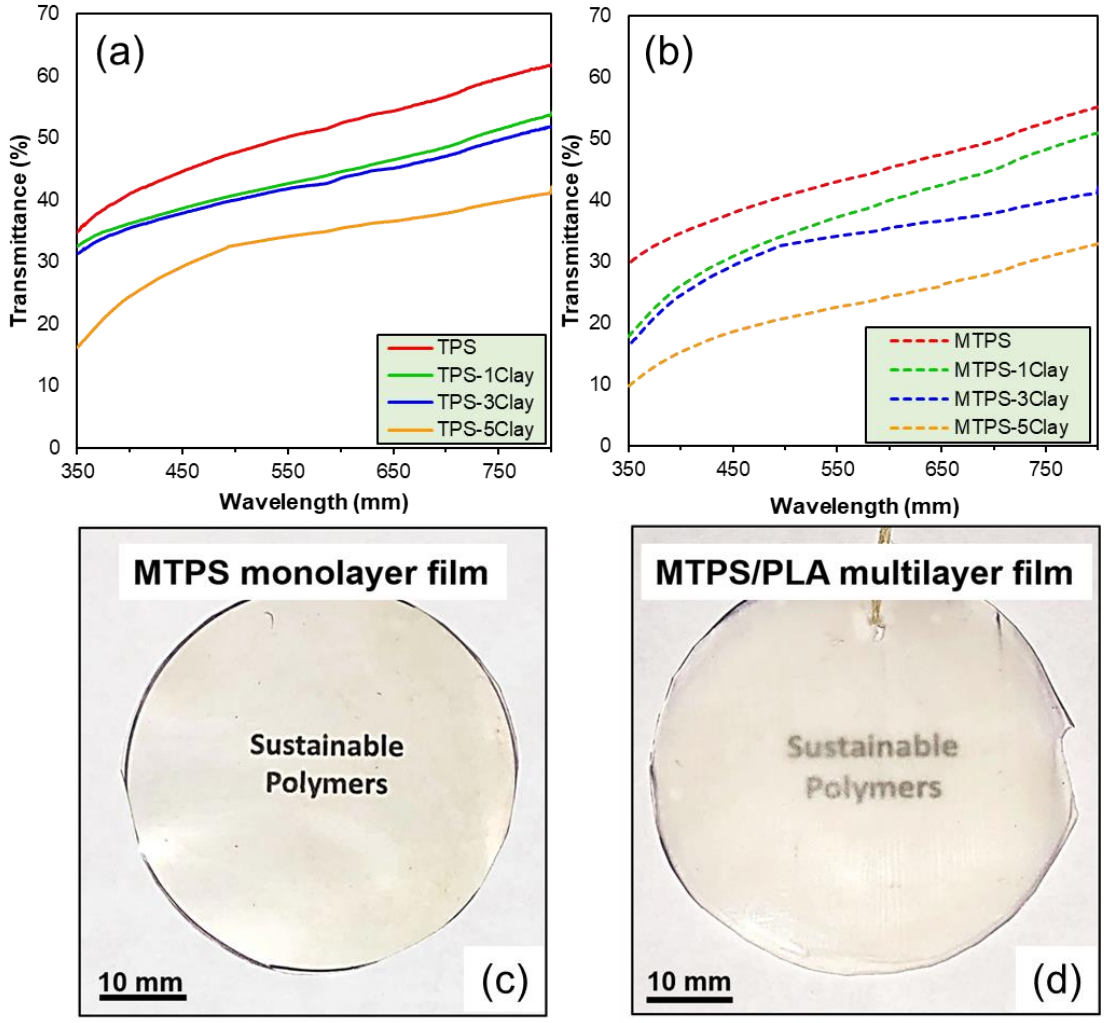

Figure 3.5. UV-Vis spectra showing the light transmittance of (a) neat TPS-Clay and (b) maleated MTPS-Clay films; Photograph of (c) MTPS monolayer film and (d) MTPS/PLA multilayer film

3.3.2.3. Tensile analysis

Evaluation of mechanical properties provides useful insight for the optimization of nanoclay dispersion and their impact in reinforcing the studied TPS and MTPS films. The baseline MTPS displayed a slightly lesser tensile strength than the TPS films (**Figure 3.6a**). This change in tensile strength can be attributed to a decrease in the crystallinity of MTPS samples, inferring from the TGA results. The partial destruction of crystallinity due to the replacement of –OH with open-ring MA groups on the starch structure causes reduction in intra- and intermolecular hydrogen bonding in the starch macromolecule chains, leading to a drop in tensile strength [142]. However, this reduction was not severe as the degree of substitution was fairly low.

The impact of nanoclay fillers on the tensile properties of the films was also investigated using tensile testing**.** It was evident that nanoclays had a clear reinforcing effect on the TPS and MTPS film's mechanical properties at 1 and 3 phr loading levels as noted from the significant improvement in the tensile strength and modulus (**Figure 3.6 a & c**). The tensile strength of neat TPS increased from 2.33 to 3.15 MPa (i.e. 35% increase), while MTPS showed a similar improvement from 2.03 to 2.84 MPa (i.e. 39% increase), respectively. Moreover, an improvement in tensile modulus by 58% and 62% were achieved at 3 phr nanoclays loading for TPS and MTPS films, respectively (**Figure 3.6b**). This indicated that nanoclays was able to restrict the chain mobility at the molecular level as well as allow stress transfer from the polymer chains to the nanoclay when tensile force was applied [168]. However, both TPS and MTPS films displayed reduction in mechanical properties with the use of the highest nanoclays loading (5 phr) in this study. The results indicated that the nanofiller loading level threshold point for both TPS and MTPS nanocomposites lies between 3 and 5 phr. This was in agreement with the SEM-EDX analysis in which the 5 phr loading manifested higher aggregation levels. Zhang et al. also reported a similar reduction in tensile strength and modulus for his potato starch derived TPS at 8 wt.%

nanoclays loading [169]. A study by Kusmono et al. on nanoclays in epoxy composites showed that effective reinforcement can be achieved at a peak loading levels of 3 wt.%, and mechanical properties progressively deteriorated beyond this level[170], which was in agreement with this study.

It appeared that nanoclays had no significant effect on the elongation at break of the bioplastic films, with the exception of the highest nanoclays loading (5 phr) due to considerable chain mobility restriction at this loading **(Figure 3.6b)**. Overall, the addition of nanoclays maintains the elongation of films, as opposed to other nanofillers. This is appealing and of great importance as the increase in tensile strength while the elongation is maintained translates into enhancement in toughness that is a desirable trait in packaging films[147]. Holding up the elongation can be associated with the energy dissipation through the reorganization of clay nanoparticles and/or dissipation via debonding at the nanoclays vs TPS/MTPS interface generating micro-cracks that has limited propagation in the films similar to polyethylene/clay composites reported by Stoeffler et al [147]. Based on the tensile results, it can be deducted that the nanoclay reinforced TPS and MTPS films with 3 phr clay loading displayed favorable properties. As a result, this formulation was utilized for the fabrication of multilayer films.

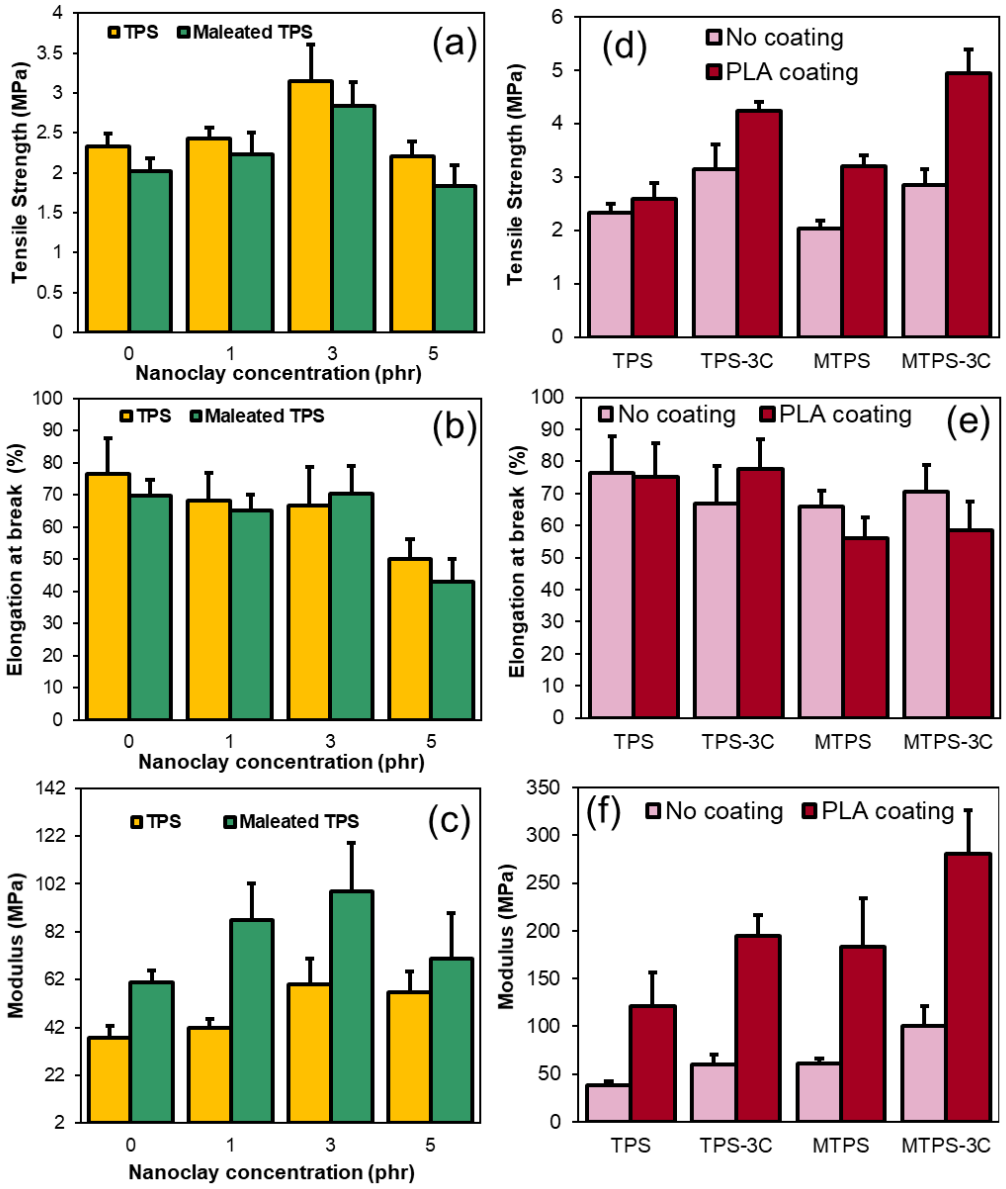

Figure 3.6. Tensile properties of TPS and MTPS bioplastic films with increasing concentration of nanoclays, showing the (a) tensile strength, (b) tensile modulus, (c) elongation at break; Tensile properties comparing the effects of PLA coating on the bioplastic film , showing the (a) tensile strength, (b) tensile modulus, and (c) elongation at break

3.3.3. Multilayer films of TPS and MTPS nanocomposites nanoclays with PLA coatings

The fabrication of multilayer films entailed coating the TPS and MTPS nanocomposites films with PLA via a dipping process. This fabrication method can be replaced with co-extrusion or lamination processes in scale-up studies or industrial settings. Since TPS and PLA have poor interaction, and hence poor interfacial adhesion, MTPS was including in the study anticipating that

it will provide augmented adhesion with PLA as compared to TPS as MA. This is because maleic anhydride is known to reduce the polarity of carbohydrates and induce hydrophobicity [144]. These films were further characterized to evaluate the effect of PLA layer on the physical and mechanical properties of the fabricated film.

3.3.4. Tensile properties of the multilayer films

The tensile strength, elongation at break, and tensile modulus of the PLA coated TPS and MTPS nanocomposite films are presented in **Figure 3.6 (d-e).** It was noted that the PLA layer improved the tensile strength of the films attributed to the high tensile strength of the semi-crystalline PLA layer, which served as the load-bearing phase when subjected to an external force [136]. Similarly, the modulus of the multilayer films also displayed a remarkable increase as compared to the non-coated (monolayer) films. The PLA grade that was used in this study had a relatively high modulus of 3.6 GPa [171], which contributed greatly to the increased modulus of multilayer film system. It was interesting to notice that the addition of PLA did not have a significant effect on the elongation at break of the film. Although, PLA coating are often associated with reductions in elongation as has been reported previously [26,172] owing to the low elasticity of PLA (about 2 % for this grade of PLA)[173], the opposite trend was observed in this study. An explanation for this behavior may stem from the variation in the thickness of the TPS and MTPS nanocomposite core layer and the PLA skin layer. Upon SEM investigation, the core layer and the skin layer had average thickness of 250 µm and 50 µm, respectively. This shows that the substantially thicker core layer contribution towards the tensile properties was much higher than the thin PLA skin layer confirming the observation.

Comparing the TPS and MTPS films, it was discernible that the MTPS/PLA multilayer films demonstrated a superior improvement in the tensile strength and modulus than those of the TPS/PLA based films. This indicated that the maleation of TPS amplified the chemical interactions

between PLA and MTPS thereby enhancing the interfacial bond adhesion and allowing more efficient stress transfer throughout the multilayer film system [136]. Most noticeably, a 73 % and 181% improvement in tensile strength and modulus were achieved for MTPS-PLA multilayer film with 3 phr nanoclays loading (MTPS-3C) compared to the monolayer counterpart, respectively.

3.3.5. Dynamic mechanical analysis (DMA)

The thermomechanical properties of TPS, MTPS, TPS-3C, MTPS-3C and their respective films coated with PLA were evaluated and the variation in the storage modulus (E') and tan delta (δ) as a function of temperature are presented in **Figure 3.7**. It was noted that the monolayer films all possessed lower modulus than their PLA coated counterparts. Among all multilayer films, TPS-3C and MTPS-3C films are the 2 samples that have the highest storage modulus in good agreement with the tensile modulus results. . It was also evident that below the onset T_g, all monolayer and multilayer films containing nanoclays exhibited higher modulus than the unfilled films. The reason for this was the restricted chain mobility caused by the presence of fillers resulting in an enhancement in the modulus [144].

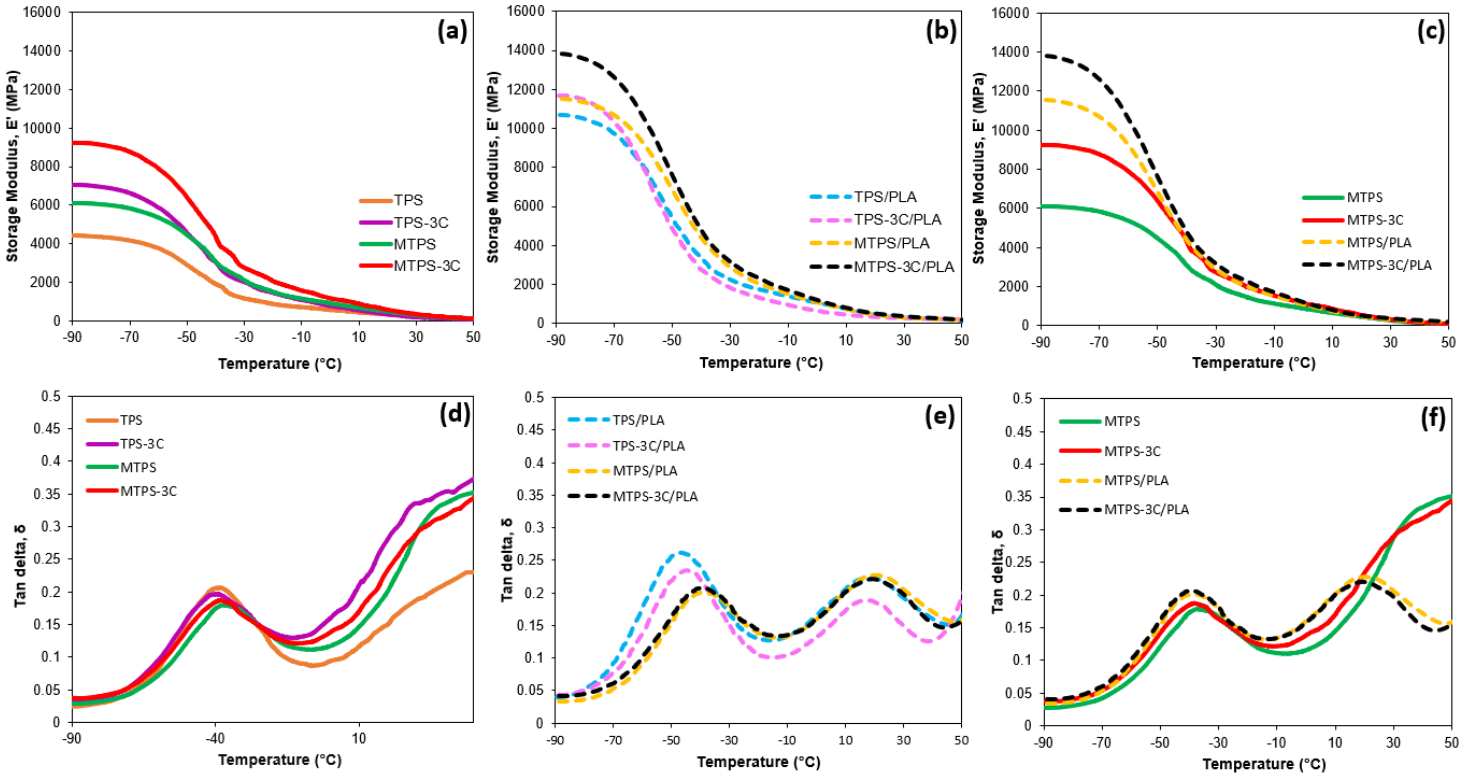

Figure 3.7. DMA results comparing the storage modulus of (a) Monolayer film, (b) Multilayer film, (c) MTPS monolayer and multilayers films at different clay concentrations; and comparing the tan delta of (d) Monolayer film, (e) Multilayer film, (f) MTPS monolayer and multilayers films at different clay concentrations

The tan delta peak was used here to evaluate the changes in the glass transition temperature (T_g) of the various films, as well as to investigate the mobility of the polymer chain segments. From **Figure 3.7(b)**, the storage modulus curve of the monolayer TPS and MTPS films showed that they were approaching the film plasticization temperature, which would be at around 90^{o}C. However, DMA is not an accurate test for the determination of plasticization temperature, thereby, it was not included in this study. For the monolayer films, a single tan delta peak was observed at approximately -38^{o}C belonging to the T_g of plasticized starch (**Figure 3.7d**).

The double tan δ peak observation (**Figure 3.7e**) is associated with the T_g of the core layer and skin layer. Higher tan delta peak intensities were also noted for neat TPS/PLA and TPS-3C/PLA in comparison with the MTPS based multilayer films (**Figure 3.7 e &f**) implying higher molecular mobility attributed to the inferior interaction between TPS and PLA layers as polymer chains

seemed to move around more freely. A narrower gap between the two T_gs' was noted for MTPS – PLA based multilayer films in comparison with the TPS – PLAs'. This was indictive of comparatively better compatibility between the MTPS and PLA as opposed to TPS and PLA.

The occurrence of the second T_g peak (**Figure 3.7 e & f),** corresponding to the T_g of the PLA layers, at only 18 – 20 ^oC was quite fascinating. This is because the typical T_g peaks of PLA is in the range of 55-60^oC [171]. This special phenomenon can be attributed to the "sliding motion" mechanism proposed by de Gennes, which suggested that polymer molecules from a thin layer can propagate their own mobility into the near-surface segment of an adjacent polymer film [174]. The perturbation caused by this PLA surface layer, which allowed some PLA molecules to propagate into the thicker TPS and MTPS film layer, resulted in a remarkable reduction in the T_g for the PLA phase.

3.3.6. Adhesive shearing strength

In order for the starch-PLA multilayer films to perform as a whole structure, each layer must provide adequate adhesion shear strength [4,175]. **Figure 3.8 (a)** shows that the adhesive shear strength necessary to separate the neat TPS from the PLA layer was 0.41 MPa, while the shear strength required for the separation of maleated MTPS from the PLA layer was 1.35 MPa, i.e. 229% increase. Similar increase in shear adhesive strength was noted for the MTPS-3C/PLA as compared to the TPS-3C/PLA nanocomposite films that represent about 135% increase. The results demonstrated that the neat TPS has inferior adhesion with the PLA layers, stemming from the poor interfacial interaction between the hydrophilic starch and the hydrophobic PLA [16,135]. The remarkable adhesive shear strength between the MTPS based films with the PLA layer is further validation that the maleic anhydride supports the interfacial interaction and interlocking between the MTPS and the PLA layer. The addition of nanoclays into the thermoplastic starch film did not have a significant effect on the layer adhesive properties. This was because nanoclays did

not significantly interfere with the hydrophilicity of the starch, resulting in the nanoclays playing statistically irrelevant role. Furthermore, it can be stipulated that the strong adhesive shear strength of the MTPS based films could have played an important role for the observed tensile properties shown in **Figure 3.6 (d-f)**.

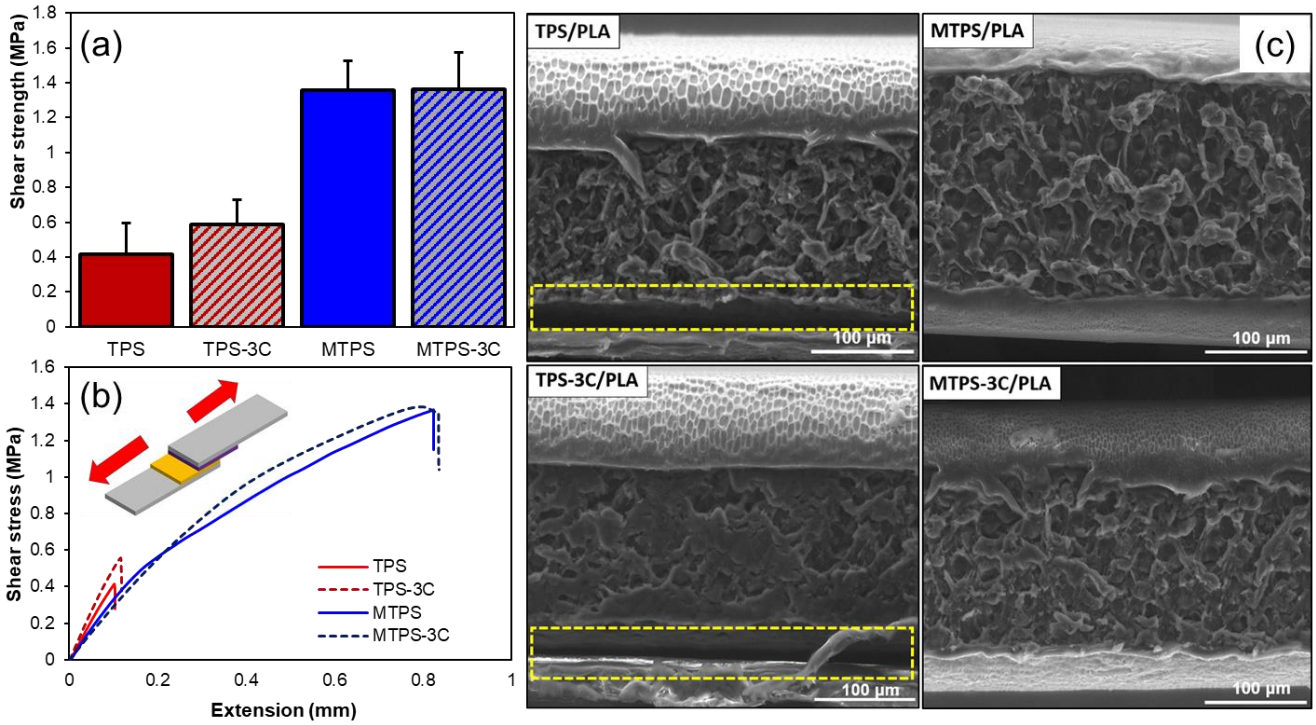

Figure 3.8. (a) Adhesive shear strength of different multilayer films, (b) Stress-extension curve for adhesive strength of the multilayer films and (c) SEM micrographs of the fractured surfaces of the TPS/MTPS and PLA multilayer films at 0 and 3 phr nanoclays concentration

3.3.7. Morphology-barrier relationship of the multilayer films

The fractured surface morphologies of the multilayers films containing TPS/PLA and MTPS/PLA at 0 and 3 phr nanoclays concentration were investigated using SEM and results are presented in **Figure 3.8c**. It was evident from the **Figure 3.8c** that the TPS and MTPS core films were sandwiched between the two PLA skin layer coatings. The fractured surfaces of the unfilled TPS and MTPS films showed a very rough surface due to the structure of starch granules. On the other

hand, both the TPS/3C and MTPS/3C nanocomposite films indicated a more homogenous and continuous matrix integrity.

Additionally, the interfacial layer adhesion behaviors between the polymer phases can be clearly observed in the micrograph. The TPS/PLA and TPS-3C/PLA displayed microscopic gaps between the PLA layer and TPS matrices. The visible gap, highlighted with yellow dotted lines, indicated insufficient compatibility and delamination between hydrophobic PLA and hydrophilic starch. On the contrary, modified MTPS/PLA and MTPS-3C/PLA samples showed excellent interfacial adhesion due to the enhanced chemical interaction and mechanical interlocking between the PLA and MTPS polymer chains in the respective layers. It was apparent that cross-layer miscibility has occurred, and it was close to impossible to clearly distinguish the layer boundaries. This is in an excellent agreement with the shear strength measurement results.

3.3.8. Moisture barrier properties

Moisture barrier is one of the most important requirements for packaging applications, because of the frequent contact of products with moisture. Water permeability test for the PLA coated TPS and MTPS films was carried out to evaluate the variation in the moisture migration as a result of the maleation modification, the inclusion of nanoclays, and the multilayer assembly. The water vapor permeation data of selected monolayers and multilayers films were investigated for 24 h and 7 days and presented in **Figure 3.9**. As anticipated, the neat TPS monolayer film had the most significant amount of water loss over the course of 7 days due to its extremely hydrophilic by nature [134,160].The incorporation of nanoclays in TPS was shown to decrease the water permeation through the film. This phenomenon was expected with the incorporation of nanofillers including nanoclays, as nanofillers induce a tortuous path for water diffusion through the films [147]. It was also noteworthy to highlight that there a stark difference was observed between the moisture permeability of the monolayer and multilayer films with PLA coatings. The inherently

hydrophobic PLA seals the core TPS/MTPS layers and helps mitigate the moisture attack and resulting in substantially reduced moisture diffusivity across the films [138,176].

The WVP data presented in **Figure 3.9 (c)** indicated that there was no statistically significant difference in the WVP values ($P > 0.05$) observed between 24 h and 7 days. The WVP results showed that the neat TPS/PLA film allowed twice as much moisture diffusion compared to the MTPS/PLA film. Since the MTPS has an enhanced layer adhesion with PLA`, it was expected that the water barrier properties of MTPS/PLA film would be superior. Furthermore, the tortuous path induced by the clay platelets further contributes to the limited mitigation of moisture through the films. This effect of nanofiller was reflected in the reduced WVP values of the nanoclays-filled films. The proposed mechanism is illustrated in **Figure 3.9 (d)**, where it was shown that the combined influences of nanoclays fillers and PLA layers can lead to enhanced water permeability behavior of the films.

Comparing the neat TPS film with the final developed multilayer film MTPS-3C/PLA, the WVP values after 7 days improved from 10.33 to 0.79×10^{-13} kg.m/s.m^2.Pa, which represents a 92.4% reduction in the WVP values and about 13 times better in term of moisture barrier properties. Overall, the interfacial compatibility of MTPS with PLA, in conjuncture with the incorporation of nanoclays in the starch polymer matrices, helped create a novel multilayer film system that has superior moisture barrier and low vapor penetration properties.

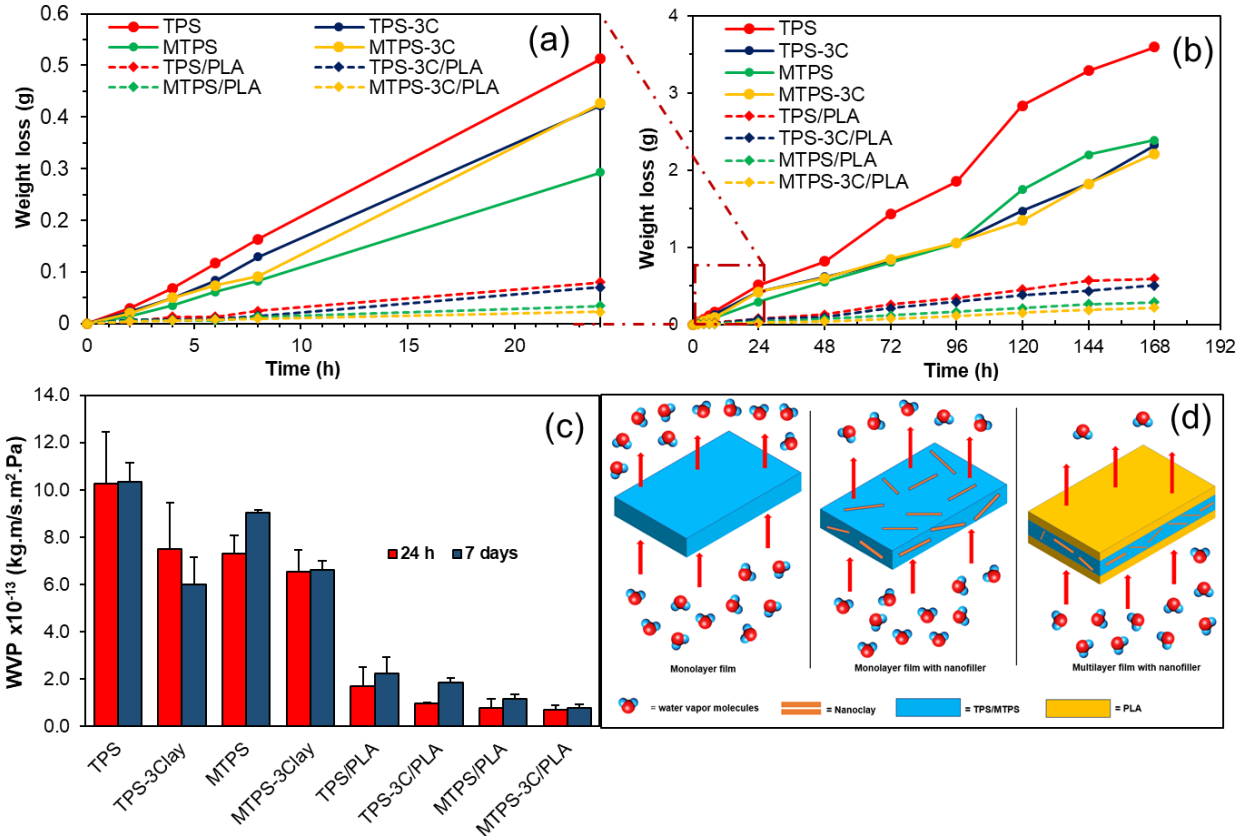

Figure 3.9. (a and b) Water vapor permeation loss of the monolayer and multilayer film systems over time, (c) Comparison of WVP values between the films over different time periods, and (d) illustration of proposed permeation mechanism though TPS/MTPS and TPS/MTPS with nanoclays and PLA coating

3.3.9. Oxygen barrier properties

Oxygen barrier properties of packaging materials is another essential property that dictates their applicability. As shown in **Figure 3.10,** the maleation of TPS slightly increased the oxygen permeability across the film assembly. This was associated with the increased crystalline structure disruption in the MTPS as compared to the TPS. Also, the reduction in polarity of the starch in the MTPS increases the interaction with the non-polar oxygen molecule leading to aggravated permeation. In general, a modest reduction in the oxygen permeability in all sample films was observed with the addition of the nanoclays. For the single layer samples, a reduction of 26.2 and 33.7% were observed for TPS and MTPS films with 3 phr nanoclay loading, respectively. This can be explained by the tortuous path created by the well-dispersed nanoclay as noted from the Al

mapping in the EDX analysis. The improved oxygen barrier properties of TPS, stemming from the addition nanoclays, is in agreement with many other studies [97,162,177]. The works of Zeppa et al. suggested that the hydrophilic montmorillonite clays form either intercalated or exfoliated structures in the starch matrices, thereby, initiating a more tortuous pathways that would reduce the permeability of oxygen molecules through the films [177].

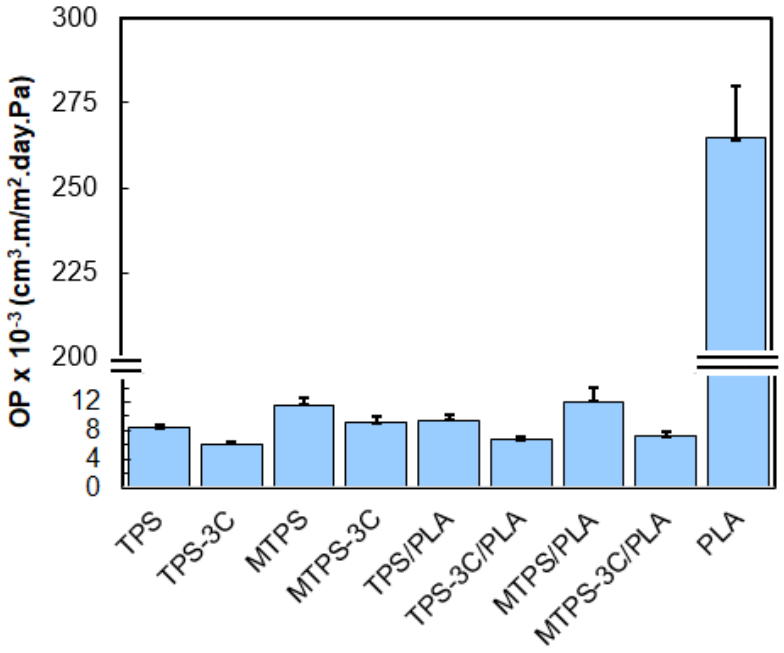

Figure 3.10. Comparison of Oxygen Permeability (OP) values between the films.

The PLA coating did not influence the OP values of any of the films, indicating that PLA's contribution towards OP reduction is substantially lower than the TPS and MTPS based nanocomposite films. It is worth highlighting that neat PLA, which is known to be an inferior polymer in providing oxygen barrier [136] displayed an OP values of $261.55 \pm 26.65 \times 10^{-3}$ ($cm^3.m/m^2.day.Pa$). This show that the optimized film in this study (MTPS-3C/PLA) provides more 3,300% improvement in oxygen barrier properties over PLA, indicating that the fabricated multilayer films provide superlative oxygen barrier properties over PLA or other similar biopolymers.

3.4. Conclusions

This research investigated the fabrication process and properties of the nanoclays-filled TPS-PLA multilayer films. Overall, the maleated TPS (MTPS) demonstrated lower crystallinity and polarity that led to improved interfacial interaction with the hydrophobic PLA layers. Due to the enhanced chemical interaction and mechanical interlocking between PLA and MTPS, the adhesive strength between each layer in the multilayer films was improved, resulting in superior mechanical and barrier properties. The incorporation of nanoclays at optimal loading (3 phr) further enhanced the physico-mechanical and barrier properties of the multilayer film assembly. Most importantly, the final MTPS-3C/PLA multilayer film exhibited excellent moisture and oxygen barrier properties in conjuncture with enhanced mechanical properties. The multilayer film assembly provided 92.4% reduction in moisture barrier compared to TPS, and 3,300% improvement in oxygen barrier properties as compared to PLA films Overall, the developed multilayer films fabricated in this study displayed good transparency and tensile properties, and excellent moisture and oxygen barrier properties. Such materials could be utilized as wrapping films for food packaging applications. Since the multilayer film system is predominantly made up of inexpensive TPS material and fabrication process involves reactive extrusion, which is a continuous solvent free process, the multilayer film will have a reasonable cost structure. The formulation ingredients are all compostable and food grade; thus, the multilayer film assembly is also expected to be compostable and food grade. However, further investigation is required to confirm the compostability of this multilayer film assembly.

CHAPTER 4: A NANOMATERIAL-STABILIZED STARCH-BEESWAX PICKERING EMULSION COATING TO EXTEND PRODUCE SHELF-LIFE

4.1. Introduction

Fruits are inherently perishable even when stored in cold storage and cannot be kept for long. Previous data showed that a high percentage of fresh fruits (20-30%) are lost after post-harvest because of over-ripening and spoilage [178]. Reducing fruits and vegetables wasted by spoilage plays a vital role in the global food system as food source security is currently one of the biggest global challenges [179,180]. To alleviate the post-harvest waste of produces, a cost-effective and green solution to extend the shelf-life of these products is among the most promising approaches.

Applying rationally designed thin layers of edible coatings on fruits and other produce to prolong their shelf-life is an appealing alternative to mitigate the spoilage challenge[9]. Unlike standard packages, which are separated from the food products, edible films are integral parts of fresh foods that can be consumed together with the foods[15]. Edible polymer coatings for fruits and vegetables have been used for centuries to delay spoilage, as well as to contribute to the texture and quality of the products [181]. Fruit spoilage is associated with microorganism attack, respiration, and senescence (climatic fruits) spoilage or dehydration (non-climatic fruits) mediated spoilage. Thus, edible coatings are designed to provide low permeability towards moisture and oxygen, retain or improve physical appearance, and provide mechanical strength to prevent physical damage, among other requirements [92]. Currently, paraffin, candelilla, shellac, and carnauba wax are the leading commercial coatings used as fruit coatings[181]. These coatings mainly improve appearance, reduce water loss, and maintain the fruits' quality by delaying ripening [28,181]. However, they have extremely poor gas permeability, which causes anaerobic conditions occurrence making them unfit for climatic fruits coating. Additionally, when removing

wax-coated fruits from cold storage, water condenses on the fruits' surface causing undesirable skin whitening and blushing [181].

Starch is a bio-based, edible, biocompatible, abundant, renewable, and low-cost polysaccharide widely utilized in the food industry [74,84]. It is an appealing candidate for food coating applications because of its excellent film-forming capability, edibility, low oxygen permeability, and ease of property tuning using simple plasticizers [182]. Pure starch, however, possesses poor mechanical properties and is susceptible to moisture damage, which is undesirable for a coating intended to keep moisture out. In order to appropriately utilize starch as a coating material, it must be combined with other materials to improve its functionalities [134]. Recent developments of starch-based films and coatings, such as a sandwich assembly film made from polylactic acid and pea starch [183] and as a gel composite films[184], indicated promising results in food coating applications.

One of the desirable materials that can be combined with starch is beeswax. This is because beeswax, composed of a mixture of over 300 hydrocarbons, free fatty acids, fatty acid esters, fatty alcohols, diesters, and exogenous substances [185], is a relatively abundant and edible natural product. Moreover, it is inherently hydrophobic that can help mitigate the hydrophilicity of starch in combined formulations. While the composition of beeswax varies slightly based on the family and breed of the bees, it invariably possesses strong water barrier properties, as well as antimicrobial and antifungal properties, making it even more desirable for edible coatings as it can protect the fruits from microbial attacks [185]. However, the starch and beeswax are incompatible due to the significant difference in polarity, which typically results in phase separation between the dispersed beeswax and the continuous starch phase resulting in a rough morphology with limited barrier properties. Thus, a compatibilizer or emulsifier is usually required to obtain a uniform dispersion of the beeswax in the starch or vice versa.

The stabilization of starch and beeswax in liquid coating formulations requires an emulsion stabilizer, such as a surfactant or solid particles (Pickering emulsifiers) [186]. The use of Pickering emulsifiers in place of the surfactants is more desirable because they offer higher stability than surfactant-based emulsions because of their excellent elastic responses [187]. Pickering emulsions also require lessor emulsifiers than conventional surfactant emulsions that are beneficial in a commercial deployment [188]. Additionally, many surfactants are toxic, which makes them unfit to be used in edible coating applications. Commonly used stabilizers in Pickering emulsions include clays, carbon nanotubes, proteins, and polysaccharides such as starch and cellulose [187].

Cellulose nanocrystals (CNCs), derived from acid hydrolysis of biomass, are green, edible, and sustainable nanomaterials that attracted substantial interest to design sustainable systems, including edible coating applications [189]. CNCs and their derivatives also provide functional attributes to coatings, such as enhancing tensile properties and improving gas barrier properties [76,173]. Moreover, CNCs and their derivatives can form stable colloidal dispersions in water, possess nanoscale size, high aspect ratio, and surface area, making them appealing in Pickering emulsion applications [189]. Researches on cellulose-based materials as colloidal stabilizers of emulsion systems is gaining substantial interest as they offer effective stability and biocompatibility compared to traditional surfactants. Gong et al. demonstrated the use of chemically modified CNCs as a Pickering emulsion stabilizer in formulations used in cleaning products or cosmetic use [190]. Zhai et al. also reported a stable peanut oil/water emulsion using bacterial cellulose (BC) nanoparticles as Pickering emulsifier without the need for any modification.

However, the stabilization mechanism of the BC nanomaterials in peanut oil/water interfaces was not throroghly investigated; thus, more researches on the same topic are required to confirm the material applicability in food [191]. Another study by Tianzhong et al. recently investigated the

effect of cellulose nanofiber (CNF) morphology on the stabilization mechanism and emulsifying capacity [192] in Pickering emulsions. Results showed that increasing the degree of CNF fibrillation improved the droplet-fiber entanglements during the emulsification process, which led to a higher stabilization between fibers and droplets 3D network structure. These researches all highlighted the potentials of nanocellulose in Pickering emulsions.

The anhydroglucose units of CNCs have three –OH moieties that are amenable to various chemical modifications to tune their physical and chemical properties. Past studies have modified CNC to improve emulsion capabilities by modifying them with BSA protein [193], octenyl succinic anhydride (OSA) [120], and benzyl-polyethyleneimine [194], among others. This study investigated the controlled succinylation of CNCs with dodecyl succinic anhydride (DDSA) to replace some hydroxyl groups with more hydrophobic aliphatic chains. The modified CNCs (CNC DDSA) were then evaluated for their performance as Pickering emulsion stabilizers of starch – beeswax colloidal dispersions for coating applications. DDSA was selected over the prominent OSA as the longer alkenyl chain of DDSA may provide the CNCs with higher hydrophobicity to interact with beeswax compared to OSA-modified CNC at similar DS. Similar to OSA, DDSA is also considered a food-grade starch-modifying agent that is safe for consumption at low quantities [195]. Moreover, the reaction between these long-chain succinic anhydrides (OSA, DDSA, etc.) with other cellulose-based materials can occur at mild reaction conditions and is frequently used in food applications [196–198]. Recent studies like those of Li et al. on physicochemical properties modified DDSA-quinoa starch [199] or Padil et al. on antibacterial properties of DDSA derived Gum Karaya [200] showcased the vast potential of DDSA modified macromolecules as emulsifying agents in food applications. Therefore, we hypothesized that the use of the modified CNC in coating applications would not only help stabilize the starch-beeswax emulsion but also

enhance the load-carrying capability of the coatings and reduce their oxygen permeability desirable in fruit coating applications.

This research aimed to investigate economic and sustainable edible starch-beeswax emulsion coating systems stabilized by a green CNC nanomaterial as a Pickering emulsifier **(Figure 4.1**). Starch-beeswax composite films were first fabricated using the CNC Pickering emulsifier system and thoroughly evaluated the physicomechanical, morphology, optical, gas, and moisture barrier properties of the film samples in order to establish the optimal film-forming coating formulations. In the next step, we evaluated the functionality and practicality of the emulsion coating systems in preserving the freshness of climatic, non-climatic, and flesh cut fruits as a proof-of-concept of the technology performances. Finally, detailed investigations on this emulsion-based coating system were carried out to ensure that the features of the study constitute novel edible coatings, such as robust mechanical properties, excellent barrier properties, and edibility.

4.2. Materials and Methods

4.2.1. Materials

Cornstarch (containing approximately 73% amylopectin and 27% amylose) and bleached beeswax were supplied by Sigma Aldrich, USA. Glycerol (99%) obtained from Thermo Fisher Scientific was used as the plasticizing agent of starch. Spray-dried cellulose nanocrystals (CNCs) powder and 5 wt.% never-dried aqueous CNCs suspension were obtained from CelluForce Inc. (Montreal, Canada). Other chemicals such as dodecyl succinic anhydride (DDSA) (90%), potassium bromide (KBr) in powder form, sodium hydroxide (NaOH) pellets, 0.5 M hydrochloric acid (HCl), deuterated dimethyl sulfoxide (DMSO-d6), phenolphthalein, reagent alcohol (EtOH) (99.0%), and acetone (99.9%), were all purchased from Sigma Aldrich, USA. All chemicals were used as received.

4.2.2. Methods

4.2.2.1. Succinylation of CNCs with DDSA

The succinylation of CNCs was carried out by using aliphatic DDSA, as illustrated in **Scheme 1.** For the reaction, about 200 mL of 5 wt.% CNCs aqueous suspension was purged into a glass reactor placed on a magnetic stir plate, and the pH was adjusted to 9.5 using 3 (w/v)% NaOH solution. 5 wt.% of DDSA with respect to the CNCs was then slowly added to the pH adjusted CNCs over 10 min and constantly agitated (250 rpm). The reaction was allowed to run for 3 h at room temperature while maintaining a pH between 9 and 10. The reaction was stopped by neutralization with the addition of dilute HCl (0.5 M HCl) solution. The modified product (referred to as CNC DDSA) was recovered via vacuum drying and washed with ethanol (three times) and acetone (two times) to remove unreacted DDSA. Complete removal of the unreacted DDSA was confirmed by infrared analysis of raffinate from the last washing step. The washed solid sample was subsequently dried at 50 ^{o}C overnight, ground into a fine powder, and stored in a glass vial at room temperature for further analysis. The procedure was repeated for the 10 and 20 wt.% DDSA loadings with respect to CNCs.

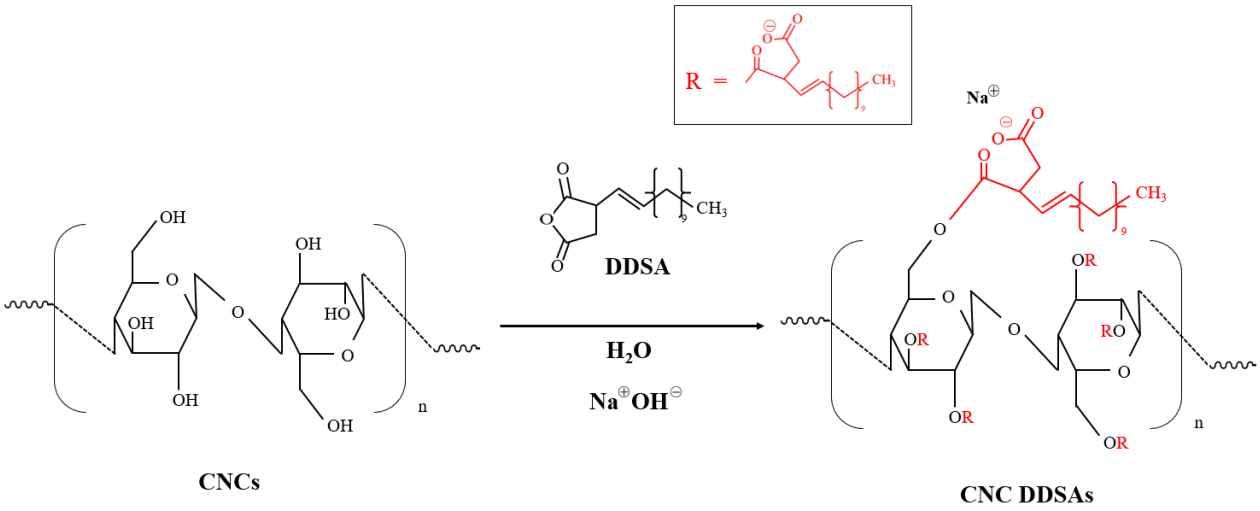

Figure 4.1. Chemical reaction of CNC with DDSA. The succinylation favors the C2 position, but the grafting is possible at C2, C3, and C6.

4.2.2.2. Characterization of the modified CNCs

Fourier transform infrared spectroscopy (FTIR)

The modification of CNCs was characterized at ambient temperature using FTIR (Nicolett 6700, Thermo Scientific Inc.). Native and modified CNC samples for the IR were prepared by mixing the powder samples with KBr salt (5 mg sample and 200 mg KBr) and pressing them into pellets at 10,000 psi for 2 min. On the other hand, DDSA was prepared by adding the liquid directly to a potassium bromide (KBr) salt pellet and dried under vacuum overnight. FTIR scans, in transmittance mode, were recorded in the range of 4000 to 500 cm^{-1} under the same conditions as the background.

Proton nuclear magnetic resonance (H-NMR)

Proton nuclear magnetic resonance (H-NMR) spectra of the baseline and modified CNCs (CNC-DDSAs) at different modification levels were recorded to analyze the chemical changes resulting from the reaction. For this, the samples were dissolved in deuterated dimethyl sulfoxide (DMSO-d6) at 50 ^{o}C and sealed in 5 mm NMR analysis tubes with a ratio of 10 mg solid sample to 0.7 mL solvent. The H-NMR spectra were collected from 0 to 7 ppm using Bruker 500 MHz high-resolution NMR (Bruker-SpectroSpin 500 MHz Ultra shield, Bruker Corporation, MA). The integration peaks of the CNC-DDSAs spectra were analyzed using TopSpin v4.1.3 to calculate the degree of substitution (DS).

Titration test

The percentage of DDSA substitute onto the anhydroglucose unit of CNCs was determined using a modified titration method adopted from Bhosale & Singhal [201]. For the titration, 25 mL of 0.5 M NaOH was added to a suspension of the modified CNCs (5 g of sample in 50 mL water). The mixtures were constantly agitated for 24 h (200 rpm) at ambient temperature in an orbital shaking incubator before titration. Then, the excess alkali was back titrated to a phenolphthalein endpoint

with 0.5 M HCl. A suspension of blank CNCs was also titrated as a baseline. Titrations were repeated three times for each sample. The percentage of DDSA substitution and the degree of substitution (DS) of –OH moieties on the anhydroglucose units were then calculated according to equations (1) and (2):

$$\%\text{DDSA substitution} = \frac{(V_{blank} - V_{sample}) * 0.1 * C_{HCl} * 100\%}{W_{sample}} \quad (1)$$

Where C_{HCl} is the concentration in molarity of the HCl solution; V_{blank} and V_{sample} are the volume (mL) of the HCl solution required for the back titration of blank CNC and modified CNC DDSA, respectively; W_{sample} is the weight (g) of the samples.

$$DS_{Titration} = \frac{162 \times \%\text{DDSA substitution}}{266 \times (100 - \%\text{DDSA substitution})} \quad (2)$$

Where 162 g/mol is the molecular weight of the anhydroglucose unit and 266 g/mol is the molecular weight of the dodecyl succinic anhydride group

Zeta potential

The zeta potential (ζ-potential) of pristine and modified CNC particles dispersed in water was obtained using a Malvern Zetasizer (Nano ZS90) by dispersing the particles in deionized water with a concentration of 0.1 wt.%. Values for zeta potential were determined from the average of three measurements, consisting of 12 runs per measurement.

Thermogravimetric analysis (TGA)

The thermal degradation behavior of the pristine and selected CNC-DDSA was evaluated using a high-resolution thermogravimetric analyzer system (TGA 2 STAR system, Mettler Toledo, Switzerland). Sample powders were dried at 70 ^{o}C overnight to remove moisture, and 10 mg of the materials were loaded onto ceramic crucibles in the machine. The TGA was carried out from 30 to 500 ^{o}C at a heating rate of 10 ^{o}C/min and a nitrogen flow of 20 mL/min.

Water contact angle (WCA)

Water contact angle (WCA) measurement of neat and modified CNCs was carried out using a custom-built optical sessile drop system. About 5 μL of a water droplet was dropped onto the prepared sample sheets, and images were taken after 10 seconds. A built-in Matlab tool was used to measure the contact angles of the water droplets.

4.2.2.3. Preparation of the starch-beeswax nanocomposite emulsion

After selecting the optimal degree of modification of the CNCs, both the native CNCs and selected CNC DDSA were added to starch and beeswax solution mixtures at various concentrations as Pickering emulsion stabilizers. The investigated formulations in this study are shown in **Table 4.1.**

Aqueous dispersions of 5% (w/v) corn starch was gelatinized at 90 ^{o}C using a stirring hot plate to prepare the emulsions. Glycerol was then added as a plasticizer at a weight ratio of 70/30 of starch/glycerol. Beeswax was fully melted at 90 ^{o}C before it is added to the plasticized starch at a ratio of 67% (plasticized starch) to 33% (beeswax) on a dry weight basis based on these preliminary experimentations. The ratio of starch to beeswax was selected based on preliminary experimentations that demonstrated that 33% beeswax is the optimal concentration to obtain a self-standing film with sufficient physical properties. The nano-sized emulsion stabilizers (native and modified CNCs) at various concentrations were dispersed in DI water, added directly to the starch-beeswax mixture, and stirred (250 rpm) at 90 ^{o}C for 30 min. Subsequently, the starch – beeswax – CNCs/modified CNCs mixture was homogenized at 10,000 rpm for 5 min using a high-speed homogenizer (Homogenizer, PowerGen 700) while maintaining the temperature at 90 ^{o}C. The generated Pickering emulsion was then kept in a water bath at 70 ^{o}C until further testing.

Table 4.1. Formulations of plasticized starch-beeswax (S-BW) emulsions that forms solid coatings and films

Sample	Emulsion compositions		Stabilizing filler (with respect to starch)	
	Starch (%)	Beeswax (%)	CNC (%)	CNC DDSA (%)
S	100	0	-	-
S-BW	67	33	-	-
S-BW-1% CNC	67	33	-	1
S-BW-2% CNC	67	33	-	2
S-BW-5% CNC	67	33	-	5
S-BW-1% CNC DDSA	67	33	1	-
S-BW-2% CNC DDSA	67	33	2	-
S-BW-5% CNC DDSA	67	33	5	-

4.2.2.4. Fabrication of starch-beeswax film

To fabricate films, each of the emulsion formulations was cast onto non-stick circular polystyrene mold. These films were then allowed to dry at 40 ^{o}C for 48 h in a conventional oven. Finally, the films were carefully peeled off the mold, conditioned at room temperature and 50% relative humidity for another 24h, and stored in sealed zip-lock bags until further testing.

4.2.2.5. Pickering emulsion characterization

An optical microscope (Olympus BX53M polarizing optical microscope, USA) with a built-in SC 100 camera system was employed to determine the dispersion of beeswax in the starch solution. The average particle sizes of beeswax of selected formulations were recorded. Pictures were collected at ×20 and ×50 objective magnifications. The stability of the selected emulsions was determined by observing beeswax particle size change over 7 days.

The blends surface morphology with and without nanoparticle stabilizers, as well as the dispersion of nanoparticles, were recorded using AFM (Veeco Digital Instrument, Dimension 3100) with a NanoScope IV controller on casted film samples. Images were taken at a size of 10×10 μm^2, and a scan rate of 1 Hz was used. Tapping phase mode was used to detect differences in stiffness of the material phases within the blends.

Rheology measurements, such as the apparent viscosity, elastic modulus (G'), and viscous modulus (G") of the various emulsion formulations were studied at 70 ^oC using a stress-controlled rotational rheometer (HAAKE Mars 3, Thermo Scientific) with a parallel plate geometry and a gap of 1 mm between the plates. Approximately 1 mL of emulsion samples were used for the rheology measurement with amplitude strain sweep measurement at 1 Hz. The emulsion rheology study was conducted one day after the initial preparation of the emulsions.

4.2.2.6. Characterization of the films

Morphology analysis

The morphology of the various starch - beeswax films was investigated using a polarizing optical microscope (Olympus BX53M polarizing optical microscope, USA). 50 μm thickness samples of S, S-BW, and S-BW-CNC and S-BW-CNC DDSA were prepared from the fabricated nanocomposite films, and images were collected using ×50 objective magnification.

Barrier properties

The water permeability of the various films was investigated in accordance with ASTM E96/E96M-16. The water vapor transmission rates (WVT) were measured using barrier cups with an exposed area of 10 cm^2. The barrier cups were filled with 7 mL distilled water (RH = 100%) with the film placed over the opening of the cups and tightly clamped with screw lids. The cups were then placed inside a sealed chamber at 23 ^oC and 30% relative humidity (RH). The weight

loss resulting from water permeation through the film was recorded at different time intervals up to seven days. WVT values (g/m^2.h) were determined according to equation (3):

$$WVT = \frac{\Delta G}{t} \times \frac{1}{A} \quad (3)$$

Where *ΔG/t (g/h)* is the linear slope of the weight loss vs. time graph, and *A (m^2)* was the exposed area of the water barrier cup. WVP values (kg. m/m^2.s.Pa), was calculated based on equation (4):

$$WVP = \frac{WVT\ x\ l}{S\ (RH_1 - RH_2)} \quad (4)$$

Where *l (m)* was the thickness of the films; *S* was the saturation vapor pressure at 23 ^{o}C; RH_1 and RH_2 were the fractional relative humidity inside and outside the test cup, respectively. Three specimens for each sample were used, and the average values were reported.

The oxygen permeability (OP) tests were performed using a customized bubble flow rate setup. Films (18.10 cm^2) were used to seal a two-chamber cartridge attached to an oxygen gas source on one end and a bubble flow meter on the other end. The pressure difference between the two chambers was set at 5 psi, allowing the oxygen to permeate through the membrane. The flux of bubbles was determined by counting the time the bubbles took to travel 50 mL volumetric unit. The OP values (cm^3.m/m^2.day.Pa) was then calculated using equation (5):

$$OP = \left(\frac{V}{t.A}\right) \times \frac{l}{\Delta P} \quad (5)$$

Where *V/(t.A) (cc/m^2.day)* is the flux of oxygen; *l* (m) was the thickness of the films; and *ΔP* (Pa) is the pressure difference between two sides of the film. Triplicate measurements were conducted at room temperature and 50% RH.

Tensile property testing

Tensile tests were carried out using a tensile testing unit (AGS-X series, Shimadzu, Japan) with a 500 N load cell according to ASTM D882-18. Films fabricated by the solvent casting method were

cut into 70 x 10 mm pieces with a gauge length of 50 mm. Testing was conducted at room temperature and a strain rate of 5 mm/min. For each formulation, at least five samples were tested, and the average was reported.

4.2.2.7. Fruit coating applications

Based on the results obtained from the emulsion and film properties characterization, an optimized coating formulation was identified as the most promising material to be tested as the representative edible coating formulations, as shown in **Figure 4.2**. Fresh Gala apples, bananas, and strawberries were purchased from a local supermarket. All the fruits were rinsed and dried with a paper towel prior to the coating studies. For banana and strawberries, the fruits were dipped in the coating formulation at 70 ^{o}C, dried for 5 h, and monitored for up to 7 days at room temperature. For apples, the fruits were freshly chopped into similar pieces, dipped in the coating, dried for 5 h at room temperature, and placed in a refrigerator (4 ^{o}C), and monitored for 7 days.

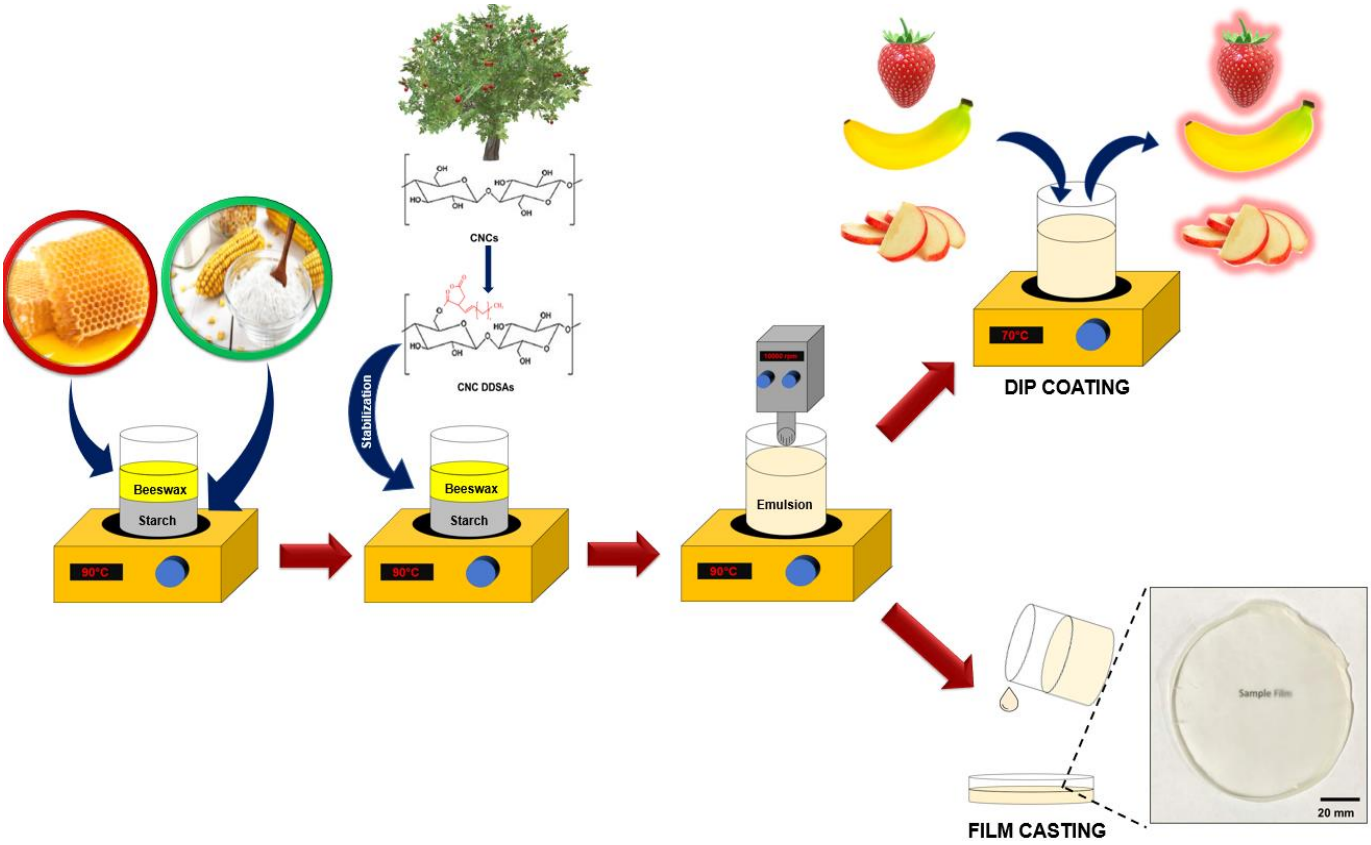

Figure 4.2. The preparation of a high performance, sustainable and edible coating.

Time-lapse study and moisture loss

Moisture loss of fresh fruits was measured daily with a digital balance. In addition, the change in color and shape of the fruits were monitored through time-lapse picture at different times over the course of the seven days.

Stiffness test

The stiffness of the fruits was obtained from the compression test using a tensile testing unit (AGS-X series, Shimadzu, Japan) with 50 mm diameter fixed compression plate and 50 N load cell capacity. Testing of the aged fruits was conducted on the last day of the time-lapse study at room temperature and a strain rate of 20 mm/min. The stiffness was obtained from the initial linear elastic region of the compression test using equation (6):

$$E = \frac{\Delta F}{\Delta x} \quad (6)$$

Where E denotes the stiffness (N/mm), ΔF denotes the applied compressive force, and Δx denoted the deformation of the fruit samples (mm).

Washability test

Optimized film samples were cut into 10 x 10 mm pieces and stirred in DI water at two different temperatures (20 ^{o}C and 40 ^{o}C). Pictures were collected after 15 minutes of constant mechanical stirring.

4.2.2.8. Statistical analysis

Replicate data in this work is presented as mean ± standard deviation. Statistical differences in data were determined using one-way analysis of variance (ANOVA). A significance level of $\alpha < 0.05$ was employed.

4.3. Results and discussions

4.3.1. Characterization of dodecyl succinic anhydride (DDSA)-modified CNCs

4.3.1.1. Fourier transform infrared spectroscopy (FTIR) analysis

FTIR was used as an initial screening tool to confirm and characterize the succinylation reaction between CNC's hydroxyl groups and DDSA. The spectra of pristine and modified CNC samples are recorded and presented in **Figure 4.3**. The native CNC showed some common characteristic peaks at 3600-3000 cm^{-1} (O-H stretching), 2920-2850 cm^{-1} (C-H stretching), 1200-980 cm^{-1} (C-O stretching, C-C stretching, and C-O-H bending from AGU ring), and 900 cm^{-1} (β -glycosidic linkages), similar to other studies [21,151,202,203].

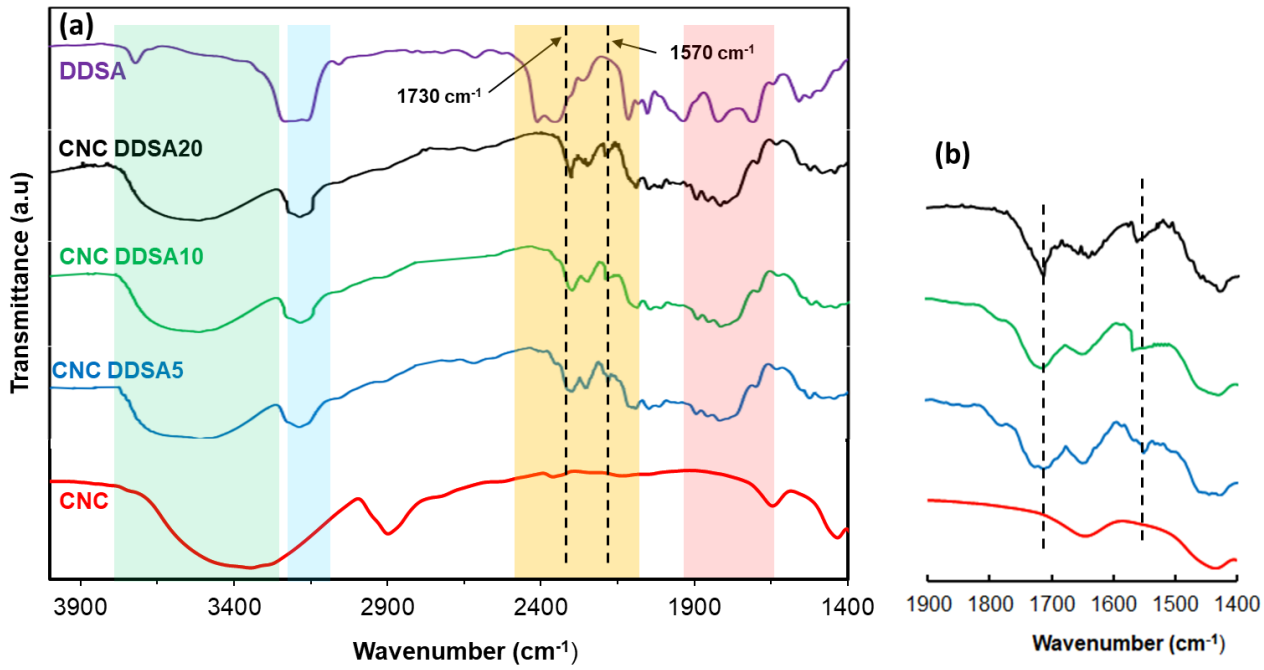

Figure 4.3. FTIR of pristine and modified CNCs at different level (5, 10, and 20 wt.% with respect to CNCs).

The emergence of new IR peaks or the change of some existing peaks displayed the reaction occurrence. The notable changes that confirm the grafting of DDSA on CNC include the presentation of new vibration peaks at 1730 and 1570 cm^{-1}, which correspond to the ester bond's carbonyl (C=O) stretching associated with the open-ring anhydride and the asymmetric stretching vibration of carboxyl group COO-, respectively. These new transmittance bands were observed in all modified CNC DDSA, as shown in **Figure 4.3**. Similar observations on the emergence of these peaks are reported in the literature for other anhydrides [201,204]. Additional evidence of the grafting of DDSA is the broadening of the C-H stretching peak at 2920-2850 cm^{-1}, attributed to the overlapping signal of the alkyl group from the long-chain succinic anhydride. Further comparison of the IR spectra revealed a slight intensity reduction in the broad O-H peak at around 3600-3000 cm^{-1} for all CNC DDSA samples compared to baseline CNCs, showing some substitutions of -OH by DDSA.

A strong transmittance peak at 1820 cm^{-1} is attributed to the close-ring anhydride group, which was presented in only the spectra of DDSA. This observation showed that free DDSA had been completely washed from the modified samples during the purification process. Overall, the IR spectra changes confirmed the progression of succinylation reaction as proposed in **Figure 4.1**.

4.3.1.2. NMR and degree of substitution (DS) analysis

The presence of new hydrogen peaks on H-NMR spectra (**Figure 4.4a)** further confirmed the chemical structure change resulting from the grafting of DDSA onto CNCs. The CNCs and modified CNCs (CNC DDSAs) exhibited characteristic peaks of anhydroglucose units (AGU) in the 5.30-3.00 ppm region. These anhydroglucose signature peaks were identified at 5.30 ppm (O-H protons at positions 2 & 3), 4.45 ppm (O-H protons at position 6), and 3.60-3.30 ppm (protons at positions 2/3/4/5/6) [105]. The peaks noted at 4.70-4.50 corresponded to the equatorial proton of the linear β -1,4 linkages (at position 1) [154].

Figure 4.4b shows the zoomed-in region of the emerging strong signal region from 3.00 to 0.00 ppm presented in all CNC DDSA samples, corresponding to the grafted DDSA on the AGUs. The strong intensity peak at 2.5 ppm was associated with deuterated DMSO (DMSO-d6) solvent used to dissolve the pristine and modified CNCs samples. The additional signals between 2.70 and 0.80 ppm (**Figure 4.4b**), and the presence of a new overlapping signal at about 5.50 ppm were also emanating from the DDSA modification of the CNCs [205]. The peaks from 5.50 ppm were attributed to the protons of the double bond (CH=CH) on the aliphatic chain, while the signals from 2.70-1.20 ppm were assigned to the protons of methylene groups of DDSA [205,206]. Finally, the peaks from 0.90-0.80 ppm represent the methylene group at the very end of the long succinic anhydride chain. It was also noted that there is a gradual increase in the intensity of this methyl peak with an increase in the concentration of DDSA. This was indicative of the successive

increase in the long-chain DDSA grafting onto CNC as more of this DDSA was used in the formulation.

Table 4.2. Zeta potential and level of CNC modification calculated from titration, H-NMR and stoichiometric calculations.

Sample	**ζ-potential (mV)**	**% DDSA substitution**	**$DS_{Titration}$**	**DS_{NMR}**	**$DS_{Theoretical}$**
CNC	-43.40±1.83[a]	0[a]	0[a]	0	0
CNC DDSA 5	-37.36±0.80[b]	1.63± 0.21[b]	0.010± 0.001[b]	0.014	0.030
CNC DDSA 10	-35.43±0.83[c]	3.53 ± 0.25[c]	0.022 ± 0.002[c]	0.028	0.061
CNC DDSA 20	-16.76±1.88[d]	5.57± 0.35[d]	0.039 ± 0.004[d]	0.045	0.122

*****Different letters within the same column are used to denote significant difference between formulations ($p < 0.05$)

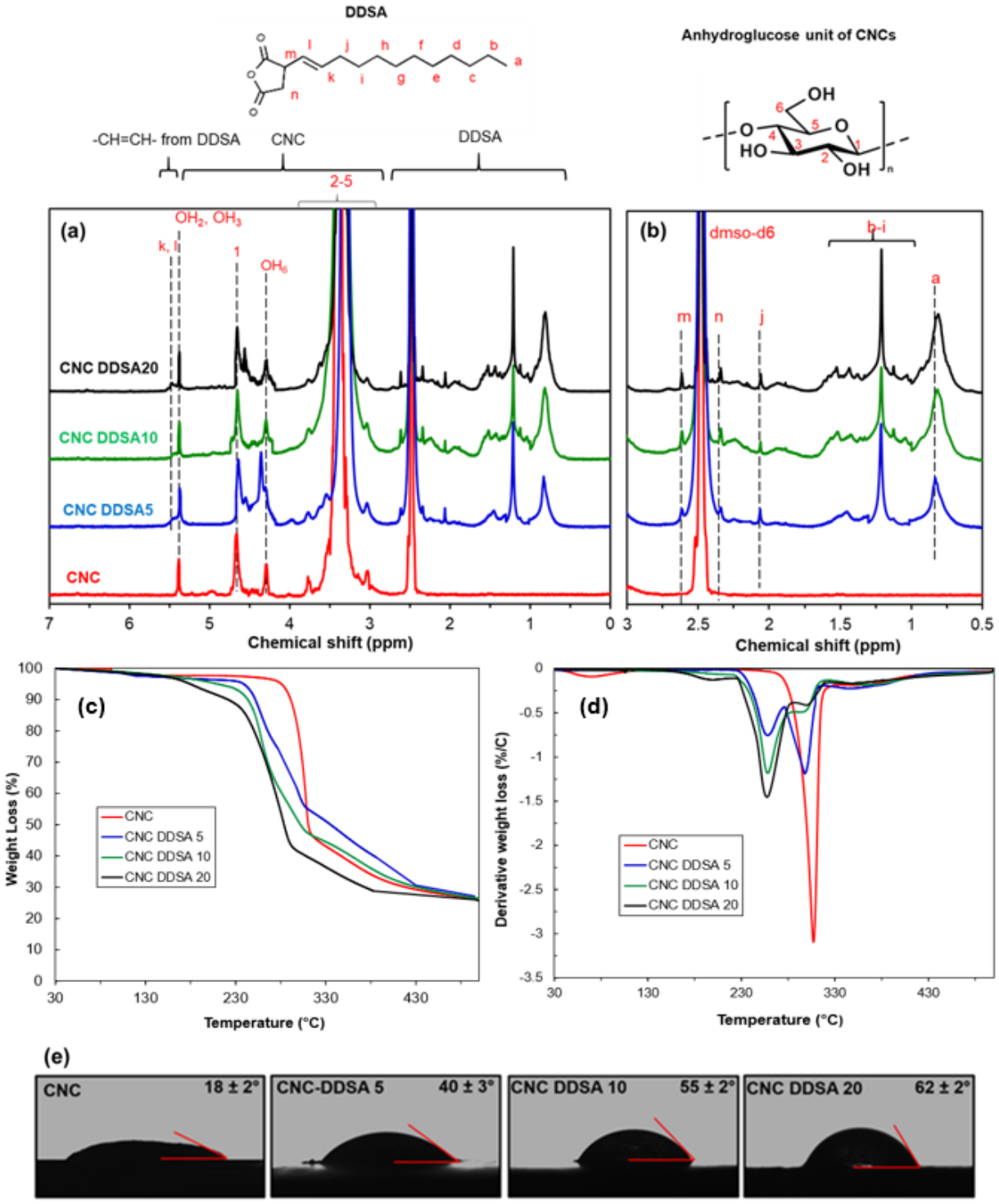

Figure 4.4. (a) H-NMR spectra of pristine and modified CNC at different level (5,10, and 20 wt.% with respect to CNCs); (b) Zoom-in picture of 3-0.5 ppm region; (c) TGA, and (d) DTG of CNC and CNC DDSA 10; (e) WCA images of pristine and modified CNCs.

The degree of substitution (DS) was also quantitatively estimated from the NMR analysis and compared with titration results. For this, the NMR signal corresponding to the reference anomeric

proton of beta glycosidic linkages at position 1 (4.70-4.50 ppm) and the functionalized methyl protons at the end of the long-chain DDSA (0.90-0.80 ppm) were integrated. The modified CNCs' DS were then calculated using Equation (7), which was a modified version from Shih and Daigle [207]:

$$DS_{NMR} = \frac{I_{0.90-0.80}}{3 * (I_{4.70-4.50})} \quad (7)$$

Where $I_{0.9\text{-}0.8}$ is the integrated peak of the methyl protons of long-chain aliphatic anhydride observed at 6.30 ppm. $I_{4.7\text{-}4.5}$ is the contribution from equatorial protons of the β-1-4 glycosidic linkage of AGUs, which is presented at around 4.70-4.50 ppm.

The DS values associated with the succinylation were also estimated using a titration method (**Table 4.2)**. Overall, the results showed that the % DDSA substitution and DS have gradually increased from 1.63 % to 5.57 %, and 0.010 to 0.039, respectively, with increasing the concentration of DDSA in the reaction from 5 to 20 wt.% with respect to CNCs. The resulting DSs were all less than 0.3, pointing out that the reaction only happens on the surface CNC, which helps maintain the crystalline structure of the CNCs. Further increase in DDSA did not seem to increase the substitution levels substantially. This was likely because the crystalline structure of CNCs was largely unaffected by the employed solvent and reaction condition. As such, the grafting reaction was limited to the surface –OH groups of CNCs as desired. Moreover, the long-chain DDSA could have caused steric hindrance that limits high levels of the succinylation reactions. The observed DS are comparable to other aliphatic succinic anhydrides reported in the literature. For instance, Bai and Shi reported a low grafting DS of 0.05 using 15% OSA in waxy corn starch [208]. The highest DS reported in the literature was a DS of 0.110 for the modification of tapioca starch at room temperature using 15% OSA[205]. Ruan et al reported a DS of 0.012 at room temperature

and a maximum DS of 0.014 at 35°C for the modification of potato starch with 3% OSA, showing that temperature slightly effects the reaction efficiency of the succinylation reaction [198].

Comparison of the DS values calculated from the titration method to H-NMR (**Table 4.2**) indicated good agreement on the succinylation trends. However, the values obtained from H-NMR were overall higher than the titration values across all samples. The lower DS values obtained from the titration method might have been contributed by the variation in the dispersibility of the modified CNCs in water that affected the titration end-point detection. The expected theoretical DS was also calculated from stoichiometry and shown in **Table 4.2**, ranging from 0.03 to 0.122. Comparison of both $DS_{Titration}$ and DS_{NMR} to $DS_{Theoretical}$ indicated that the reaction of CNC with DDSA has comparatively low efficiency, which was magnified at higher DDSA loadings. This low reaction efficiency was anticipated due to the low reactivity of DDSA due the molecular hindrance caused by long alkenyl chains during the reactions.

For food-grade applications, it is preferable to keep the modification of the pristine CNCs low, and DS value should only be around 0.02 [209,210]. Thus, CNC DDSA10 was selected as the representative Pickering emulsion stabilizer for the fruit coating study and referred to as CNC DDSA in the subsequent sections of the manuscript.

4.3.1.3. Zeta potential, WCA, and thermal analysis of CNC and CNC DDSA

The change in the zeta potential of CNCs with the progression of the modifications is shown in **Table 4.2**. Pristine CNCs possessed a strong negative zeta potential (-43.4 mV) associated with the sulfate groups generated during the sulfuric acid hydrolysis of cellulose to produce CNCs[188,211]. Cheng et al. suggested that the negative charge of CNC can help the nanoparticles to manifest better interaction with other negative charged materials such as gold nanorods, as presented in their study [212]. Modified CNCs with DDSA substitutions of 1.63, 3.53, and 5.57% exhibited zeta potentials of -37.36, -35.43, and -16.76 mV, respectively. The increase in the surface

charge with increasing modification levels was attributed to the incremental introduction of carboxyl groups from the ring-opening esterification of the DDSA anhydride (Scheme 1). Based on these observations, it can be anticipated that the higher-level modifications could transition the hydrophilic CNCs to amphiphilic nanoparticles. The results from WCA provided another evidence for the gradual changes in polarity as DDSA is grafted onto the CNCs. In the most modified sample, the contact angle increased up to 74°. This is due to the incremental replacement of the polar –OH groups with the long-chain succinic anhydride groups.

Thermal analysis was carried out to investigate the changes in the thermal stability or decomposition of CNCs due to the succinylation reaction. TG and DTG curves of CNC and CNC DDSAs were evaluated from 30 to 500 ^{o}C and results are presented in **Figure 4.4 (c&d)**, respectively. Native CNCs exhibited rapid thermal decomposition at a peak temperature of around 307 ^{o}C, and generated about 25 wt.% solid residue at 500 ^{o}C, which agrees with other researches on thermal degradation of polysaccharides [74,213]. On the other hand, all of the CNC DDSA samples displayed an early onset degradation (~ 258 ^{o}C) and gradual weight loss as compared to the native CNCs. These two degradation peaks presented in the DTG curves provided further validation of the modification of the CNCs because of the succinylation reaction. The lower thermal stability of CNC DDSA compared to CNC was ascribed to the replacement of surface -OH group by long-chain DDSA, which hinders inter- and intramolecular hydrogen bonding CNCs that effectively reduce its thermal stability stemming from the bonding of materials.

4.3.2. Emulsion study

4.3.2.1. Beeswax particle sizes in emulsion

Figure 4.5(a) displayed the complete plasticization of starch in water with the addition of glycerol. Since both glycerol and starch are soluble in water, starch solution was shown as a single homogenous phase on the microscope and no crystals were detected. The CNC DDSA

nanomaterials were then incorporated into the starch-beeswax emulsion as a Pickering emulsion stabilizer to generate coating emulsions. The Pickering emulsions were kept warm (70 ^{o}C) in a water bath to prevent the beeswax from solidifying. The dispersion and particle size of beeswax in starch solution 24 h after preparation was recorded and displayed in **Figure 4.5(b-h).** The S-BW emulsion without a stabilizer exhibited the largest average particle sizes as the emulsion was destabilized within 24 h. On the other hand, the beeswax maintained their excellent dispersion, as noted from the small particle sizes using CNCs and CNC DDSA as emulsion stabilizers. Comparison of the CNC and CNC DDSA stabilized samples showed that the CNC DDSA has an overall better stabilizing effect. This phenomenon was due to the amphiphilic behavior of the CNCs DDSA resulting from the grafting of the aliphatic chains on the surface of otherwise hydrophilic CNCs. While the hydrophobicity of the aliphatic chains helps the modified CNCs (CNC DDSA) associate with the hydrophobic beeswax phase, the remaining –OH groups allow it to associate with the starch with an overall amphiphilic behavior as illustrated in **Figure 4.5l**.

. It was evident that the beeswax particles size gradually increased as much as twice its original size over the course of 7 days. On the contrary, the formulations with CNC and CNC DDSA stabilizers maintained a high level of stability over time. Comparison of formulations containing CNC and CNC DDSA, the beeswax particle size displayed a higher level of stability with the use of CNC DDSA compared to formulations stabilized with CNC. In particular, agglomeration of beeswax particles was evident on day 5 in formulations containing CNCs, indicating that CNC did not have a similar level of stabilizing effect as the CNC DDSA in the starch-beeswax emulsion.

Similar stabilization of oil/water emulsion with the use of octenyl succinic anhydride modified starch was reported by Tesch et al., in which the OSA moieties of the modified starch was able to adsorb onto the oil phase to prevent oil droplet coalescence [214]. A decreasing trend in beeswax diameter with increasing concentration (1 to 2 wt.%) of both CNC and CNC DDSA samples

suggests that particles are available to stabilize higher amount of starch/beeswax interface and therefore small droplet size. However, increasing the emulsion stabilizer loading from 2 to 5 wt.% showed minimal effect on the particle droplet size, indicating that the emulsion stabilization capacity is limited and has already peaked at 2 wt.% loadings. The stability of S-BW, S-BW-2% CNC, and S-BW 2% CNC DDSA was also investigated using the microscope over the course of 7 days and illustrated in Figure S3.

4.3.2.2. Distribution of nanoparticles in emulsion blend

Atomic force microscopy (AFM) images were collected to visualize the dispersion of the wax with (**Figure 4.5i**) and without (**Figure 4.5j**) the nano-Pickering emulsion stabilizer in the starch phase. Phase images obtained from the tapping mode of AFM imaging, which detects the variation in the stiffness of materials, is an effective method to study the distribution of different components in polymer blends [215]. In this case, beeswax was seen as the bright yellow dispersed phase, while the TPS was indicated as the continuous orange phase. Overall, there was a stark improvement in the beeswax dispersion with the addition of the CNC DDSA emulsion stabilizer, owing to the improved interfacial interaction and compatibility between the TPS and beeswax. CNC DDSA nanoparticles were also observed as bright white nanoparticles (**Figure 4.5j**), which is characteristic of nanocellulose reported in literature [216]. The nanoparticles are fairly well dispersed around the beeswax regions, further supporting the suggested mechanism that these amphiphilic nanomaterials are latching at the interface of the beeswax and starch phases and preventing the beeswax phases from agglomeration in the continuous starch matrices.

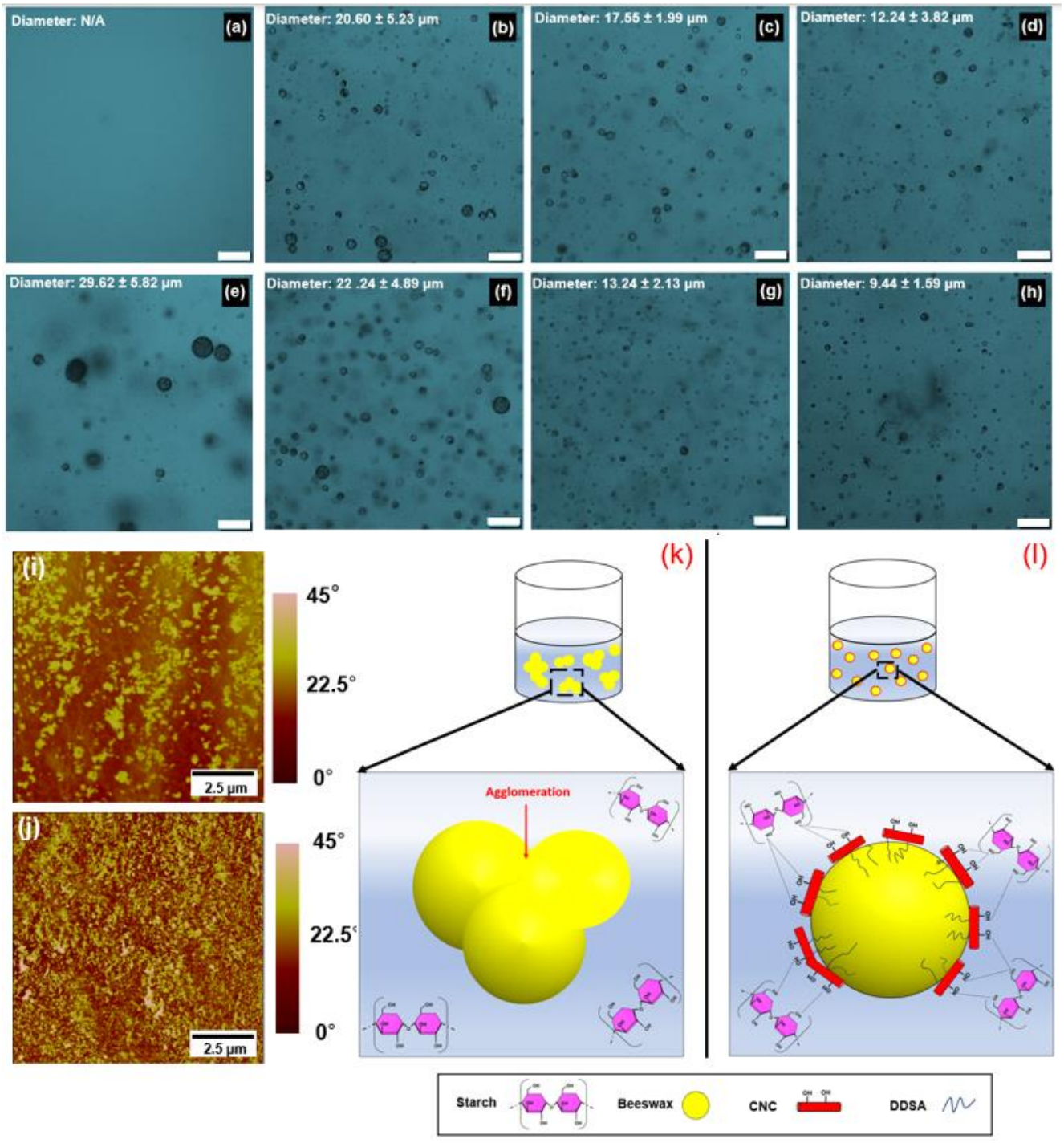

Figure 4.5. Microscope pictures (x 20 magnification) of (a) Starch solution, and starch-beeswax emulsion with ; (b) 1.0% CNC; (c) 2.0% CNC; (d) 5.0% CNC; (e)No emulsion stabilizer (f) 1.0% CNC DDSA; (g) 2.0% CNC DDSA, (h) 5.0% CNC DDSA. The white scale bars are 50 µm. AFM phase image of starch-beeswax emulsion film (i) without emulsion stabilizer and (j) with 2.0% CNC DDSA. Illustration of CNC DDSA as Pickering emulsion stabilizer: (k) Starch-beeswax interface without emulsifier and (l) Starch-beeswax interface stabilized by CNC DDSA

4.3.2.3. Rheology

The rheology of the starch-beeswax nanocomposite emulsion at 70 ^{o}C as a function of shear strain was also collected to determine the emulsion's processability as a coating. The plots of storage (G') and loss (G") moduli versus shear strain were generated (**Figure 4.6a&b**) to evaluate the viscoelastic properties of starch solution and starch-beeswax emulsion microstructure with increasing strain percentage. In general, the starch-beeswax emulsion has much higher emulsion strength compared to the plasticized starch solution alone. The addition of CNC and CNC DDSA nanoparticles increased the overall moduli. At higher concentration loading of 2 and 5 wt.%, G' was significantly higher than G" at low shear strain range and similar values at high shear strain, suggesting the formation of stronger gel-like dispersions with higher viscosity. Emulsions that use CNC DDSA as a Pickering emulsifier showed higher storage and loss modulus, meaning that the emulsion strength is higher at higher concentration loading than emulsions that contain pristine CNCs. This behavior is attributed to the decrease in beeswax droplet size, resulting in increased surface area that increases the droplet network between beeswax and starch interaction present in the stabilized emulsion [217]. Overall, starch and beeswax Pickering emulsions exhibited substantial improvement in the viscoelasticity properties as the storage modulus and loss modulus increased with increasing nanoparticle concentrations, showing signs that the emulsions are integral fluids.

The plots of viscosity versus shear strain were also plotted and displayed in **Figure 4.6c**. Starch-beeswax emulsions exhibited a shear-thinning behavior beyond a strain rate of 10%. This is typical of gel-like hydrocolloids, such as dilute starch solutions, due to the gelatinization from glycerol, as reported in the literature [113,218]. A study by Myeongsu et al. suggested that the shear-thinning behavior is caused by the shear-induced structural breakdown and elongation of the swollen starch granules in the shear direction [196]. The addition of beeswax increased the viscosity due to the

introduction of a new hydrophobic phase in the starch solution. Since no nanoparticle emulsifier was added in the baseline formulation, the viscosity was fairly low, and the viscosity behavior leaned towards a continuous starch solution phase. The incorporation of nano-sized emulsion stabilizers, CNC and CNC DDSA, cause an overall drastic increase in the viscosity of the emulsion at lower shear strain**.** This effect increased with the increase in the concentration of nanoparticle emulsion stabilizer from 1 to 2 wt.%. However, the viscosity remains at the same level when the loading concentration increased to 5 wt.%, indicating that only a certain level of nanoparticles can cover the beeswax droplets and cause the stabilization effect. Overall, increasing viscosity prevents the merger of the dispersed phase, increases the coalescent time, and reduces coalescent stability, leading to a more stable emulsion [219]. In this study, the S-BW-2% CNC DDSA and S-BW-5% CNC DDSA nanocomposite formulations displayed high viscosity and consequently presented high emulsion stability. The slight modification of the CNC that retains most of the –OH functional groups while introducing long aliphatic chains of DDSA provided amphiphilic behavior to the CNCs that stabilized the hydrophilic starch and hydrophobic beeswax phase, resulting in a stable Pickering emulsion.

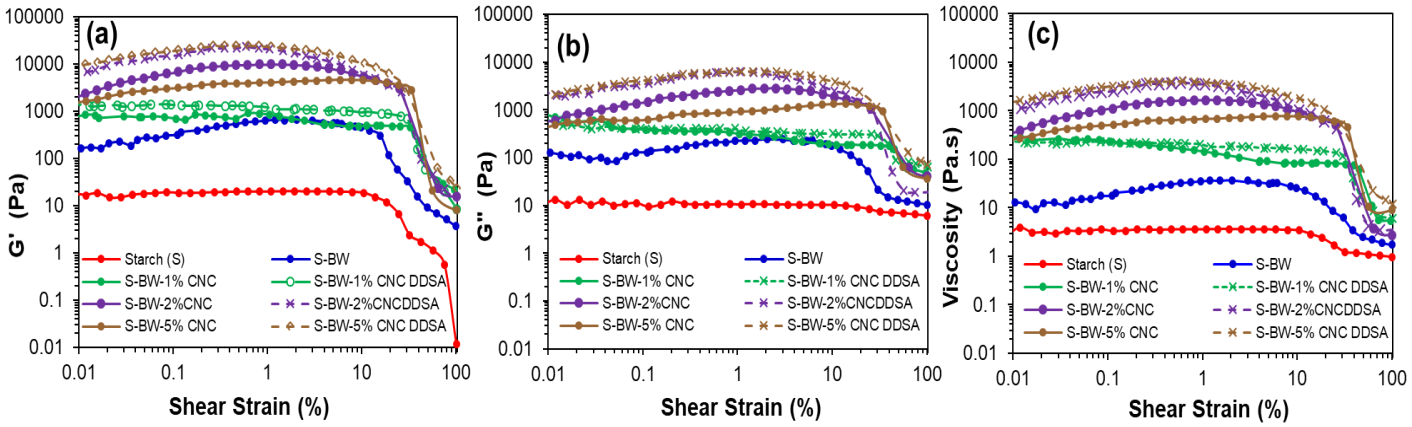

Figure 4.6. Amplitude sweep measurements showing (a) Storage modulus, (b) Loss modulus, (c) and apparent viscosity vs shear strain of starch and starch-beeswax emulsion with different concentrations of emulsion stabilizers.

4.3.3. Characterization of films made from starch-beeswax emulsion

4.3.3.1. Starch-beeswax films and their microstructure

Figure 4.7(i) displays images of plasticized starch and plasticized starch-beeswax emulsion -based films fabricated via a solvent casting process. The incorporation of beeswax has slightly reduced the transparency of the starch films. Nonetheless, all starch-beeswax based films showed good transparency. The S-BW displayed signs of beeswax coalescence indicating that the starch – beeswax emulsion was not stable without the CNC nanomaterial emulsifier as the beeswax colloids separated and solidified to form hydrophobic pockets. In contrast, films that involve the emulsion stabilizers are homogeneous indicating the stability of the starch and beeswax phase in the film.

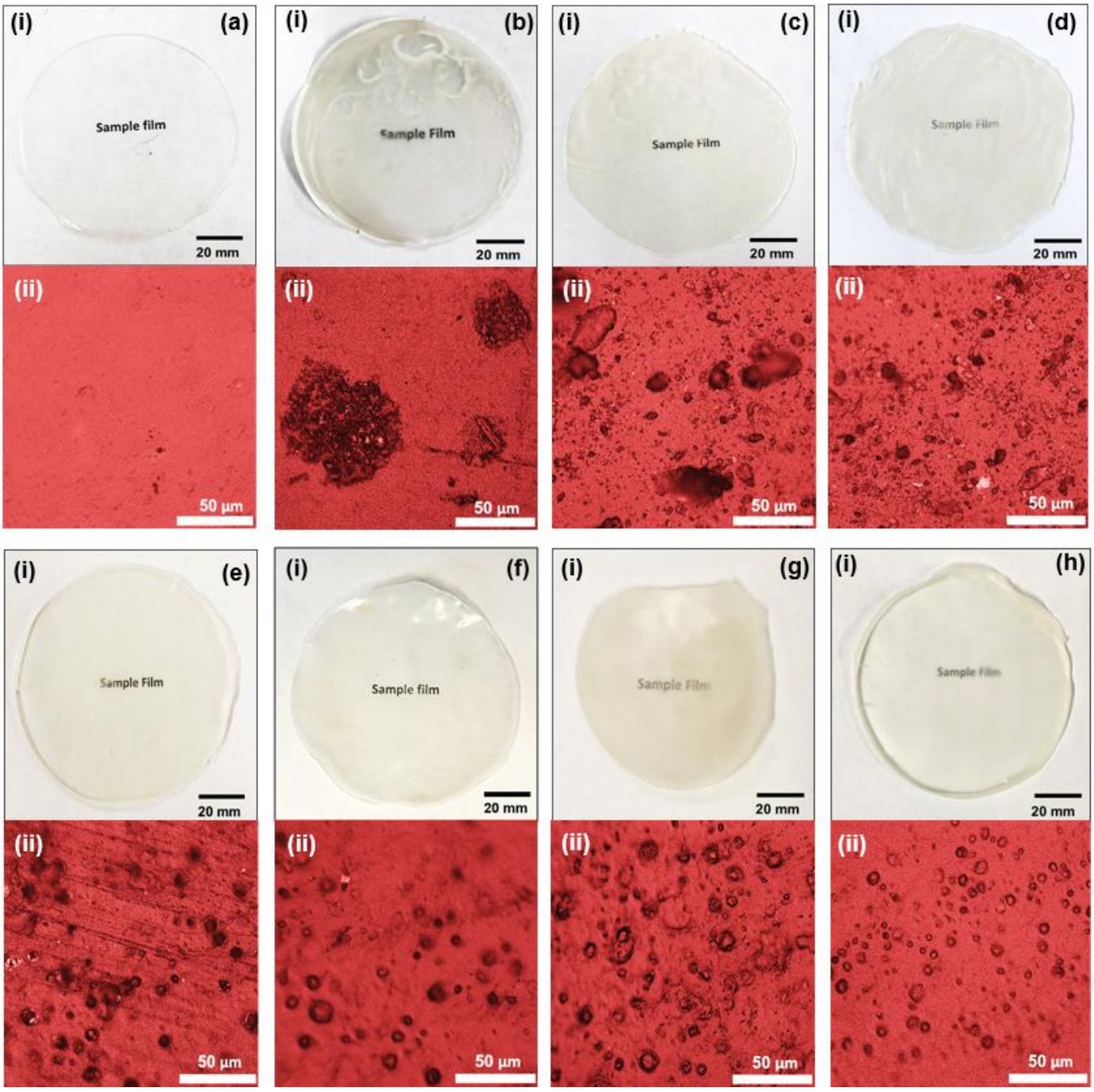

Figure 4.7. (i) Pictures of emulsion film and (ii) optical microscope of the structure of (a) Starch (S), (b) Starch-beeswax (S-BW), (c) S-BW-1.0% CNC, (d) S-BW-2.0% CNC, (e) S-BW-5.0% CNC, (f) S-BW-1.0% CNC DDSA, (f) S-BW-2.0% CNC DDSA, and (f) S-BW-5.0% CNC DDSA films

The microstructures of the formulated films were further investigated with an optical microscope, and images are presented in **Figure 4.7ii**. As anticipated, the beeswax colloids in the S-BW film coalesced together during the drying process resulting in uneven distribution of beeswax in the starch matrices. This is due to the difference in the inherent polarity of the starch and the beeswax. On the other hand, the beeswax colloids were well-distributed in the starch phase with the addition of the nanoparticle (CNC and CNC DDSA) emulsion stabilizers. It was also observed that increasing the concentrations of the CNC and CNC DDSA further reduced the particle size, indicating a greater stabilizing effect at higher nanoparticle concentrations.

Comparison of CNC and CNC DDSA as the emulsion stabilizer indicated that the CNC DDSA based films provided smaller beeswax colloid size and better distribution, indicating greater efficiency as an emulsion stabilizer. This was because of the amphiphilic nature of the CNC DDSA. The grafted DDSA aliphatic tails on the AGU units of CNCs interacted with the non-polar beeswax colloid, while the remaining hydroxyl groups of CNCs stick out into the starch phase and protect the beeswax colloids against aggregation through steric repulsion. Overall, the modification of CNCs with DDSA made it an effective Pickering emulsifier of starch – beeswax emulsion.

4.3.3.2. Oxygen barrier properties

Oxygen permeability (OP) is one of the most important properties that dictate the coatings' applicability in the agriculture and food industries. Oxygen barrier properties of the coating material are necessary to prevent detrimental contacts between the coating surface and the atmosphere to deaccelerate the rate of oxidation of fresh fruits, ultimately protecting the fruits from oxidative rancidity and spoilage [3]. Starch films exhibited excellent oxygen barrier properties, displaying the lower oxygen permeability (OP) (10.82×10^{-3} $cm^3 \cdot m/(m^2 \cdot day \cdot Pa)$) from all the other formulations consisting of beeswax, as shown in **Figure 4.8a.** This is due to the crystalline

structure of starch accrued from the intermolecular and intramolecular hydrogen bonding. However, the corporation of beeswax to the starch film has drastically increased the oxygen permeability (up to 20.80× 10^{-3} $cm^3 \cdot m/(m^2 \cdot day \cdot Pa)$). This observation was anticipated as beeswax has mediocre oxygen gas barrier properties. The poor oxygen barrier property of beeswax is attributed to the ease of the non-polar oxygen molecules to diffuse through the hydrophobic beeswax channel, in conjuncture with the increased adsorption of oxygen from the atmosphere by the beeswax due to the reduced surface tension caused by the beeswax hydrophobicity [22].

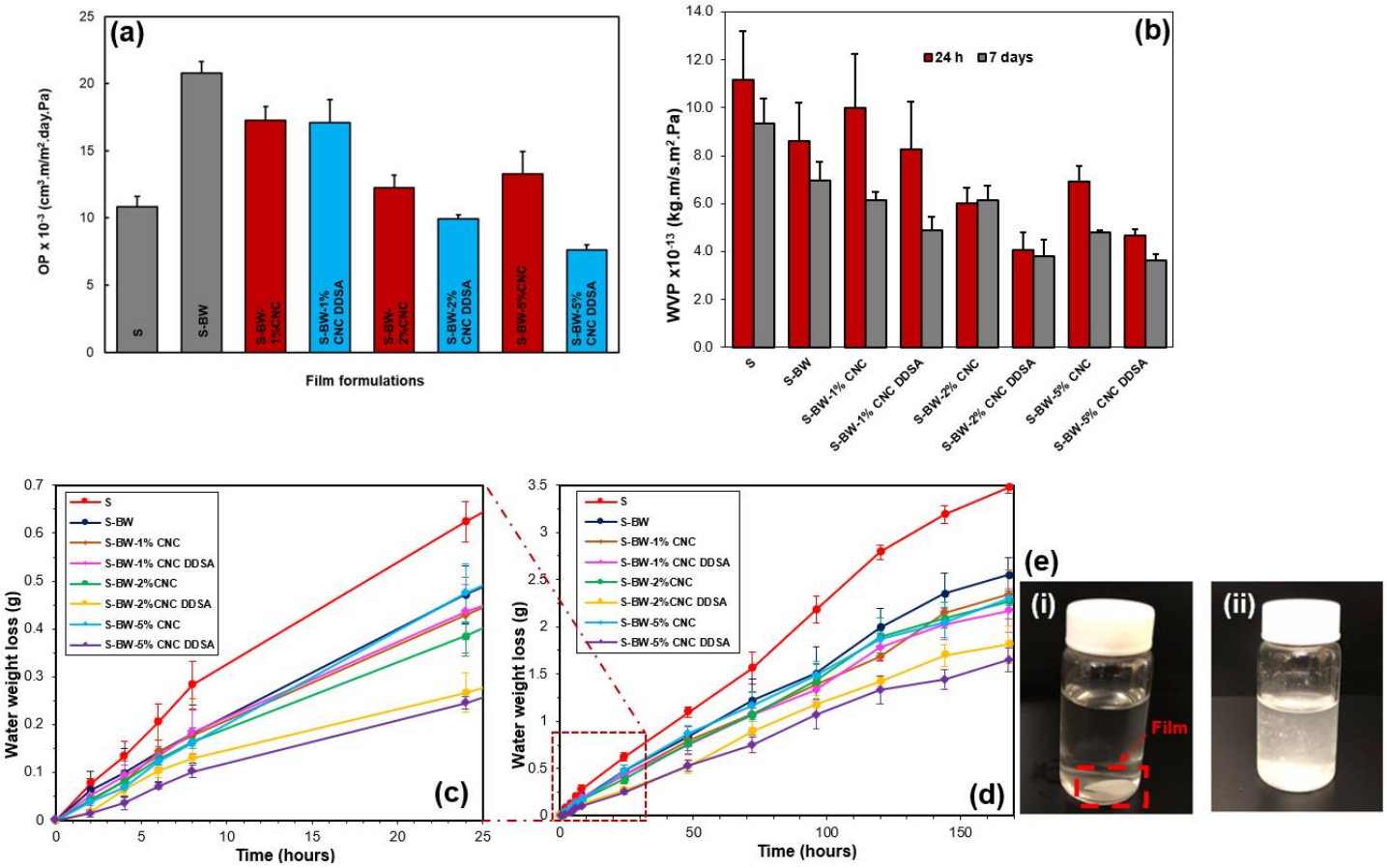

Figure 4.8. (a) Comparison of Oxygen Permeability (OP) values between the films, (b) Comparison of WVP values between the films over different time periods (c and d) Water vapor permeation loss of the starch and starch-beeswax films over time, and (e) Solubility of films after 15 min of mechanical stirring in (i) Room temperature water (20 ^oC) and (ii) lukewarm water (40 ^oC)

On the other hand, the application of CNC and CNC DDSA as emulsion stabilizer additives also affected the oxygen barrier properties of the films, especially at higher loading concentrations. For CNCs, a reduction in the oxygen permeability by 17.1, 41.1, and 37.3 % was observed for CNC concentrations of 1, 2, and 5%, respectively. Contrarily, a greater reduction of 17.9, 52.2, and 63.3% were achieved with the use of CNC DDSA at concentrations of 1, 2, and 5%, respectively. The improved oxygen barrier properties of TPS, stemming from the addition of pristine and modified CNCs as emulsion stabilizers, were the combined effect of the excellent barrier properties of the highly crystalline CNCs and its derivatives in conjuncture with the fine and even dispersion of beeswax in the starch matrices promoted by the Pickering emulsion stabilizers. The CNC DDSA caused a markedly reduced oxygen permeability of the coating films compared to blank CNC, because of its enhanced emulsion stabilizer capability, which reduced the beeswax colloidal particle sizes in the starch film when the film is dried as noted from the optical microscope (**Figure 4.7**). Since CNCs and CNC DDSA are highly crystalline and polar additives, they typically display good barrier properties against the non-polar oxygen molecules and create a tortuous pathway for oxygen in the film resulting in the observed enhancement in the oxygen barrier properties [220].

4.3.3.3. Moisture barrier properties

Moisture barrier is another essential requirement for fruit coating applications because of the frequent moisture migration between the fruit and the environment. One of the most common challenges in the development of starch fruit coating is the poor moisture-barrier properties of the naturally hydrophilic starch and the plasticizers (e.g., glycerol). On the other hand, beeswax is inherently hydrophobic. The incorporation of the beeswax can thus improve the poor moisture barrier properties of starch films and maintains the fruit juices and succulents intact as much as possible when used as a fruit coating. **Figure 4.8 (c & d)** display the water permeation of the

various formulations over 24h and 7 days (168h) duration, respectively. As anticipated, starch films were poor moisture barriers and showed water loss of 8.92 and 44.43% over the course of 24 h and 7 days, respectively. Results in **Figure 4.8b** further highlighted the poor water vapor permeation of the starch (9.35×10^{-13} kg·m/(s·m^2·Pa)), which was consistent with other published results using the similar technique [74,137].

The WVP data presented in **Figure 4.8b** indicated that the inclusion of the beeswax alone in the starch formulation reduced the WVP value over 7 days by 25.6%. It is also important to highlight that the addition of emulsion stabilizers, CNC and CNC DDSA, further improved the water vapor permeability of the starch-beeswax system. Remarkable reductions in the WVP were obtained in the S-BW- 2% CNC DDSA and S-BW-5% CNC DDSA with reductions of 59.5 and 61.3% compared to the starch film, respectively. This was attributed to the fine and even dispersion of the hydrophobic beeswax in the starch film in these formulations, the tortuous pathway created by the CNC DDSA nanoparticles in conjuncture with the hydrophobicity of the modified CNCs (CNC DDSA) emanating from the aliphatic tails. The mechanism of tailoring moisture and gas permeability of films by incorporating nano-sized particles is illustrated in **Figure 4.9**. However, the WVP data (**Figure 4.8b**) did not present a statistical difference between the use of 2 and 5% CNC DDSA. Thus, considering the cost implication as well as the effectiveness of the CNC DDSA material, the 2% CNC DDSA loading could be sufficient to provide the desired moisture barrier properties. Overall, the incorporation of CNC DDSA as a Pickering emulsion stabilizer has improved the water permeability without compromising the oxygen barrier properties of starch, making the combination a suitable candidate in edible fruit coating applications.

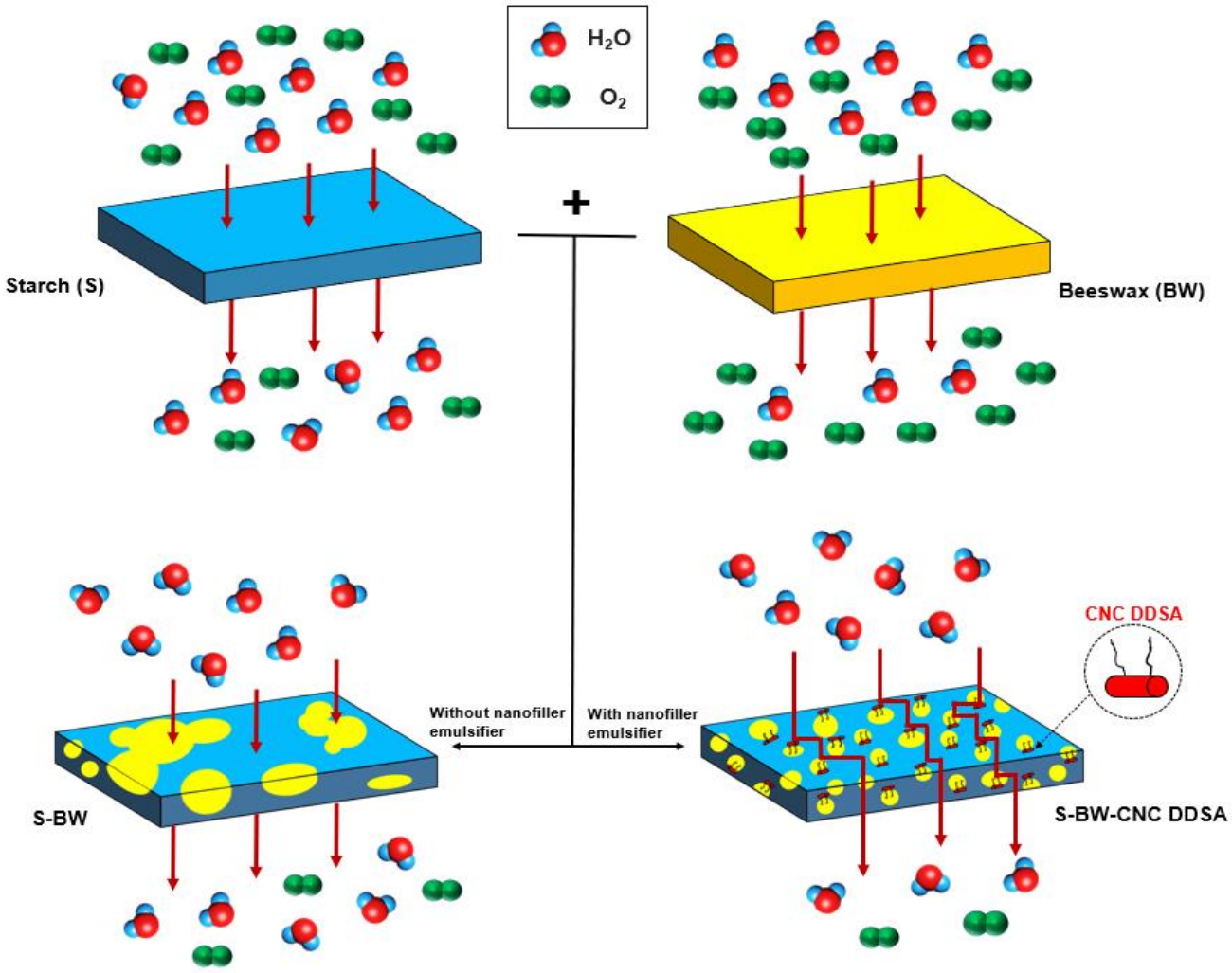

Figure 4.9. Mechanism of water vapor and oxygen permeability through the S-BW edible emulsion film

4.3.3.4. Tensile properties

To investigate the physical integrity of the coating formulations and the effect of the Pickering emulsion stabilizers, tensile testing of the casted films was carried out. It was evident that the addition of beeswax in the starch matrices had deteriorated the overall mechanical properties, as noted from the reduction in the tensile strength, elastic modulus, and elongation. This was because the starch and beeswax mixtures without a stabilizer generated a rough morphology film with poor integrity and immiscible phase separation, as observed from the optical microscope images (**Figure 4.7**).

Contrarily, incorporating CNC and CNC DDSA into the starch – beeswax allowed the generation of a fine dispersion of beeswax, and reduced the effect of phase separation between beeswax solid phase and starch continuous phase during the drying process. Consequently, a significant improvement in the tensile strength and modulus of starch-beeswax film was noted (**Figure 4.10 a & c)** with CNC and CNC DDSA at 1 and 2% loading levels. It is important to highlight that the CNC and modified CNCs also have reinforcing effects in the film in addition to the emulsion stabilization effect. While the CNC DDSA displayed a slight reinforcing effect at 5%, the pristine CNC at 5% deteriorated the mechanical properties of the films. This is attributed to the agglomeration of CNC at high loading levels, as reported in many other studies [221,222]. Overall, the CNC DDSA exhibited great promise as it simultaneously provides emulsion stability and mechanical reinforcement to the coating formulations. Considering the results from this tensile test, as well as barrier properties, the optimized formulation S-BW-CNC 2% DDSA was chosen as a representative material for the fruit coating studies. Comparison of the tensile strength and ductility of the edible coating from this work with other materials such as pectin, chitosan, gelatin, polysaccharide gum, and cassava starch/carnauba wax are shown in **Figure 4.10d** [19,223–225]. Overall, the emulsion film in this study showed much higher ductility compared to other typical food coating materials despite the comparatively low tensile strength. These results suggest that the corn starch-beeswax emulsion coating is quite flexible, which can be beneficial when applied as produce coating.

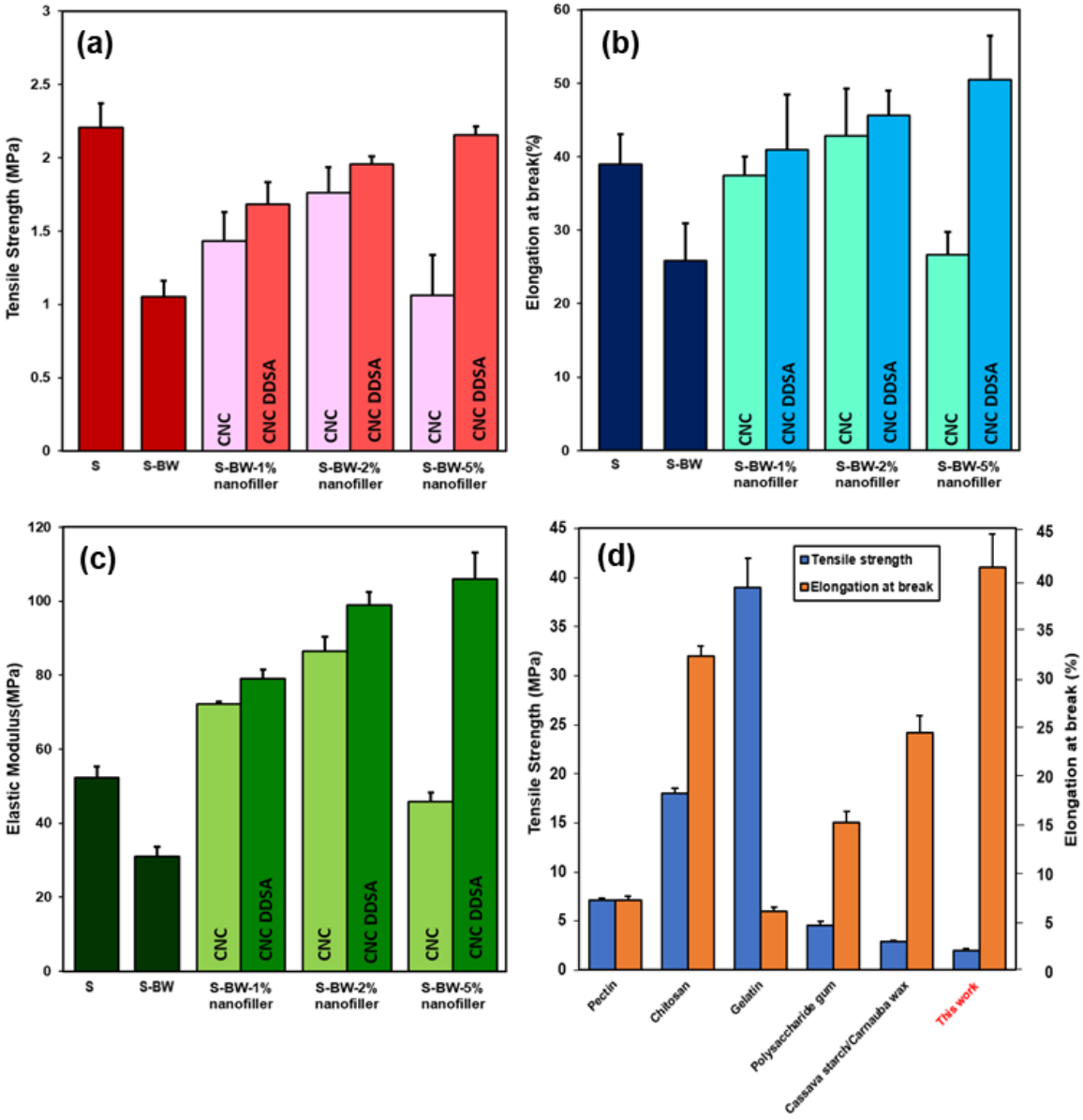

Figure 4.10. Tensile properties of starch and starch-beeswax edible emulsion films with increasing concentration of nanofillers, showing the (a) tensile strength, (b) elongation at break, and (c) elastic modulus. (d) Mechanical properties of the emulsion film compared to other edible coating materials.

4.3.4. Fruit coatings application

4.3.4.1. Fruit quality during storage

To investigate the effectiveness of the optimized emulsion in preserving the freshness of fruits, the S-BW-CNC 2% DDSA formulation was applied on selected fruits by a quick dip-coating

process and then compared with fruit samples without any coating layers. The level of ripening and signs of spoilage was recorded for the selected fruits, bananas (climatic fruits), strawberries (non-climatic fruits), and fresh apple slices, which were then monitored over seven days.

The coatings employed via the dip-coating process were thin with an average thickness and grammage of 25 ± 5 μm and 67.5 ± 7.2 mg/cm^2, respectively. These coatings are transparent and are invisible to the naked eye, indicating that the coatings do not negatively affect the normal appeal of the fruits. Time-lapse images of banana ripening indicated that starch-beeswax emulsion coating decreased the ripening rate of the climatic fruits (**Figure 4.11a**). After 7 days post-purchase, the uncoated bananas showed substantial browning on the exterior due to the accelerated cell respiration rate caused by the production of ethylene gas, which is typical for climatic fruits [226]. On the contrary, the coated bananas showed little to no brown spots on the exterior, indicating that the emulsion coating has significantly prolonged the shelf-life and preserved the banana peel colors.

Moreover, the coated banana's flesh showed a light-yellow color, while the non-coated bananas revealed a darker brown color, demonstrating that the coating preserved the freshness of the bananas (**Figure 4.11b**). Since over-ripen and perished fruits usually become softer in texture, a compressibility test was conducted to investigate the freshness of the fruits further. The coated bananas were shown to have higher stiffness compared to their non-coated samples (**Figure 4.11e**). The higher firmness of the coated bananas is associated with the water retention in the plant cells, which results in an improved cellular elasticity. To help visualize the difference in the firmness of the bare and coated bananas, a weight of 330 g was applied onto both bananas, which are shown in **Figure 4.11c**. While the coated banana retained its integrity, the bare banana displayed a clear dimple due to over-ripening and spoilage.

The coating's efficiency on non-climatic strawberries indicated that the coated strawberries demonstrated a slow and gradual change in appearance and color compared to the non-coated strawberries samples, which underwent a stark decaying and dehydration transformation within the 7 days study time. The time-lapse study displayed that the non-coated strawberries have rotten entirely. In contrast, the coated strawberries showed signs of slight dehydration and a darker color at day 7, exhibiting the deceleration of rotting with the coating (**Figure 4.12a (i)**). The moisture weight loss data for strawberries shown in **Figure 4.12b(i)** indicated that the employed coatings provided a substantial barrier that assisted in limiting the moisture loss from the strawberries. The stiffness of the strawberries was carried out at day 5 when both the coated and non-coated strawberries are still relatively healthy. As expected, the coated samples exhibited much-improved stiffness, with a compressibility value about three times higher compared to their non-coated counterparts (**Figure 4.12c(i)**).

This research also evaluated the benefits of the formulated coatings on fresh-cut fruits, which was demonstrated on sliced apple pieces. When apples are cut into pieces, the flesh color rapidly turned brown due to the release of the polyphenol oxidase (PPO) enzymes and reaction with oxygen from the atmosphere[227]. Moreover, the dehydration rate of cut apple flesh is rapid when exposed to the atmosphere at room temperature, and as such, apple slices are typically stored in a refrigerator. Thus, to observe the effect of the coating on the storage stability of apple slices, both the coated and bare slices were stored in a refrigerator (4 ^{o}C) and monitored over 7 days. The time-lapse images (**Figure 4.12a(ii)**) showed that the coated apple slices had better appearances and retained more moisture compared to the non-coated samples. The difference was most remarkable on day 7, with a reduction of over 15% moisture in the coated slices versus the uncoated slices. The observation is likely due to the protection provided by the coating to the apple flesh from getting in contact with oxygen in the air. This reduces the PPO enzymatic activities and slow down

enzymatic browning in conjuncture with the reduction in moisture migration. The moisture loss and compressibility data (**Figure 4.12b(ii) and c(ii)**, respectively**)** validated the positive impact of the formulated coatings on the apple slices. Overall, water losses of non-coated apples are significantly higher than the non-coated counterparts, which shows the coatings are very effective in maintaining the water content in the apples.

Additionally, apple slices sustained a stiffness of 35 N/mm compared to the mere 15 N/mm value obtained from the non-coated slices, indicating that the emulsion coating helps maintain the freshness and integrity of the apple flesh. In term of efficiency in maintaining moisture loss of flesh apple slices, results of this research are comparable to the recent multilayered edible coatings made from silk fibroin and poly(vinyl alcohol) [9], and better than a previous study by Gago et al. on edible coatings using isolated whey protein and beeswax [228]. Based on the stability of the studied fruits, it was noted that the green and edible Pickering emulsion coating developed in this study has a great potential to be used as a preservation technique to protect fruits from oxidation and preserve the intactness of perishable fruits.

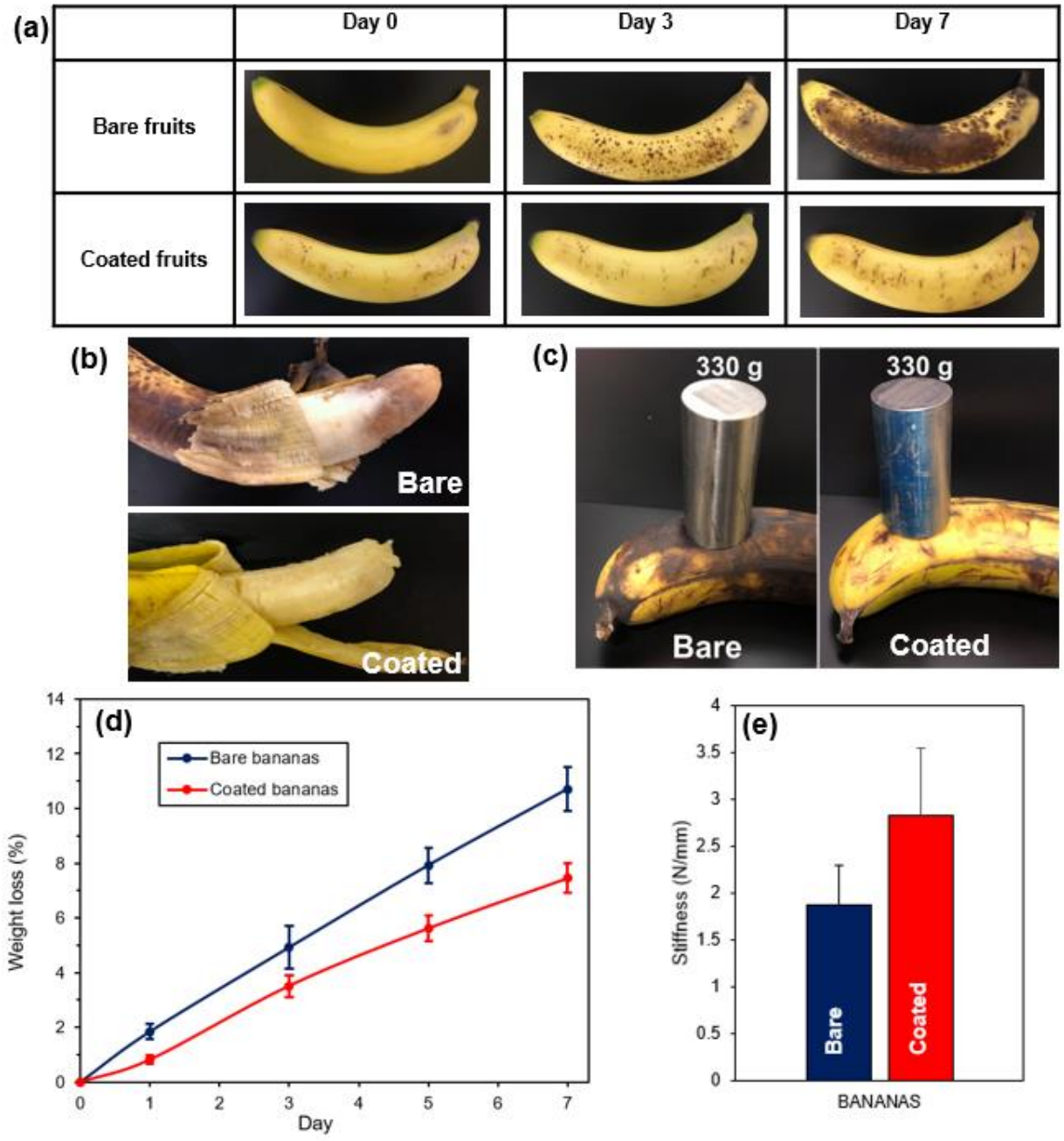

Figure 4.11. Effect of edible emulsion coatings on bananas. (a) Time-lapse photographs of bare and coated bananas over 7 days, (b) Flesh of bananas after 7 days, (c) Illustration of the softness of bare and coated bananas by applying a weight of 330g on top of the fruits, (d) Water weight loss of bananas over 7 days, and (e) comparison between stiffness of bare and coated bananas

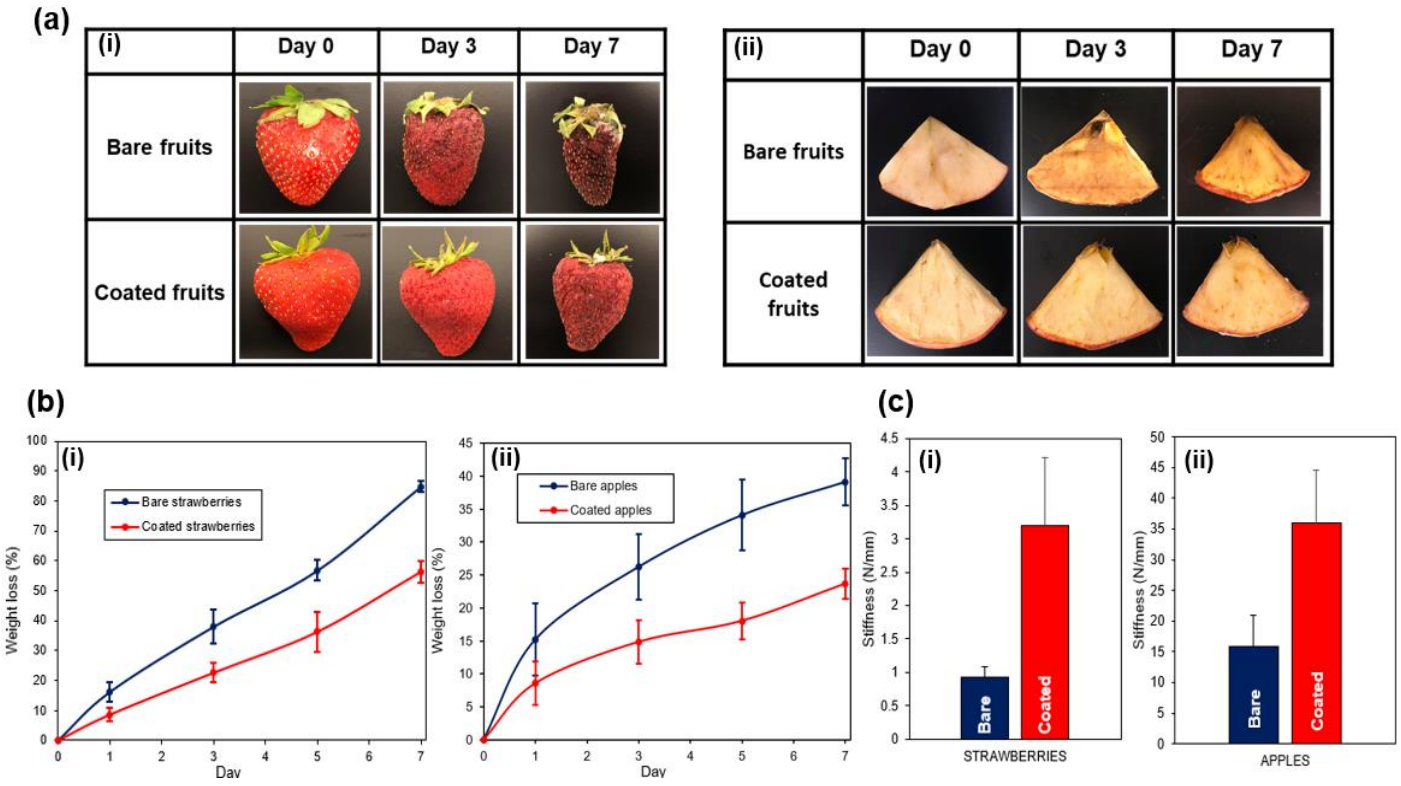

Figure 4.12. Effect of edible emulsion coatings on strawberries and apples. (a) Time-lapse photographs of bare and coated (i) strawberries and (ii) flesh-cut apples over 7 days. (b) Water weight loss of (i) strawberries and (ii) flesh-cut apples over 7 days, and (c) comparison between stiffness of bare and coated (i) strawberries and (ii) flesh-cut apples

4.3.4.2. Coating washability

The washability test was conducted to evaluate the solubility of the coating in water, as most consumers would prefer to eat their fruits without any coatings on them despite that these coatings are considered safe for consumption. **Figure 4.8e** showed the solubility of the coating film at room temperature (20 ^{o}C) and lukewarm (40 ^{o}C) DI water after 10 minutes under slow stirring (50 rpm). The results showed that the starch-beeswax emulsion films maintained their structural integrity when stirred in water at room temperature (20 ^{o}C), owing to the stabilized hydrophobic phase of beeswax inside the films. This waterproof property agrees with the results obtained from water vapor permeability. On the other hand, the films constantly stirred at 40 ^{o}C were mostly disintegrated and dispersed into the DI water. This observation showed that the coatings could be easily washed from the fruit's surface by rinsing with warm water. These results are of great

importance to the applicability of these coatings as it reduces food safety concerns or provide preference flexibility to consumers.

4.4. Conclusions

This research proposed an edible emulsion coating system stabilized and reinforced with green and edible nanomaterials by exploiting a combination of two common nature-derived sustainable materials, starch and beeswax. Characterization of the coating films displayed that the modified CNC stabilized Pickering emulsion generated an excellent barrier film with robust mechanical strength, simultaneous oxygen, and moisture barrier properties. The research has also demonstrated that the starch-beeswax formulated films are effective as edible coatings to preserve the freshness of perishable fruits by preventing contact of the fruits to oxygen and sustaining the moisture content within the fruits. The seven-day fruit freshness study on bananas, strawberries, and flesh-cut apples validated that the formulated coating could retain freshness and appearances of both climatic and non-climatic fruits, potentially extending to other kinds of fruits. Since most of the materials used to fabricate these coatings are edible, abundant, and inexpensive, it is anticipated that the emulsion coating can compete with commercial fruit coatings already in the market.

CHAPTER 5: CONCLUDING REMARKS AND FUTURE WORKS

The transition towards sustainable materials from traditional plastics requires more progressive developments of biodegradable polymer systems, especially in the field of food packaging and food preservation due to their hefty contribution toward landfill waste. There is much interest in the use of different biodegradable and bio-based materials in the multi-phase polymer systems in these packaging and coating applications, as their required barrier properties can be significantly improved compared to individual stand-alone materials. In this thesis, two distinguished multi-phase polymer systems for food packaging and preservation were investigated, and their conclusions from previous chapters are summarized as follows:

1) **Multilayer assembly films made from TPS and PLA:** The structural-barrier relationships were thoroughly analyzed in this study**.** The morphologies obtained by SEM showed that TPS and PLA by themselves showed signs of microscopic gap and delamination, which would potentially inhibit the maximum moisture and oxygen barrier capabilities of the multilayer films. However, this problem was overcome by the enhancement of interfacial interaction between the TPS and PLA layers with the addition of MA chemical grafting onto the backbone of TPS to create MTPS. The WVP results showed that the maleation of TPS in a multilayer system (MTPS/PLA) reduced the water diffusion rate across the films by twice as much as the neat TPS/PLA films. Incorporating nanoclays at optimal loading (3 phr) in the MTPS layer further enhanced the physico-mechanical and moisture/oxygen barrier properties of the multilayer film assembly. Moreover, these multilayer films are composed of compostable, food-grade, inexpensive, and bio-based ingredients, and as such, they are expected to be compostable with great cost structure and environmentally friendly.

2) **Pickering emulsion nanocomposite coatings made from starch and BW:** This research showed that by stabilizing cornstarch and beeswax emulsion with CNC, a sustainable and edible coating that substantially reduces the spoilage of fruits and other produce could be obtained. Surface modification of CNC with aliphatic succinic anhydride DDSA successfully increases the amphiphilicity of the nanomaterials; thus, enhancing the effects of stabilization of lipid BW in starch matrices and reducing the agglomeration of BW when cooling down to room temperature. The fine dispersion of BW particles helps with the reduction of moisture barrier properties of the films. Furthermore, the modified CNC-DDSA also acted as reinforcing nanocomposites materials, which effectively improved both WVP and OP values of the edible films. Banana, strawberries, and apples were dip-coated in this formulated emulsion blend; and the time-lapse images evidently indicated that the fruits with applied coating still maintain decent color and freshness after a week of observations. This studied emulsion is edible and inexpensive, making it an exciting material that can be used to combat fresh produce waste caused by oxidative and enzymatic over-ripening.

To conclude, this chapter will also address the challenges associated with these renewable polymer coatings in the context of food preservation applications such as sustainable packaging and potential edible coating. Although the renewable multi-phase coatings and films presented in this thesis showed enhanced barrier properties and untapped potentials in the food packaging and preservation applications, there is also significant room for further additional improvements such as compostability studies, antimicrobial analysis, and safety assessments.

REFERENCES

[1] A.K. Mohanty, M. Misra, G. Hinrichsen, Biofibres, biodegradable polymers and biocomposites: An overview, Macromol. Mater. Eng. 276–277 (2000) 1–24. https://doi.org/10.1002/(SICI)1439-2054(20000301)276:1<1::AID-MAME1>3.0.CO;2-W.

[2] Y. Zhu, C. Romain, C.K. Williams, Sustainable polymers from renewable resources, Nature. 540 (2016) 354–362. https://doi.org/10.1038/nature21001.

[3] D. Lin, Y. Zhao, Innovations in the development and application of edible coatings for fresh and minimally processed fruits and vegetables, Compr. Rev. Food Sci. Food Saf. 6 (2007) 60–75. https://doi.org/10.1111/j.1541-4337.2007.00018.x.

[4] B.A. Morris, Adhesion, in: Sci. Technol. Flex. Packag., Elsevier, 2017: pp. 351–400. https://doi.org/10.1016/B978-0-323-24273-8.00010-1.

[5] D. Jubinville, E. Esmizadeh, S. Saikrishnan, C. Tzoganakis, T. Mekonnen, A comprehensive review of global production and recycling methods of polyolefin (PO) based products and their post-recycling applications, Sustain. Mater. Technol. 25 (2020) e00188. https://doi.org/10.1016/J.SUSMAT.2020.E00188.

[6] S. Saikrishnan, D. Jubinville, C. Tzoganakis, T.H. Mekonnen, Thermo-mechanical degradation of polypropylene (PP) and low-density polyethylene (LDPE) blends exposed to simulated recycling, Polym. Degrad. Stab. 182 (2020). https://doi.org/10.1016/j.polymdegradstab.2020.109390.

[7] R. Geyer, J.R. Jambeck, K.L. Law, Production, use, and fate of all plastics ever made, Sci. Adv. 3 (2017). https://doi.org/10.1126/SCIADV.1700782.

[8] R. Muthuraj, T. Mekonnen, Recent progress in carbon dioxide (CO 2) as feedstock for sustainable materials development: Co-polymers and polymer blends, Polymer (Guildf). 145 (2018) 348–373. https://doi.org/10.1016/j.polymer.2018.04.078.

[9] E. Ruggeri, D. Kim, Y. Cao, S. Farè, L. De Nardo, B. Marelli, A Multilayered Edible Coating to Extend Produce Shelf Life, ACS Sustain. Chem. Eng. 8 (2020) 14312–14321. https://doi.org/10.1021/acssuschemeng.0c03365.

[10] L.S. Dilkes-Hoffman, S. Pratt, P.A. Lant, I. Levett, B. Laycock, Polyhydroxyalkanoate coatings restrict moisture uptake and associated loss of barrier properties of thermoplastic starch films, J. Appl. Polym. Sci. 135 (2018) 46379. https://doi.org/10.1002/app.46379.

[11] T.H. Mekonnen, T. Haile, M. Ly, Hydrophobic functionalization of cellulose nanocrystals for enhanced corrosion resistance of polyurethane nanocomposite coatings, Appl. Surf. Sci. 540 (2021) 148299. https://doi.org/10.1016/J.APSUSC.2020.148299.

[12] T. Mekonnen, P. Mussone, H. Khalil, D. Bressler, Progress in bio-based plastics and plasticizing modifications, J. Mater. Chem. A. 1 (2013) 13379–13398. https://doi.org/10.1039/c3ta12555f.

[13] A. Chamas, H. Moon, J. Zheng, Y. Qiu, T. Tabassum, J.H. Jang, M. Abu-Omar, S.L. Scott, S. Suh, Degradation Rates of Plastics in the Environment, ACS Sustain. Chem. Eng. 8 (2020) 3494–3511. https://doi.org/10.1021/ACSSUSCHEMENG.9B06635.

[14] V.M. Pathak, Navneet, Review on the current status of polymer degradation: a microbial approach, Bioresour. Bioprocess. 4 (2017). https://doi.org/10.1186/S40643-017-0145-9.

[15] H.J. Park, Development of advanced edible coatings for fruits, Trends Food Sci. Technol. 10 (1999) 254–260. https://doi.org/10.1016/S0924-2244(00)00003-0.

[16] N. Le Bolay, A. Lamure, N. Gallego Leis, A. Subhani, How to combine a hydrophobic matrix and a hydrophilic filler without adding a compatibilizer - Co-grinding enhances use properties of Renewable PLA-starch composites, Chem. Eng. Process. Process Intensif. 56 (2012) 1–9. https://doi.org/10.1016/j.cep.2012.03.005.

[17] Y. Parulekar, A.K. Mohanty, Extruded Biodegradable Cast Films from Polyhydroxyalkanoate and Thermoplastic Starch Blends: Fabrication and Characterization, Macromol. Mater. Eng. 292 (2007) 1218–1228. https://doi.org/10.1002/MAME.200700125.

[18] R. Ortega-Toro, I. Morey, P. Talens, A. Chiralt, Active bilayer films of thermoplastic starch and polycaprolactone obtained by compression molding, Carbohydr. Polym. 127 (2015) 282–290. https://doi.org/10.1016/j.carbpol.2015.03.080.

[19] M. Chiumarelli, M.D. Hubinger, Stability, solubility, mechanical and barrier properties of cassava starch – Carnauba wax edible coatings to preserve fresh-cut apples, Food Hydrocoll. 28 (2012) 59–67. https://doi.org/10.1016/J.FOODHYD.2011.12.006.

[20] J.F. Mendes, R.T. Paschoalin, V.B. Carmona, A.R. Sena Neto, A.C.P. Marques, J.M. Marconcini, L.H.C. Mattoso, E.S. Medeiros, J.E. Oliveira, Biodegradable polymer blends based on corn starch and thermoplastic chitosan processed by extrusion, Carbohydr. Polym. 137 (2016) 452–458. https://doi.org/10.1016/j.carbpol.2015.10.093.

[21] M. Ly, T.H. Mekonnen, Cationic surfactant modified cellulose nanocrystals for corrosion protective nanocomposite surface coatings, J. Ind. Eng. Chem. 83 (2020) 409–420. https://doi.org/10.1016/j.jiec.2019.12.014.

[22] J.H. Han, G.H. Seo, I.M. Park, G.N. Kim, D.S. Lee, Physical and mechanical properties of pea starch edible films containing beeswax emulsions, J. Food Sci. 71 (2006) 290–296. https://doi.org/10.1111/j.1750-3841.2006.00088.x.

[23] A. Rodríguez, R. Batlle, C. Nerín, The use of natural essential oils as antimicrobial solutions in paper packaging. Part II, Prog. Org. Coatings. 60 (2007) 33–38. https://doi.org/10.1016/J.PORGCOAT.2007.06.006.

[24] A. Alissandratos, N. Baudendistel, S.L. Flitsch, B. Hauer, P.J. Halling, Lipase-catalysed acylation of starch and determination of the degree of substitution by methanolysis and GC, BMC Biotechnol. 10 (2010). https://doi.org/10.1186/1472-6750-10-82.

[25] S. Kandasamy, J. Yoo, J. Yun, H.-B. Kang, K.-H. Seol, H.-W. Kim, J.-S. Ham, Application of Whey Protein-Based Edible Films and Coatings in Food Industries: An Updated Overview, Coatings 2021, Vol. 11, Page 1056. 11 (2021) 1056. https://doi.org/10.3390/COATINGS11091056.

[26] J.F. Martucci, R.A. Ruseckaite, Three-layer sheets based on gelatin and poly(lactic acid), part 1: Preparation and properties, J. Appl. Polym. Sci. 118 (2010) 3102–3110. https://doi.org/10.1002/app.32751.

[27] H.J. PARK, M.S. CHINNAN, R.L. SHEWFELT, EDIBLE CORN-ZEIN FILM COATINGS to EXTEND STORAGE LIFE of TOMATOES, J. Food Process. Preserv. 18 (1994) 317–331. https://doi.org/10.1111/j.1745-4549.1994.tb00255.x.

[28] R.K. Dhall, Application of edible films and coatings on fruits and vegetables, Edible Film. Coatings Fundam. Appl. (2016) 363–390. https://doi.org/10.1201/9781315373713.

[29] B.W. Chieng, N.A. Ibrahim, W.M.Z.W. Yunus, M.Z. Hussein, Poly(lactic acid)/poly(ethylene glycol) polymer nanocomposites: Effects of graphene nanoplatelets, Polymers (Basel). 6 (2014) 93–104. https://doi.org/10.3390/polym6010093.

[30] T. Mekonnen, M. Misra, A.K. Mohanty, Fermented Soymeals and Their Reactive Blends with Poly(butylene adipate-co-terephthalate) in Engineering Biodegradable Cast Films for Sustainable Packaging, ACS Sustain. Chem. Eng. 4 (2016) 782–793. https://doi.org/10.1021/acssuschemeng.5b00782.

[31] John Dixon, Packaging Materials 9. Multilayer Packaging for food and Beverages ILSI Europe Report Series RepoRt Commissioned by the ilsi Europe Packaging Materials Task Force, (2011).

[32] P.K. Samantaray, A. Little, D.M. Haddleton, T. McNally, B. Tan, Z. Sun, W. Huang, Y. Ji, C. Wan, Poly(glycolic acid) (PGA): a versatile building block expanding high performance and sustainable bioplastic applications, Green Chem. 22 (2020) 4055–4081. https://doi.org/10.1039/D0GC01394C.

[33] I. Vroman, L. Tighzert, Biodegradable Polymers, Materials (Basel). 2 (2009) 307. https://doi.org/10.3390/MA2020307.

[34] P.J. Halley, R.W. Truss, M.G. Markotsis, C. Chaleat, M. Russo, A.L. Sargent, I. Tan, P.A. Sopade, A Review of Biodegradable Thermoplastic Starch Polymers, in: 2007: pp. 287–300. https://doi.org/10.1021/bk-2007-0978.ch024.

[35] Q. Sun, T. Mekonnen, M. Misra, A.K. Mohanty, Novel Biodegradable Cast Film from Carbon Dioxide Based Copolymer and Poly(Lactic Acid), J. Polym. Environ. 24 (2016) 23–36. https://doi.org/10.1007/s10924-015-0743-6.

[36] A. Gupta, B. Chudasama, B.P. Chang, T. Mekonnen, Robust and sustainable PBAT – Hemp residue biocomposites: Reactive extrusion compatibilization and fabrication, Compos. Sci. Technol. 215 (2021) 109014. https://doi.org/10.1016/J.COMPSCITECH.2021.109014.

[37] E. Ojogbo, J. Jardin, T.H. Mekonnen, Robust and sustainable starch ester nanocomposite films for packaging applications, Ind. Crops Prod. (2020) 113153. https://doi.org/10.1016/j.indcrop.2020.113153.

[38] R. Grewal, W. Sweesy, J.S. Jur, J. Willoughby, Moisture vapor barrier properties of biopolymers for packaging materials, ACS Symp. Ser. 1107 (2012) 271–296. https://doi.org/10.1021/bk-2012-1107.ch015.

[39] P.E. Keller, R. Kouzes, Water Vapour Permeation in Plastics, United States. (2017) 29.

[40] R.J. Hernandez, Effect of water vapor on the transport properties of oxygen through polyamide packaging materials, J. Food Eng. 22 (1994) 495–507.

https://doi.org/10.1016/0260-8774(94)90050-7.

[41] S.S. Hosseini, J.A. Dehkordi, P.K. Kundu, Mathematical Modeling and Investigation on the Temperature and Pressure Dependency of Permeation and Membrane Separation Performance for Natural gas Treatment, Chem. Prod. Process Model. 11 (2016) 7–10. https://doi.org/10.1515/cppm-2015-0051.

[42] D. Feldman, Polymer nanocomposite barriers, J. Macromol. Sci. Part A Pure Appl. Chem. 50 (2013) 441–448. https://doi.org/10.1080/10601325.2013.768440.

[43] T.K. Goswami, S. Mangaraj, Advances in polymeric materials for modified atmosphere packaging (MAP), Multifunct. Nanoreinforced Polym. Food Packag. (2011) 163–242. https://doi.org/10.1533/9780857092786.1.163.

[44] R.M. Venable, A. Krämer, R.W. Pastor, Molecular Dynamics Simulations of Membrane Permeability, Chem. Rev. 119 (2019) 5954–5997. https://doi.org/10.1021/ACS.CHEMREV.8B00486.

[45] G.A. Pogany, Anomalous diffusion of water in glassy polymers, Polymer (Guildf). 17 (1976) 690–694. https://doi.org/10.1016/0032-3861(76)90209-3.

[46] J. Kim, S. Oh, S.M. Cho, J. Jun, S. Kwak, Oxygen barrier properties of polyketone/EVOH blend films and their resistance to moisture, J. Appl. Polym. Sci. 137 (2020) 49537. https://doi.org/10.1002/APP.49537.

[47] N. Panapitiya, S. Wijenayake, D. Nguyen, C. Karunaweera, Y. Huang, K. Balkus, I. Musselman, J. Ferraris, Compatibilized Immiscible Polymer Blends for Gas Separations, Mater. 2016, Vol. 9, Page 643. 9 (2016) 643. https://doi.org/10.3390/MA9080643.

[48] H. Vinh-Thang, S. Kaliaguine, Predictive Models for Mixed-Matrix Membrane Performance: A Review, Chem. Rev. 113 (2013) 4980–5028. https://doi.org/10.1021/CR3003888.

[49] J.C. Maxwell, A treatise on electricity and magnetism, (1998). https://global.oup.com/academic/product/a-treatise-on-electricity-and-magnetism-9780198503736 (accessed November 10, 2021).

[50] BRUGGEMAN, DAG., The calculation of various physical constants of heterogeneous substances. I. The dielectric constants and conductivities of mixtures composed of isotropic substances, Ann. Phys. (N. Y). 416 (1935) 636–791. https://ci.nii.ac.jp/naid/10027369104 (accessed November 10, 2021).

[51] W.I. Higuchi, T. Higuchi, Theoretical Analysis of Diffusional Movement Through Heterogeneous Barriers, J. Am. Pharm. Assoc. (Scientific Ed.). 49 (1960) 598–606. https://doi.org/10.1002/JPS.3030490910.

[52] J.H. Petropoulos, A comparative study of approaches applied to the permeability of binary composite polymeric materials, J. Polym. Sci. Polym. Phys. Ed. 23 (1985) 1309–1324. https://doi.org/10.1002/POL.1985.180230703.

[53] T.B. Lewis, L.E. Nielsen, Dynamic mechanical properties of particulate-filled composites, J. Appl. Polym. Sci. 14 (1970) 1449–1471. https://doi.org/10.1002/APP.1970.070140604.

[54] R.H.B. Bouma, A. Checchetti, G. Chidichimo, E. Drioli, Permeation through a

heterogeneous membrane: the effect of the dispersed phase, J. Memb. Sci. 128 (1997) 141–149. https://doi.org/10.1016/S0376-7388(96)00303-1.

[55] D. Bhattacharyya, R.J. Shields, Modeling of Fibre Formation and Oxygen Permeability in Micro-fibrillar Polymer-Polymer Composites, IUTAM Bookseries. 19 (2010) 111–119. https://doi.org/10.1007/978-90-481-3771-8_12.

[56] S.Y. Zhou, H.D. Huang, X. Ji, D.X. Yan, G.J. Zhong, B.S. Hsiao, Z.M. Li, Super-Robust Polylactide Barrier Films by Building Densely Oriented Lamellae Incorporated with Ductile in Situ Nanofibrils of Poly(butylene adipate- co -terephthalate), ACS Appl. Mater. Interfaces. 8 (2016) 8096–8109. https://doi.org/10.1021/ACSAMI.6B00451/SUPPL_FILE/AM6B00451_SI_001.PDF.

[57] C.C. Sarath, R.A. Shanks, S. Thomas, Polymer Blends, Nanostructured Polym. Blends. (2014) 1–14. https://doi.org/10.1016/B978-1-4557-3159-6.00001-8.

[58] M.A. Aroon, A.F. Ismail, T. Matsuura, M.M. Montazer-Rahmati, Performance studies of mixed matrix membranes for gas separation: A review, Sep. Purif. Technol. 75 (2010) 229–242. https://doi.org/10.1016/J.SEPPUR.2010.08.023.

[59] E.E. Gonzo, M.L. Parentis, J.C. Gottifredi, Estimating models for predicting effective permeability of mixed matrix membranes, J. Memb. Sci. 277 (2006) 46–54. https://doi.org/10.1016/J.MEMSCI.2005.10.007.

[60] H. Wu, M. Zamanian, B. Kruczek, J. Thibault, Gas permeation model of mixed-matrix membranes with embedded impermeable cuboid nanoparticles, Membranes (Basel). 10 (2020) 1–20. https://doi.org/10.3390/membranes10120422.

[61] A. Rybak, A. Rybak, P. Sysel, Modeling of gas permeation through mixed-matrix membranes using novel computer application MOT, Appl. Sci. 8 (2018) 1–20. https://doi.org/10.3390/app8071166.

[62] J. Lange, Y. Wyser, Recent innovations in barrier technologies for plastic packaging—a review, Packag. Technol. Sci. 16 (2003) 149–158. https://doi.org/10.1002/PTS.621.

[63] S. Fu, Z. Sun, P. Huang, Y. Li, N. Hu, Some basic aspects of polymer nanocomposites: A critical review, Nano Mater. Sci. 1 (2019) 2–30. https://doi.org/10.1016/J.NANOMS.2019.02.006.

[64] G. Choudalakis, A.D. Gotsis, Permeability of polymer/clay nanocomposites: A review, Eur. Polym. J. 45 (2009) 967–984. https://doi.org/10.1016/j.eurpolymj.2009.01.027.

[65] L. Ge, Z. Zhu, F. Li, S. Liu, L. Wang, X. Tang, V. Rudolph, Investigation of Gas Permeability in Carbon Nanotube (CNT)−Polymer Matrix Membranes via Modifying CNTs with Functional Groups/Metals and Controlling Modification Location, J. Phys. Chem. C. 115 (2011) 6661–6670. https://doi.org/10.1021/JP1120965.

[66] L.E. Nielsen, Models for the Permeability of Filled Polymer Systems, Http://Dx.Doi.Org/10.1080/10601326708053745. 1 (2006) 929–942. https://doi.org/10.1080/10601326708053745.

[67] E.L. Cussler, S.E. Hughes, W.J. Ward, R. Aris, Barrier membranes, J. Memb. Sci. 38 (1988) 161–174. https://doi.org/10.1016/S0376-7388(00)80877-7.

[68] J.P. DeRocher, B.T. Gettelfinger, J. Wang, E.E. Nuxoll, E.L. Cussler, Barrier membranes with different sizes of aligned flakes, J. Memb. Sci. 254 (2005) 21–30. https://doi.org/10.1016/J.MEMSCI.2004.12.025.

[69] G.D. Moggridge, N.K. Lape, C. Yang, E.L. Cussler, Barrier films using flakes and reactive additives, Prog. Org. Coatings. 46 (2003) 231–240. https://doi.org/10.1016/S0300-9440(02)00180-7.

[70] R.K. Bharadwaj, Modeling the Barrier Properties of Polymer-Layered Silicate Nanocomposites, Macromolecules. 34 (2001) 9189–9192. https://doi.org/10.1021/MA010780B.

[71] S. Nazarenko, P. Meneghetti, P. Julmon, B.G. Olson, S. Qutubuddin, Gas barrier of polystyrene montmorillonite clay nanocomposites: Effect of mineral layer aggregation, J. Polym. Sci. Part B Polym. Phys. 45 (2007) 1733–1753. https://doi.org/10.1002/POLB.21181.

[72] E.E. Nuxoll, E.L. Cussler, The third parameter in reactive barrier films, AIChE J. 51 (2005) 456–463. https://doi.org/10.1002/AIC.10316.

[73] N.K. Lape, H. Mao, D. Camper, M.A. Hillmyer, E.L. Cussler, Barrier membranes of self-assembled lamellar poly(lactide-isoprene-lactide) triblock copolymers, J. Memb. Sci. 259 (2005) 1–9. https://doi.org/10.1016/J.MEMSCI.2004.11.035.

[74] B.M. Trinh, C.C. Chang, T.H. Mekonnen, Facile fabrication of thermoplastic starch/poly (lactic acid) multilayer films with superior gas and moisture barrier properties, Polymer (Guildf). 223 (2021) 123679. https://doi.org/10.1016/J.POLYMER.2021.123679.

[75] E. Ojogbo, E.O. Ogunsona, T.H. Mekonnen, Chemical and physical modifications of starch for renewable polymeric materials, Mater. Today Sustain. 7–8 (2020) 100028. https://doi.org/10.1016/j.mtsust.2019.100028.

[76] B.M. Trinh, T. Mekonnen, Hydrophobic esterification of cellulose nanocrystals for epoxy reinforcement, Polymer (Guildf). 155 (2018) 64–74. https://doi.org/10.1016/j.polymer.2018.08.076.

[77] M. Mashkour, E. Afra, H. Resalati, M. Mashkour, Moderate surface acetylation of nanofibrillated cellulose for the improvement of paper strength and barrier properties, RSC Adv. 5 (2015) 60179–60187. https://doi.org/10.1039/C5RA08161K.

[78] F. Wu, M. Misra, A.K. Mohanty, Challenges and new opportunities on barrier performance of biodegradable polymers for sustainable packaging, Prog. Polym. Sci. 117 (2021) 101395. https://doi.org/10.1016/j.progpolymsci.2021.101395.

[79] U. Witt, M. Yamamoto, U. Seeliger, R.-J. Müller, V. Warzelhan, Biodegradable Polymeric Materials-Not the Origin but the Chemical Structure Determines Biodegradability, Angew. Chem. Int. Ed. 38 (1999). https://doi.org/10.1002/(SICI)1521-3773(19990517)38:10.

[80] D.H. Weinkauf, D.R. Paul, Effects of Structural Order on Barrier Properties, (1990) 60–91. https://doi.org/10.1021/BK-1990-0423.CH003.

[81] P.K. Sandhya, R. Lakshmipriya, M.S. Sreekala, Gas Permeability Through Thermosets,

Transp. Prop. Polym. Membr. (2018) 475–516. https://doi.org/10.1016/B978-0-12-809884-4.00023-9.

[82] M.Á. Corres, Á. Mayor, A. Sangroniz, J. del Río, M. Iriarte, A. Etxeberria, Blends based on biodegradable poly(caprolactone) with outstanding barrier properties for packaging applications: The role of free volume and interactions, Eur. Polym. J. 135 (2020). https://doi.org/10.1016/J.EURPOLYMJ.2020.109869.

[83] H.M.C. Azeredo, K.W. Waldron, Crosslinking in polysaccharide and protein films and coatings for food contact – A review, Trends Food Sci. Technol. 52 (2016) 109–122. https://doi.org/10.1016/J.TIFS.2016.04.008.

[84] T. Mekonnen, P. Mussone, H. Khalil, D. Bressler, Progress in bio-based plastics and plasticizing modifications, J. Mater. Chem. A. 1 (2013) 13379–13398. https://doi.org/10.1039/C3TA12555F.

[85] T. Mekonnen, P. Mussone, K. Alemaskin, L. Sopkow, J. Wolodko, P. Choi, D. Bressler, Biocomposites from hydrolyzed waste proteinaceous biomass: mechanical, thermal and moisture absorption performances, J. Mater. Chem. A. 1 (2013) 13186–13196. https://doi.org/10.1039/C3TA13560H.

[86] P. Hernández-Muñoz, R. Villalobos, A. Chiralt, Effect of cross-linking using aldehydes on properties of glutenin-rich films, Food Hydrocoll. 18 (2004) 403–411. https://doi.org/10.1016/S0268-005X(03)00128-0.

[87] Y. Gao, H. Zheng, J. Wang, J. Wu, X. Li, G. Liu, Physicochemical properties of zein films cross-linked with glutaraldehyde, Polym. Bull. (2021) 1–19. https://doi.org/10.1007/S00289-021-03723-9/FIGURES/11.

[88] J. Uranga, I. Leceta, A. Etxabide, P. Guerrero, K. De La Caba, Cross-linking of fish gelatins to develop sustainable films with enhanced properties, Eur. Polym. J. 78 (2016) 82–90. https://doi.org/10.1016/J.EURPOLYMJ.2016.03.017.

[89] K. Yuniarto, B.A. Welt, C. Irawan, Morphological, Thermal and Oxygen Barrier Properties Plasticized Film Polylactic Acid, J. Appl. Packag. Res. 1 (n.d.).

[90] J.M. Lagaron, R. Catalá, R. Gavara, Structural characteristics defining high barrier properties in polymeric materials, Http://Dx.Doi.Org/10.1179/026708304225010442. 20 (2013) 1–7. https://doi.org/10.1179/026708304225010442.

[91] H. Bai, C. Huang, H. Xiu, Q. Zhang, H. Deng, K. Wang, F. Chen, Q. Fu, Significantly Improving Oxygen Barrier Properties of Polylactide via Constructing Parallel-Aligned Shish-Kebab-Like Crystals with Well-Interlocked Boundaries, Biomacromolecules. 15 (2014) 1507–1514. https://doi.org/10.1021/BM500167U.

[92] M. Sapper, A. Chiralt, Starch-Based Coatings for Preservation of Fruits and Vegetables, (n.d.). https://doi.org/10.3390/coatings8050152.

[93] A. Chiralt, C. González-Martínez, M. Vargas, L. Atarés, Edible films and coatings from proteins, Proteins Food Process. Second Ed. (2018) 477–500. https://doi.org/10.1016/B978-0-08-100722-8.00019-X.

[94] J.W. Rhim, T.H. Shellhammer, Lipid-based edible films and coatings, Innov. Food

Packag. (2005) 362–383. https://doi.org/10.1016/B978-012311632-1/50053-X.

[95] S. Galus, J. Kadzińska, Food applications of emulsion-based edible films and coatings, Trends Food Sci. Technol. 45 (2015) 273–283. https://doi.org/10.1016/J.TIFS.2015.07.011.

[96] L. Chen, F. Ao, X. Ge, W. Shen, Food-grade pickering emulsions: Preparation, stabilization and applications, Molecules. 25 (2020). https://doi.org/10.3390/molecules25143202.

[97] T. Anukiruthika, P. Sethupathy, A. Wilson, K. Kashampur, J.A. Moses, C. Anandharamakrishnan, Multilayer packaging: Advances in preparation techniques and emerging food applications, Compr. Rev. Food Sci. Food Saf. 19 (2020) 1156–1186. https://doi.org/10.1111/1541-4337.12556.

[98] High Barrier Packaging Films Market Size Estimation, Industry Demand, Growth Trend, Chain Structure, Supply and Demand Forecast (2020-2027) – Techno Geeks TMR, (n.d.). https://technogeekstmr.wordpress.com/2020/07/13/high-barrier-packaging-films-market-size-estimation-industry-demand-growth-trend-chain-structure-supply-and-demand-forecast-2020-2027/ (accessed December 5, 2021).

[99] Multilayer Flexible Packaging Market Analysis and Review 2019 - 2029 | Future Market Insights (FMI), (n.d.). https://www.futuremarketinsights.com/reports/multilayer-flexible-packaging-market?utm_source=pr_distribution&utm_medium=accesswire&utm_campaign=Multilayer Flexible Packaging Market (accessed December 5, 2021).

[100] Z. Li, A. Olah, E. Baer, Micro- and nano-layered processing of new polymeric systems, Prog. Polym. Sci. 102 (2020) 101210. https://doi.org/10.1016/J.PROGPOLYMSCI.2020.101210.

[101] Blown Film | Which Applications Are Most Suited for 7/9/11 Layers? Part 3 - Paper, Film & Foil Converter, (n.d.). https://www.pffc-online.com/flexpack/14617-blown-film-which-applications-are-most-suited-for-7-9-11-layers-part-3 (accessed December 13, 2021).

[102] K. Kaiser, M. Schmid, M. Schlummer, Recycling of Polymer-Based Multilayer Packaging: A Review, Recycl. 2018, Vol. 3, Page 1. 3 (2017) 1. https://doi.org/10.3390/RECYCLING3010001.

[103] T. Mazerolles, M.C. Heuzey, M. Soliman, H. Martens, R. Kleppinger, M.A. Huneault, Development of multilayer barrier films of thermoplastic starch and low-density polyethylene, J. Polym. Res. 27 (2020) 1–15. https://doi.org/10.1007/s10965-020-2015-y.

[104] C. Thellen, S. Cheney, J.A. Ratto, Melt processing and characterization of polyvinyl alcohol and polyhydroxyalkanoate multilayer films, J. Appl. Polym. Sci. 127 (2013) 2314–2324. https://doi.org/10.1002/APP.37850.

[105] C.C. Chang, B.M. Trinh, T.H. Mekonnen, Robust multiphase and multilayer starch/polymer (TPS/PBAT) film with simultaneous oxygen/moisture barrier properties, J. Colloid Interface Sci. 593 (2021) 290–303. https://doi.org/10.1016/J.JCIS.2021.03.010.

[106] C. Ge, B. Lansing, C.L. Lewis, Thermoplastic starch and poly(vinyl alcohol) blends centered barrier film for food packaging applications, Food Packag. Shelf Life. 27 (2021)

100610. https://doi.org/10.1016/J.FPSL.2020.100610.

[107] E.O. Ogunsona, T.H. Mekonnen, Multilayer assemblies of cellulose nanocrystal – Polyvinyl alcohol films with robust physical integrity and multi-functional properties, J. Colloid Interface Sci. 580 (2020) 56–67. https://doi.org/10.1016/j.jcis.2020.07.012.

[108] P. Scarfato, L. Di Maio, M.R. Milana, S. Giamberardini, M. Denaro, L. Incarnato, Performance properties, lactic acid specific migration and swelling by simulant of biodegradable poly(lactic acid)/nanoclay multilayer films for food packaging, Https://Doi.Org/10.1080/19440049.2017.1321786. 34 (2017) 1730–1742. https://doi.org/10.1080/19440049.2017.1321786.

[109] H. Liu, J. Wu, C. Liu, B. Pan, N.H. Kim, J.H. Lee, Differently-charged graphene-based multilayer films by a layer-by-layer approach for oxygen gas barrier application, Compos. Part B Eng. 155 (2018) 391–396. https://doi.org/10.1016/J.COMPOSITESB.2018.08.137.

[110] N. Lavoine, I. Desloges, A. Dufresne, J. Bras, Microfibrillated cellulose – Its barrier properties and applications in cellulosic materials: A review, Carbohydr. Polym. 90 (2012) 735–764. https://doi.org/10.1016/J.CARBPOL.2012.05.026.

[111] X. Tang, S. Alavi, T.J. Herald, Barrier and Mechanical Properties of Starch-Clay Nanocomposite Films, Cereal Chem. 85 (2008) 433–439. https://doi.org/10.1094/CCHEM-85-3-0433.

[112] A. bin Ali, A.S. Mohammed, N. Merah, Tribological investigations of UHMWPE nanocomposites reinforced with three different organo-modified clays, Polym. Compos. 39 (2018) 2224–2231. https://doi.org/10.1002/pc.24186.

[113] Y. Iida, T. Tuziuti, K. Yasui, A. Towata, T. Kozuka, Control of viscosity in starch and polysaccharide solutions with ultrasound after gelatinization, Innov. Food Sci. Emerg. Technol. 9 (2008) 140–146. https://doi.org/10.1016/J.IFSET.2007.03.029.

[114] N. Bumbudsanpharoke, S. Ko, Nanoclays in food and beverage packaging, J. Nanomater. 2019 (2019). https://doi.org/10.1155/2019/8927167.

[115] P. Bordes, E. Pollet, L. Avérous, Nano-biocomposites: Biodegradable polyester/nanoclay systems, Prog. Polym. Sci. 34 (2009) 125–155. https://doi.org/10.1016/J.PROGPOLYMSCI.2008.10.002.

[116] R. Crétois, N. Follain, E. Dargent, J. Soulestin, S. Bourbigot, S. Marais, L. Lebrun, Microstructure and barrier properties of PHBV/organoclays bionanocomposites, J. Memb. Sci. 467 (2014) 56–66. https://doi.org/10.1016/J.MEMSCI.2014.05.015.

[117] B.L. Peng, N. Dhar, H.L. Liu, K.C. Tam, Chemistry and applications of nanocrystalline cellulose and its derivatives: A nanotechnology perspective, Can. J. Chem. Eng. 89 (2011) 1191–1206. https://doi.org/10.1002/CJCE.20554.

[118] P. Panchal, E. Ogunsona, T. Mekonnen, Trends in advanced functional material applications of nanocellulose, Processes. 7 (2019). https://doi.org/10.3390/pr7010010.

[119] H. Du Le, S.M. Loveday, H. Singh, A. Sarkar, Pickering emulsions stabilised by hydrophobically modified cellulose nanocrystals: Responsiveness to pH and ionic strength, Food Hydrocoll. 99 (2020) 105344.

https://doi.org/10.1016/j.foodhyd.2019.105344.

[120] Q.H. Chen, J. Zheng, Y.T. Xu, S.W. Yin, F. Liu, C.H. Tang, Surface modification improves fabrication of pickering high internal phase emulsions stabilized by cellulose nanocrystals, Food Hydrocoll. 75 (2018) 125–130. https://doi.org/10.1016/J.FOODHYD.2017.09.005.

[121] S. Zhang, S.N. Li, Q. Wu, Q. Li, J. Huang, W. Li, W. Zhang, S. Wang, Phosphorus containing group and lignin toward intrinsically flame retardant cellulose nanofibril-based film with enhanced mechanical properties, Compos. Part B Eng. 212 (2021) 108699. https://doi.org/10.1016/J.COMPOSITESB.2021.108699.

[122] H.M. Seo, M. Seo, K. Shin, S. Choi, J.W. Kim, Bacterial cellulose nanofibrils-armored Pickering emulsions with limited influx of metal ions, Carbohydr. Polym. 258 (2021) 117730. https://doi.org/10.1016/J.CARBPOL.2021.117730.

[123] Y. Yin, L.A. Lucia, L. Pal, X. Jiang, M.A. Hubbe, Lipase-catalyzed laurate esterification of cellulose nanocrystals and their use as reinforcement in PLA composites, Cellulose. 27 (2020) 6263–6273. https://doi.org/10.1007/S10570-020-03225-3/TABLES/2.

[124] R. Shorey, A. Gupta, T.H. Mekonnen, Hydrophobic modification of lignin for rubber composites, Ind. Crops Prod. 174 (2021) 114189. https://doi.org/10.1016/J.INDCROP.2021.114189.

[125] S.S. Nair, H. Chen, Y. Peng, Y. Huang, N. Yan, Polylactic Acid Biocomposites Reinforced with Nanocellulose Fibrils with High Lignin Content for Improved Mechanical, Thermal, and Barrier Properties, ACS Sustain. Chem. Eng. 6 (2018) 10058–10068. https://doi.org/10.1021/ACSSUSCHEMENG.8B01405/SUPPL_FILE/SC8B01405_SI_001.PDF.

[126] M. Batra, G.K. Malik, J. Mitra, Enhancing the properties of gelatin–chitosan bionanocomposite films by incorporation of silica nanoparticles, J. Food Process Eng. 43 (2020) e13329. https://doi.org/10.1111/JFPE.13329.

[127] Q. Sun, T. Xi, Y. Li, L. Xiong, Characterization of Corn Starch Films Reinforced with CaCO3 Nanoparticles, PLoS One. 9 (2014) 106727. https://doi.org/10.1371/JOURNAL.PONE.0106727.

[128] A.M. Nafchi, R. Nassiri, S. Sheibani, F. Ariffin, A.A. Karim, Preparation and characterization of bionanocomposite films filled with nanorod-rich zinc oxide, Carbohydr. Polym. 96 (2013) 233–239. https://doi.org/10.1016/J.CARBPOL.2013.03.055.

[129] J. Ma, W. Zhu, Y. Tian, Z. Wang, Preparation of Zinc Oxide-Starch Nanocomposite and Its Application on Coating, Nanoscale Res. Lett. 2016 111. 11 (2016) 1–9. https://doi.org/10.1186/S11671-016-1404-Y.

[130] A.M. Nafchi, M. Moradpour, M. Saeidi, A.K. Alias, Thermoplastic starches: Properties, challenges, and prospects, Starch/Staerke. 65 (2013) 61–72. https://doi.org/10.1002/STAR.201200201.

[131] A.K. Mohanty, M. Misra, G. Hinrichsen, Biofibres, biodegradable polymers and biocomposites: An overview, Macromol. Mater. Eng. 276–277 (2000) 1–24.

https://doi.org/10.1002/(SICI)1439-2054(20000301)276:1<1::AID-MAME1>3.0.CO;2-W.

[132] E.O. Ogunsona, A. Codou, M. Misra, A.K. Mohanty, A critical review on the fabrication processes and performance of polyamide biocomposites from a biofiller perspective, Mater. Today Sustain. 5 (2019) 100014. https://doi.org/10.1016/j.mtsust.2019.100014.

[133] R. Muthuraj, T. Mekonnen, Carbon dioxide derived poly (propylene carbonate) polymer for composites and nanocomposites: performance, biodegradation and applications., Macromol. Mater. Eng. (2018). https://doi.org/10.1002/mame.201800366.

[134] E. Ogunsona, E. Ojogbo, T. Mekonnen, Advanced material applications of starch and its derivatives, Eur. Polym. J. 108 (2018) 570–581. https://doi.org/10.1016/j.eurpolymj.2018.09.039.

[135] M.L. Sanyang, S.M. Sapuan, M. Jawaid, M.R. Ishak, J. Sahari, Development and characterization of sugar palm starch and poly(lactic acid) bilayer films, Carbohydr. Polym. 146 (2016) 36–45. https://doi.org/10.1016/j.carbpol.2016.03.051.

[136] J. Muller, C. González-Martínez, A. Chiralt, Poly(lactic) acid (PLA) and starch bilayer films, containing cinnamaldehyde, obtained by compression moulding, Eur. Polym. J. 95 (2017) 56–70. https://doi.org/10.1016/j.eurpolymj.2017.07.019.

[137] R. Turco, R. Ortega-Toro, R. Tesser, S. Mallardo, S. Collazo-Bigliardi, A.C. Boix, M. Malinconico, M. Rippa, M. Di Serio, G. Santagata, Poly (lactic acid)/thermoplastic starch films: Effect of cardoon seed epoxidized oil on their chemicophysical, mechanical, and barrier properties, Coatings. 9 (2019) 1–20. https://doi.org/10.3390/coatings9090574.

[138] S. Detyothin, A. Kathuria, W. Jaruwattanayon, S.E.M. Selke, R. Auras, Poly(Lactic Acid) Blends, in: Poly(Lactic Acid), John Wiley & Sons, Inc., Hoboken, NJ, USA, 2010: pp. 227–271. https://doi.org/10.1002/9780470649848.ch16.

[139] J. Lunt, Large-scale production, properties and commercial applications of poly lactic acid polymers, Polym. Degrad. Stab. 59 (1998) 145–152. https://doi.org/10.1016/s0141-3910(97)00148-1.

[140] R. Auras, L.T. Lim, S.E.M. Selke, H. Tsuji, Poly(Lactic Acid), John Wiley & Sons, Inc., Hoboken, NJ, USA, 2010. https://doi.org/10.1002/9780470649848.

[141] J.M. Raquez, Y. Nabar, M. Srinivasan, B.Y. Shin, R. Narayan, P. Dubois, Maleated thermoplastic starch by reactive extrusion, Carbohydr. Polym. 74 (2008) 159–169. https://doi.org/10.1016/j.carbpol.2008.01.027.

[142] Y. Zuo, J. Gu, L. Yang, Z. Qiao, Y. Zhang, Study on the preparation of maleated thermoplastic starch by reactive extrusion, J. Thermoplast. Compos. Mater. 29 (2016) 397–409. https://doi.org/10.1177/0892705713518809.

[143] J. Wootthikanokkhan, P. Kasemwananimit, N. Sombatsompop, A. Kositchaiyong, S. Isarankura na Ayutthaya, N. Kaabbuathong, Preparation of modified starch-grafted poly(lactic acid) and a study on compatibilizing efficacy of the copolymers in poly(lactic acid)/thermoplastic starch blends, J. Appl. Polym. Sci. 126 (2012) E389–E396. https://doi.org/10.1002/app.36896.

[144] B.M. Trinh, E.O. Ogunsona, T.H. Mekonnen, Thin-structured and compostable wood fiber-polymer biocomposites: Fabrication and performance evaluation, Compos. Part A Appl. Sci. Manuf. 140 (2021) 106150. https://doi.org/10.1016/j.compositesa.2020.106150.

[145] H.M. Li, H. biao Chen, Z.G. Shen, S. Lin, Preparation and characterization of maleic anhydride-functionalized syndiotactic polystyrene, Polymer (Guildf). 43 (2002) 5455–5461. https://doi.org/10.1016/S0032-3861(02)00369-5.

[146] M. Bhattacharya, Polymer nanocomposites-A comparison between carbon nanotubes, graphene, and clay as nanofillers, Materials (Basel). 9 (2016). https://doi.org/10.3390/ma9040262.

[147] K. Stoeffler, P.G. Lafleur, F. Perrin-Sarazin, M.N. Bureau, J. Denault, Micro-mechanisms of deformation in polyethylene/clay micro- and nanocomposites, Compos. Part A Appl. Sci. Manuf. 42 (2011) 916–927. https://doi.org/10.1016/j.compositesa.2011.03.020.

[148] B.F. Bergel, S. Dias Osorio, L.M. da Luz, R.M.C. Santana, Effects of hydrophobized starches on thermoplastic starch foams made from potato starch, Carbohydr. Polym. 200 (2018) 106–114. https://doi.org/10.1016/j.carbpol.2018.07.047.

[149] Y. Wen, F. Ye, J. Zhu, G. Zhao, Corn starch ferulates with antioxidant properties prepared by N,N′-carbonyldiimidazole-mediated grafting procedure, Food Chem. 208 (2016) 1–9. https://doi.org/10.1016/j.foodchem.2016.03.094.

[150] J. Liu, X. Wang, R. Bai, N. Zhang, J. Kan, C. Jin, Synthesis, characterization, and antioxidant activity of caffeic-acid-grafted corn starch, Starch - Stärke. 70 (2018) 1700141. https://doi.org/10.1002/star.201700141.

[151] E. Ojogbo, R. Blanchard, T. Mekonnen, Hydrophobic and Melt Processable Starch-Laurate Esters: Synthesis, Structure-Property Correlations, J. Polym. Sci. Part A Polym. Chem. 56 (2018) 2611–2622. https://doi.org/10.1002/pola.29237.

[152] Glycerol(56-81-5) 1H NMR, (n.d.). https://www.chemicalbook.com/SpectrumEN_56-81-5_1HNMR.htm (accessed December 4, 2020).

[153] E. Ojogbo, V. Ward, T.H. Mekonnen, Functionalized starch microparticles for contact-active antimicrobial polymer surfaces, Carbohydr. Polym. 229 (2020) 115422. https://doi.org/10.1016/j.carbpol.2019.115422.

[154] M.J. Tizzotti, M.C. Sweedman, D. Tang, C. Schaefer, R.G. Gilbert, New 1H NMR procedure for the characterization of native and modified food-grade starches, J. Agric. Food Chem. 59 (2011) 6913–6919. https://doi.org/10.1021/jf201209z.

[155] M.J. Gidley, Quantification of the structural features of starch polysaccharides by n.m.r. spectroscopy, Carbohydr. Res. 139 (1985) 85–93. https://doi.org/10.1016/0008-6215(85)90009-6.

[156] S. Park, Novel Starch Nanocomposites, 2019.

[157] N.A. Nikonenko, D.K. Buslov, N.I. Sushko, R.G. Zhbankov, Investigation of stretching vibrations of glycosidic linkages in disaccharides and polysaccarides with use of IR spectra deconvolution, Biopolym. - Biospectroscopy Sect. 57 (2000) 257–262. https://doi.org/10.1002/1097-0282(2000)57:4<257::AID-BIP7>3.0.CO;2-3.

[158] E. Ojogbo, R. Blanchard, T. Mekonnen, Hydrophobic and Melt Processable Starch-Laurate Graft Polymers: Synthesis, Structure – Property Correlations, J. Polym. Sci. Part A-Polymer Chem. (2018). https://doi.org/10.1002/pola.29237.

[159] J.-M. Raquez, Y. Nabar, R. Narayan, P. Dubois, In situ compatibilization of maleated thermoplastic starch/polyester melt-blends by reactive extrusion, Polym. Eng. Sci. 48 (2008) 1747–1754. https://doi.org/10.1002/pen.21136.

[160] E. Hablot, S. Dewasthale, Y. Zhao, Y. Zhiguan, X. Shi, D. Graiver, R. Narayan, Reactive extrusion of glycerylated starch and starch-polyester graft copolymers, Eur. Polym. J. 49 (2013) 873–881. https://doi.org/10.1016/j.eurpolymj.2012.12.005.

[161] X. Liu, Y. Wang, L. Yu, Z. Tong, L. Chen, H. Liu, X. Li, Thermal degradation and stability of starch under different processing conditions, Starch - Stärke. 65 (2013) 48–60. https://doi.org/10.1002/star.201200198.

[162] V.P. Cyras, L.B. Manfredi, M.T. Ton-That, A. Vázquez, Physical and mechanical properties of thermoplastic starch/montmorillonite nanocomposite films, Carbohydr. Polym. 73 (2008) 55–63. https://doi.org/10.1016/j.carbpol.2007.11.014.

[163] Y. Nabar, J.M. Raquez, P. Dubois, R. Narayan, Production of starch foams by twin-screw extrusion: Effect of maleated poly(butylene adipate-co-terephthalate) as a compatibilizer, Biomacromolecules. 6 (2005) 807–817. https://doi.org/10.1021/bm0494242.

[164] D. Le Corre, J. Bras, A. Dufresne, Starch nanoparticles: A review, Biomacromolecules. 11 (2010) 1139–1153. https://doi.org/10.1021/bm901428y.

[165] N. Bumbudsanpharoke, S. Ko, A Study of Thermal Properties of LDPE-Nanoclay Composite Films, KOREAN J. Packag. Sci. Technol. 21 (2015) 107–113. https://doi.org/10.20909/kopast.2015.21.3.107.

[166] T. Mekonnen, M. Misra, A.K. Mohanty, Fermented Soymeals and Their Reactive Blends with Poly(butylene adipate-co-terephthalate) in Engineering Biodegradable Cast Films for Sustainable Packaging, ACS Sustain. Chem. Eng. 4 (2016) 782–793. https://doi.org/10.1021/ACSSUSCHEMENG.5B00782.

[167] A. Kelarakis, K. Yoon, Optical transparency in a polymer blend induced by clay nanofillers, Eur. Polym. J. 44 (2008) 3941–3945. https://doi.org/10.1016/j.eurpolymj.2008.08.030.

[168] C.M.O. Müller, J.B. Laurindo, F. Yamashita, Composites of thermoplastic starch and nanoclays produced by extrusion and thermopressing, Carbohydr. Polym. 89 (2012) 504–510. https://doi.org/10.1016/j.carbpol.2012.03.035.

[169] Y. Zhang, Q. Liu, A. Hrymak, J.H. Han, Characterization of Extruded Thermoplastic Starch Reinforced by Montmorillonite Nanoclay, J. Polym. Environ. 21 (2013) 122–131. https://doi.org/10.1007/s10924-012-0528-0.

[170] Kusmono, M.W. Wildan, Z.A. Mohd Ishak, Preparation and properties of clay-reinforced epoxy nanocomposites, Int. J. Polym. Sci. 2013 (2013). https://doi.org/10.1155/2013/690675.

[171] M. Applications, Ingeo™ Biopolymer 4043D Technical Data Sheet 3D Printing

Monofilament-General Purpose Grade, n.d. http://www.fda.gov/food/ingredientspackaginglabeling/ (accessed March 28, 2020).

[172] A. González, C.I. Alvarez Igarzabal, Soy protein - Poly (lactic acid) bilayer films as biodegradable material for active food packaging, Food Hydrocoll. 33 (2013) 289–296. https://doi.org/10.1016/j.foodhyd.2013.03.010.

[173] E.O. Ogunsona, P. Panchal, T.H. Mekonnen, Surface grafting of acrylonitrile butadiene rubber onto cellulose nanocrystals for nanocomposite applications, Compos. Sci. Technol. 184 (2019). https://doi.org/10.1016/j.compscitech.2019.107884.

[174] P.G. De Gennes, Glass transitions in thin polymer films, Eur. Phys. J. E. 2 (2000) 201–205. https://doi.org/10.1007/PL00013665.

[175] R.R. Costa, A.I. Neto, I. Calgeris, C.R. Correia, A.C.M. Pinho, J. Fonseca, E.T. Öner, J.F. Mano, Adhesive nanostructured multilayer films using a bacterial exopolysaccharide for biomedical applications, J. Mater. Chem. B. 1 (2013) 2367–2374. https://doi.org/10.1039/c3tb20137f.

[176] Q. Sun, T. Mekonnen, M. Misra, A. Mohanty, Novel Biodegradable Cast Film from Carbon Dioxide Based Copolymer and Poly(Lactic Acid), J. Polym. Environ. 24 (2016) 23–36. https://doi.org/10.1007/s10924-015-0743-6.

[177] C. Zeppa, F. Gouanvé, E. Espuche, Effect of a plasticizer on the structure of biodegradable starch/clay nanocomposites: Thermal, water-sorption, and oxygen-barrier properties, J. Appl. Polym. Sci. 112 (2009) 2044–2056. https://doi.org/10.1002/app.29588.

[178] F. Salehi, Edible Coating of Fruits and Vegetables Using Natural Gums: A Review, Https://Doi.Org/10.1080/15538362.2020.1746730. 20 (2020) S570–S589. https://doi.org/10.1080/15538362.2020.1746730.

[179] S. Jung, Y. Cui, M. Barnes, C. Satam, S. Zhang, R.A. Chowdhury, A. Adumbumkulath, O. Sahin, C. Miller, S.M. Sajadi, L.M. Sassi, Y. Ji, M.R. Bennett, M. Yu, J. Friguglietti, F.A. Merchant, R. Verduzco, S. Roy, R. Vajtai, J.C. Meredith, J.P. Youngblood, N. Koratkar, M.M. Rahman, P.M. Ajayan, Multifunctional Bio-Nanocomposite Coatings for Perishable Fruits, Adv. Mater. 32 (2020) 1–9. https://doi.org/10.1002/adma.201908291.

[180] B. Marelli, M.A. Brenckle, D.L. Kaplan, F.G. Omenetto, Silk Fibroin as Edible Coating for Perishable Food Preservation, Sci. Rep. 6 (2016). https://doi.org/10.1038/srep25263.

[181] F.D. Conforti, J.A. Totty, Effect of three lipid/hydrocolloid coatings on shelf life stability of Golden Delicious apples, (n.d.). https://doi.org/10.1111/j.1365-2621.2006.01365.x.

[182] A. Pérez-Gallardo, B. García-Almendárez, G. Barbosa-Cánovas, D. Pimentel-González, L.R. Reyes-González, C. Regalado, Effect of starch-beeswax coatings on quality parameters of blackberries (Rubus spp.), (n.d.). https://doi.org/10.1007/s13197-014-1665-3.

[183] X. Zhou, R. Cheng, B. Wang, J. Zeng, J. Xu, J. Li, L. Kang, Z. Cheng, W. Gao, K. Chen, Biodegradable sandwich-architectured films derived from pea starch and polylactic acid with enhanced shelf-life for fruit preservation, Carbohydr. Polym. 251 (2021) 117117. https://doi.org/10.1016/J.CARBPOL.2020.117117.

[184] M.I. Pinzon, L.T. Sanchez, O.R. Garcia, R. Gutierrez, J.C. Luna, C.C. Villa, Increasing shelf life of strawberries (Fragaria ssp) by using a banana starch-chitosan-Aloe vera gel composite edible coating, Int. J. Food Sci. Technol. 55 (2020) 92–98. https://doi.org/10.1111/IJFS.14254.

[185] F. Fratini, G. Cilia, B. Turchi, A. Felicioli, Beeswax: A minireview of its antimicrobial activity and its application in medicine, Asian Pac. J. Trop. Med. 9 (2016) 839–843. https://doi.org/10.1016/J.APJTM.2016.07.003.

[186] Y. Yang, Z. Fang, X. Chen, W. Zhang, Y. Xie, Y. Chen, Z. Liu, W. Yuan, An Overview of Pickering Emulsions: Solid-Particle Materials, Classification, Morphology, and Applications, Front. Pharmacol. 0 (2017) 287. https://doi.org/10.3389/FPHAR.2017.00287.

[187] H. Dai, J. Wu, H. Zhang, Y. Chen, L. Ma, H. Huang, Y. Huang, Y. Zhang, Recent advances on cellulose nanocrystals for Pickering emulsions: Development and challenge, Trends Food Sci. Technol. 102 (2020) 16–29. https://doi.org/10.1016/J.TIFS.2020.05.016.

[188] C. Tang, S. Spinney, Z. Shi, J. Tang, B. Peng, J. Luo, K.C. Tam, Amphiphilic Cellulose Nanocrystals for Enhanced Pickering Emulsion Stabilization, (2018). https://doi.org/10.1021/acs.langmuir.8b02437.

[189] D. Saidane, E. Perrin, F. Cherhal, F. Guellec, I. Capron, Some modification of cellulose nanocrystals for functional Pickering emulsions, (n.d.). https://doi.org/10.1098/rsta.2015.0139.

[190] X. Gong, Y. Wang, L. Chen, Enhanced emulsifying properties of wood-based cellulose nanocrystals as Pickering emulsion stabilizer, Carbohydr. Polym. 169 (2017) 295–303. https://doi.org/10.1016/J.CARBPOL.2017.04.024.

[191] X. Zhai, D. Lin, D. Liu, X. Yang, Emulsions stabilized by nanofibers from bacterial cellulose: New potential food-grade Pickering emulsions, Food Res. Int. 103 (2018) 12–20. https://doi.org/10.1016/J.FOODRES.2017.10.030.

[192] T. Yuan, J. Zeng, B. Wang, Z. Cheng, K. Chen, Pickering emulsion stabilized by cellulosic fibers: Morphological properties-interfacial stabilization-rheological behavior relationships, Carbohydr. Polym. 269 (2021) 118339. https://doi.org/10.1016/J.CARBPOL.2021.118339.

[193] F. Liu, J. Zheng, C.H. Huang, C.H. Tang, S.Y. Ou, Pickering high internal phase emulsions stabilized by protein-covered cellulose nanocrystals, Food Hydrocoll. 82 (2018) 96–105. https://doi.org/10.1016/J.FOODHYD.2018.03.047.

[194] W. Li, B. Ju, S. Zhang, Novel amphiphilic cellulose nanocrystals for pH-responsive Pickering emulsions, Carbohydr. Polym. 229 (2020) 115401. https://doi.org/10.1016/J.CARBPOL.2019.115401.

[195] S. Y, G. J, T. H, Z. Y, H. P, Physicochemical properties of starch adhesives enhanced by esterification modification with dodecenyl succinic anhydride, Int. J. Biol. Macromol. 112 (2018) 1257–1263. https://doi.org/10.1016/J.IJBIOMAC.2018.01.222.

[196] M. Jo, M.J. Chang, K.K.T. Goh, C. Ban, Y.J. Choi, Rheology, microstructure, and storage stability of emulsion-filled gels stabilized solely by maize starch modified with octenyl

succinylation and pregelatinization, Foods. 10 (2021). https://doi.org/10.3390/foods10040837.

[197] R.C. Amos, J. Mesnager, M. Kuska, M. Gauthier, Production of Cyclic Anhydride - Modified Starches, (2020).

[198] R. Hui, C. Qi-he, F. Ming-liang, X. Qiong, H. Guo-qing, Preparation and properties of octenyl succinic anhydride modified potato starch, Food Chem. 114 (2009) 81–86. https://doi.org/10.1016/j.foodchem.2008.09.019.

[199] G. Li, X. Xu, F. Zhu, Physicochemical properties of dodecenyl succinic anhydride (DDSA) modified quinoa starch, Food Chem. 300 (2019) 125201. https://doi.org/10.1016/J.FOODCHEM.2019.125201.

[200] V.V.T. Padil, C. Senan, M. Černík, Dodecenylsuccinic Anhydride Derivatives of Gum Karaya (Sterculia urens): Preparation, Characterization, and Their Antibacterial Properties, J. Agric. Food Chem. 63 (2015) 3757–3765. https://doi.org/10.1021/JF505783E.

[201] R. Bhosale, R. Singhal, Process optimization for the synthesis of octenyl succinyl derivative of waxy corn and amaranth starches, Carbohydr. Polym. 66 (2006) 521–527. https://doi.org/10.1016/J.CARBPOL.2006.04.007.

[202] A. Junior de Menezes, G. Siqueira, A.A.S. Curvelo, A. Dufresne, Extrusion and characterization of functionalized cellulose whiskers reinforced polyethylene nanocomposites, Polymer (Guildf). 50 (2009) 4552–4563. https://doi.org/10.1016/J.POLYMER.2009.07.038.

[203] W.T. Wulandari, A. Rochliadi, I.M. Arcana, Nanocellulose prepared by acid hydrolysis of isolated cellulose from sugarcane bagasse, IOP Conf. Ser. Mater. Sci. Eng. 107 (2016). https://doi.org/10.1088/1757-899X/107/1/012045.

[204] U.S. Rashid, S. Simsek, S.R. Kanel, A.N. Bezbaruah, Modified tapioca starch for iron nanoparticle dispersion in aqueous media: potential uses for environmental remediation, SN Appl. Sci. 1 (2019). https://doi.org/10.1007/s42452-019-1364-9.

[205] U.S. Rashid, S. Simsek, S.R. Kanel, A.N. Bezbaruah, Modified tapioca starch for iron nanoparticle dispersion in aqueous media: potential uses for environmental remediation, SN Appl. Sci. 1 (2019). https://doi.org/10.1007/S42452-019-1364-9.

[206] Y. Guo, Q. Liu, H. Chen, X. Wang, Z. Shen, X. Shu, R. Sun, Direct grafting modification of pulp in ionic liquids and self-assembly behavior of the graft copolymers, Cellulose. 20 (2013) 873–884. https://doi.org/10.1007/S10570-012-9847-5.

[207] F.F. Shih, K.W. Daigle, Gelatinization and pasting properties of rice starch modified with 2-octen-1-ylsuccinic anhydride, Nahrung - Food. 47 (2003) 64–67. https://doi.org/10.1002/FOOD.200390015.

[208] Y. Bai, Y.C. Shi, Structure and preparation of octenyl succinic esters of granular starch, microporous starch and soluble maltodextrin, Carbohydr. Polym. 83 (2011) 520–527. https://doi.org/10.1016/J.CARBPOL.2010.08.012.

[209] M.C. Sweedman, M.J. Tizzotti, C. Schäfer, R.G. Gilbert, Structure and physicochemical

properties of octenyl succinic anhydride modified starches: A review, Carbohydr. Polym. 92 (2013) 905–920. https://doi.org/10.1016/J.CARBPOL.2012.09.040.

[210] S. Plate, S. Diekmann, U. Steinhäuser, S. Drusch, Determination of the degree of substitution of hydrolysed octenylsuccinate-derivatised starch, LWT - Food Sci. Technol. 46 (2012) 580–582. https://doi.org/10.1016/J.LWT.2011.12.014.

[211] D. Beyene, M. Chae, J. Dai, C. Danumah, F. Tosto, A.G. Demesa, D.C. Bressler, Characterization of Cellulase-Treated Fibers and Resulting Cellulose Nanocrystals Generated through Acid Hydrolysis, Materials (Basel). 11 (2018). https://doi.org/10.3390/MA11081272.

[212] Z. Cheng, Y. Ma, L. Yang, F. Cheng, Z. Huang, A. Natan, H. Li, Y. Chen, D. Cao, Z. Huang, Y. Wang, Y. Liu, R. Yang, H. Zhu, Plasmonic-Enhanced Cholesteric Films: Coassembling Anisotropic Gold Nanorods with Cellulose Nanocrystals, Adv. Opt. Mater. 7 (2019) 1801816. https://doi.org/10.1002/ADOM.201801816.

[213] M. Hayashi, F. Tournilhac, Thermal stability enhancement of hydrogen bonded semicrystalline thermoplastics achieved by combination of aramide chemistry and supramolecular chemistry, Polym. Chem. 8 (2017) 461–471. https://doi.org/10.1039/C6PY01833E.

[214] S. Tesch, C. Gerhards, H. Schubert, Stabilization of emulsions by OSA starches, J. Food Eng. 54 (2002) 167–174. https://doi.org/10.1016/S0260-8774(01)00206-0.

[215] E. Jalali Dil, P.J. Carreau, B.D. Favis, Morphology, miscibility and continuity development in poly(lactic acid)/poly(butylene adipate-co-terephthalate) blends, Polymer (Guildf). 68 (2015) 202–212. https://doi.org/10.1016/j.polymer.2015.05.012.

[216] D. Klemm, E.D. Cranston, D. Fischer, M. Gama, S.A. Kedzior, D. Kralisch, F. Kramer, T. Kondo, T. Lindström, S. Nietzsche, K. Petzold-Welcke, F. Rauchfuß, Nanocellulose as a natural source for groundbreaking applications in materials science: Today's state, Mater. Today. 21 (2018) 720–748. https://doi.org/10.1016/J.MATTOD.2018.02.001.

[217] S.A. Kedzior, S. Cranmer-Smith, N. Behabtu, K. Kim, C. Lenges, S.L. Bryant, M. Trifkovic, Elucidating the effect of enzymatic polymerized polysaccharide particle morphology on emulsion properties, Carbohydr. Polym. 251 (2021) 117112. https://doi.org/10.1016/j.carbpol.2020.117112.

[218] H.F. ZOBEL, GELATINIZATION OF STARCH AND MECHANICAL PROPERTIES OF STARCH PASTES, Starch Chem. Technol. (1984) 285–309. https://doi.org/10.1016/B978-0-12-746270-7.50015-X.

[219] U. Bains, R. Pal, Rheology and catastrophic phase inversion of emulsions in the presence of starch nanoparticles, ChemEngineering. 4 (2020) 1–15. https://doi.org/10.3390/chemengineering4040057.

[220] Christian Aulin, German Salazar-Alvarez, Tom Lindström, High strength, flexible and transparent nanofibrillated cellulose–nanoclay biohybrid films with tunable oxygen and water vapor permeability, Nanoscale. 4 (2012) 6622–6628. https://doi.org/10.1039/C2NR31726E.

[221] V. Khoshkava, M.R. Kamal, Effect of drying conditions on cellulose nanocrystal (CNC)

agglomerate porosity and dispersibility in polymer nanocomposites, Powder Technol. 261 (2014) 288–298. https://doi.org/10.1016/J.POWTEC.2014.04.016.

[222] Y. Cao, P. Zavattieri, J. Youngblood, R. Moon, J. Weiss, The relationship between cellulose nanocrystal dispersion and strength, Constr. Build. Mater. 119 (2016) 71–79. https://doi.org/10.1016/j.conbuildmat.2016.03.077.

[223] M.A. Rojas-Graü, M.S. Tapia, O. Martín-Belloso, Using polysaccharide-based edible coatings to maintain quality of fresh-cut Fuji apples, LWT - Food Sci. Technol. 41 (2008) 139–147. https://doi.org/10.1016/J.LWT.2007.01.009.

[224] T.M.P. Ngo, T.H. Nguyen, T.M.Q. Dang, T.X. Tran, P. Rachtanapun, Characteristics and antimicrobial properties of active edible films based on pectin and nanochitosan, Int. J. Mol. Sci. 21 (2020). https://doi.org/10.3390/ijms21062224.

[225] H. Wang, F. Ding, L. Ma, Y. Zhang, Edible films from chitosan-gelatin: Physical properties and food packaging application, Food Biosci. 40 (2021) 100871. https://doi.org/10.1016/J.FBIO.2020.100871.

[226] S.D.T. Maduwanthi, R.A.U.J. Marapana, Induced Ripening Agents and Their Effect on Fruit Quality of Banana, Int. J. Food Sci. 2019 (2019). https://doi.org/10.1155/2019/2520179.

[227] D.F. Holderbaum, T. Kon, T. Kudo, M.P. Guerra, Enzymatic Browning, Polyphenol Oxidase Activity, and Polyphenols in Four Apple Cultivars: Dynamics during Fruit Development, HortScience. 45 (2010) 1150–1154. https://doi.org/10.21273/HORTSCI.45.8.1150.

[228] M.B. Perez-Gago, M. Serra, M.A.D. Río, Color change of fresh-cut apples coated with whey protein concentrate-based edible coatings, Postharvest Biol. Technol. 39 (2006) 84–92. https://doi.org/10.1016/J.POSTHARVBIO.2005.08.002.